

AN INVESTIGATION INTO ANTERIOR SEGMENT ANATOMY AND  
GENETICS OF PIGMENT DISPERSION SYNDROME

Mr Ameet Shah  
(M.B.,B.S., FRCOphth.)

Thesis submitted to  
University College London  
in fulfillment of the  
MD(Res)

Authors Declaration

I, Ameet Shah, confirm that the work presented in this thesis is my own. Where information has been derived from other sources, I confirm that this has been indicated in the thesis.

Signed.....

Date.....

## ABSTRACT

Pigment dispersion syndrome (PDS) is an ocular condition predisposing to glaucomatous optic neuropathy in patients at a relatively young age. Concavity of the iris is considered to be important in the pathogenesis of PDS, however, it is also appears to be a feature of non-PDS eyes, particularly in young myopes. Much of the current understanding of anterior segment anatomy is derived from studies using ultrasound biomicroscopy, a relatively invasive imaging modality that involves direct ocular contact. Anterior-segment optical coherence tomography (AS-OCT) allows imaging of the anterior segment with the patient in the upright position without the need for contact with the ocular surface. AS-OCT may allow a more physiological assessment of anterior segment anatomy as well as being better suited to paediatric subjects. AS-OCT was used to conduct a case-control study of anterior segment anatomy in PDS subjects and age-, sex- and refraction- matched controls to determine which features of anterior segment anatomy best discriminated between the 2 groups. In addition AS-OCT was used to assess anterior segment anatomy, with particular emphasis on iris curvature, in a cohort of 10-12 year old school children and explore correlations with ocular biometry and parameters reflecting corneal biomechanical properties. Longitudinal data was collected through re-visiting the cohort 2 years later.

Chromosomal susceptibility loci for PDS have been described, although no causative gene has been identified. Two approaches were used to identify novel disease

susceptibility loci: 1) linkage analysis was used in a 3-generation family segregating for PDS/pigmentary glaucoma, and, 2) DNA from a large cohort of unrelated PDS probands was collected and sent for genotyping with a view to conducting a pilot genome-wide association study. Finally a candidate gene, *GPNMB*, the human homologue of a causative gene in a mouse model of pigmentary glaucoma was sequenced in a panel of 96 unrelated PDS/pigmentary glaucoma subjects.

## **ACKNOWLEDGEMENTS**

The work in this thesis could not have been done without the support and encouragement of a large number of people.

I would especially like to thank my supervisors Professors David Garway-Heath and Professor Shomi Bhattacharya for their advice and guidance as well as Dr Naushin Waseem for her teaching and supervision in the laboratory. I am also indebted to my family without whose support and patience this work could not have been completed.

## LIST OF CONTENTS

Title page	1
Author's declaration	2
Abstract	3
Acknowledgements	5
List of contents	6
List of figures	9
List of tables	11
Abbreviations	13

<b>1</b>	<b>INTRODUCTION</b>	
1.1	Glaucoma	19
1.2	Pigment dispersion syndrome	25
<b>2</b>	<b>ANTERIOR SEGMENT BIOMETRY IN PIGMENT DISPERSION: BETWEEN- AND WITHIN-OBSERVER AGREEMENT AND COMPARISON WITH AGE-, SEX- AND REFRACTION- MATCHED CONTROLS</b>	
2.1	Introduction	42
2.2	Methods	46
2.3	Results	54
2.4	Discussion	66
<b>3</b>	<b>PREVALENCE OF IRIS CONCAVITY IN 10-12 YEAR OLD SCHOOL BOYS AND LONGITUDINAL 2 YEAR FOLLOW UP</b>	
3.1	Introduction	74
3.2	Methods	77
3.3	Results	82
3.4	Discussion	93
<b>4</b>	<b>LINKAGE ANALYSIS</b>	
4.1	Introduction	103
4.2	Methods	109

4.3	Results	112
4.4	Discussion	125
<b>5</b>	<b>GENOME-WIDE ASSOCIATION STUDY OF PIGMENT DISPERSION SYNDROME AND MUTATION SCREENING OF <i>GPNMB</i></b>	
5.1	Introduction	134
5.2	Methods	142
5.3	Results	146
5.4	Discussion	157
<b>6</b>	<b>SUMMARY</b>	165
<b>7</b>	<b>APPENDIX</b>	170
<b>8</b>	<b>REFERENCES</b>	176

## LIST OF FIGURES

- 2.1 Line construction for iris concavity
- 2.2 Example AS-OCT screenshot illustrating semi-automated measurements
- 2.3 Determining posterior displacement of iris root from scleral spur
- 2.4 Bland-Altman plot to show within-observer agreement in the temporal quadrant
- 2.5 Bland-Altman plot to show between-observer agreement in the temporal quadrant
- 2.6 Receiver operating characteristic curves for iris curvature and anterior chamber angle
- 2.7 Receiver operating characteristic curves for iris curvature, lens vault and spur-to-root distance
- 2.8 Scatterplot of accommodative iris curvature against age in PDS/PG cohort
- 3.1 Scatterplot of lens vault against non-accommodating iris curvature iris curvature in 2009 schoolboy cohort
- 3.2 Histogram to show the distribution of non-accommodating iris curvature in 2009 and 2011
- 3.3 Histogram to show the distribution of accommodating iris curvature in 2009 and 2011

- 3.4 Scatterplot of corneal hysteresis against spur-to-spur distance on accommodation for 2011 schoolboy cohort
- 4.1 Autosomal dominant pigment dispersion pedigree
- 4.2 Parametric genome-wide LOD scores for chromosome 1
- 4.3 Parametric genome-wide LOD scores for chromosome 10
- 4.4 Parametric genome-wide LOD scores for chromosome 22
- 4.5 Haplotype analysis for region of interest on chromosome 1
- 4.6 Haplotype analysis for region of interest on chromosome 10
- 4.7 Haplotype analysis for region of interest on chromosome 22
- 5.1 Proportion of individuals with missing genotypes
- 5.2 Proportion of SNPs with missing genotypes
- 5.3 X-chromosome homozygosity for PDS cohort
- 5.4 Clustering of PDS subjects in comparison with HapMap III populations
- 5.5 Plot of principal components 1 and 2 for genotypic data from PDS cohort
- 5.6 Plot of principal components 1 and 3 for genotypic data from PDS cohort
- 5.7 Quantile-quantile plot showing the departure from Hardy-Weinberg equilibrium
- 5.8 Plot of observed to expected heterozygosity ratio
- 5.9 Estimated relatedness between any 2 samples in the PDS cohort
- 5.10 Missense change in exon 6 of GPNMB
- 5.11 Nucleotide insertion in exon 1 of GPNMB

## LIST OF TABLES

- 2.1 Within-observer agreement for classifying temporal quadrant
- 2.2 Between-observer agreement for classifying temporal quadrant
- 2.3 Bias and 95% limits of agreement for between- and within-observer difference in estimate of iris concavity
- 2.4 Summary of anterior segment optical coherence tomography parameters in cases and controls
- 2.5 Receiver Operating Characteristic analysis for anterior segment optical coherence tomography parameters in cases and controls
- 2.6 Correlation matrix to show correlation between non-accommodating AS-OCT parameters
- 2.7 Correlation matrix to show correlation between accommodating AS-OCT parameters
- 2.8 Results of robust regression of iris curvature on age with and without outlier exclusion
- 3.1 Baseline ocular characteristics of 2009 schoolboy cohort
- 3.2 Summary of AS-OCT parameters in 2009 schoolboy cohort
- 3.3 Between-observer agreement on AS-OCT parameters on images from 2009 schoolboy cohort
- 3.4 Ocular and non-ocular characteristics of 2011 schoolboy cohort

- 3.5 Comparison of ocular biometric parameters between 2009 and 2011 schoolboy cohorts
- 3.6 Summary data for AS-OCT parameters in 2011 schoolboy cohort
- 4.1 Clinical characteristics of generation III of PDS/PG family
- 4.2 Clinical characteristics of generation IV of PDS/PG family
- 5.1 Illumina 660w Quad beadchip genotyping call rates for 8 pilot samples from PDS cohort
- 5.2 Illumina 660w Quad beadchip genotyping call rates for remaining samples from PDS cohort

## ABBREVIATIONS

5-FU	5-fluorouracil
ACD	anterior chamber depth
AL	axial length
ALT	argon laser trabeculoplasty
AMD	age-related macula degeneration
AOD	angle opening distance
AS-OCT	anterior segment optical coherence tomography
AUC	area under the curve
ccIOP	corneal-compensated intraocular pressure
CCT	central corneal thickness
CH	corneal hysteresis
cM	centimorgan
cm	centimetre
CNV	copy number variations
CRF	corneal resistance factor

D	diopetre
DNA	deoxyribonucleic acid
FED	fuchs' endothelial dystrophy
GON	glaucomatous optic neuropathy
GWAS	genome-wide association study
HLA	human leucocyte antigen
HWE	Hardy-Weinberg Equilibrium
IBD	identity by descent
IBS	identity by state
ICE	irido-corneal endothelial
IOL	intra-ocular lens
IOP	intraocular pressure
JOAG	juvenile open angle glaucoma
kg	kilogram
LD	linkage disequilibrium
LE	left eye
LoA	limits of agreement

LOD	logarithm of the odds
LogMAR	logarithm of the minimal angle of resolution
LPI	laser peripheral iridotomy
LV	lens vault
µm	micron
mm	millimetre
MMC	mitomycin C
mmHg	millimetres of mercury
NC	neural crest
NICE	National Institute for Health and Care Excellence
OAG	open angle glaucoma
OHT	ocular hypertension
OR	odds ratio
ORA	ocular response analyser
<i>P</i>	probability value
PDS	pigment dispersion syndrome
PG	pigmentary glaucoma

POAG	primary open angle glaucoma
QC	quality control
RD	retinal detachment
RE	right eye
RNA	ribonucleic acid
ROC	receiver operating characteristic
SD	standard deviation
SE	spherical equivalent
SLT	selective laser trabeculoplasty
SNP	single nucleotide polymorphism
TGF	transforming growth factor
TISA	trabecular-iris space area
TM	trabecular meshwork
UBM	ultrasound biomicroscopy
VF	visual field
XFG	exfoliative glaucoma
YAG	yttrium-aluminium-garnet

<b>1</b>	<b>INTRODUCTION</b>	
1.1	Glaucoma	19
1.1.1	Definition	19
1.1.2	Classification of glaucoma	19
1.1.3	Epidemiology	20
1.1.4	Pathophysiology	20
1.1.5	Clinical evaluation	21
1.1.6	Management	21
1.1.6.1	Topical therapy	
1.1.6.2	Laser trabeculoplasty	
1.1.6.3	Surgery	
1.1.6.4	Management of angle closure	
1.2	Pigment dispersion syndrome	25
1.2.1	Prevalence of pigment dispersion syndrome	25
1.2.2	Epidemiology	27
1.2.3	Risk of conversion	27
1.2.4	Economic cost of pigmentary glaucoma	28

1.2.5	Pathophysiology	28
1.2.5.1	Damage to outflow	
1.2.6	Management	30
1.2.6.1	Topical therapy	
1.2.6.2	Laser trabeculoplasty	
1.2.6.3	Role of laser peripheral iridotomy	
1.2.6.4	Trabeculectomy	
1.2.7	Pigment dispersion as a heritable phenotype	34
1.2.7.1	Gene mapping in PDS/PG families	
1.2.7.2	DBA/2J mouse model	
1.2.7.3	Myocilin and pigmentary glaucoma	
1.3	Aims	38

## **1.1 Glaucoma**

### **1.1.1 Definition**

The term 'glaucoma' encompasses a heterogeneous number of conditions which have in common an optic neuropathy characterized by specific structural findings in the optic disc and specific functional deficits detected by automated visual field testing (1). Raised intraocular pressure (IOP) is an important risk factor but not a defining feature of the disease.

### **1.1.2 Classification**

Glaucoma may be broadly classified as either open-angle, where the irido-corneal angle appears clinically normal, or closed-angle, where tissue (commonly peripheral iris) physically obstructs the drainage of aqueous humour into the trabecular meshwork (TM). Differentiation between the 2 forms is significant with regard to management. Both open-angle and closed-angle glaucoma may be further divided into primary (no identifiable ocular comorbidity) and secondary causes. Secondary causes of open angle glaucoma (OAG) include pigment dispersion and pseudoexfoliation whilst secondary causes of closed angle glaucoma include rubeosis, plateau iris syndrome and uveitis (in the context of causing extensive adhesions between the peripheral iris and drainage angle (peripheral anterior synechiae). A proportion of

patients with open angles will have glaucomatous optic neuropathy (GON) with IOP consistently less than the upper limit of the normal range (considered to be 21mmHg) and these patients are classified as having low- or normal-tension glaucoma.

### **1.1.3 Epidemiology**

Glaucoma is the 2<sup>nd</sup> leading cause of blindness (defined as visual acuity of less than 3/60, or a corresponding visual field loss to less than 10 degrees in the better eye with best possible correction) worldwide after cataracts (2). Quigley et al. (3) estimated the combined prevalence of open and closed angle glaucoma to be 60 million with 8.4 million bilaterally blind in 2010. Women were estimated to comprise 55% of OAG and 70% of angle closure glaucoma (3). OAG is most prevalent in people of African descent whilst angle closure glaucoma is most prevalent in Chinese people (3). The projected numbers for 2020 are a combined prevalence of 79.6 million and 11.2 million bilaterally blind (3).

### **1.1.4 Pathophysiology**

Raised IOP is the major risk factor for GON as evidenced by unilateral secondary glaucoma, experimentally induced glaucoma and observation of the effects of IOP lowering in glaucoma patients (4) whilst the Collaborative Normal Tension Study was the first clinical trial to demonstrate that IOP lowering reduced the rate of glaucoma

progression (5). Raised IOP may cause compression of retinal nerve fibres against lamina cribrosa with interruption of axoplasmic flow (mechanical theory). An alternative theory is that raised IOP compromises blood supply to the optic nerve head (ischaemic theory). Disturbance in autoregulation of the blood supply to the optic nerve may also contribute with raised IOP leading to reduced perfusion or the occurrence of vasospasm even at normal levels of IOP (4).

### **1.1.5 Clinical evaluation**

The National Institute for Health and Clinical Excellence (NICE) have issued guidance on diagnosis, monitoring and treatment of chronic open angle glaucoma and OHT (6). Initial evaluation should include IOP measurement using Goldmann applanation tonometry, central corneal thickness (CCT) measurement, peripheral anterior chamber configuration and depth assessments using gonioscopy, visual field measurement using standard automated perimetry, optic nerve assessment after pupil dilatation, using stereoscopic slit lamp biomicroscopy with fundus examination. Automated imaging technologies have been developed which allow assessment of the optic disc and nerve fibre layer. Scanning laser ophthalmoscopy and optical coherence tomography (OCT) have a role in baseline assessment and monitoring for progression of GON.

### **1.1.6 Management**

IOP is the major modifiable risk factor for development of GON and current treatment options aim to lower IOP to a 'target pressure', which a clinician determines would prevent the development of visual disability (or prevent its worsening) within the patient's lifetime. Typically the target pressure is set lower if there is greater initial damage or multiple risk factors for progression. Treatment options include IOP lowering drops, laser treatment or surgery. Ocular perfusion pressure may also play a role in glaucoma pathogenesis (7) and clinicians may choose to modify blood pressure in order to achieve a more favourable perfusion pressure. Finally, there has been considerable interest in the role of neuroprotective agents in protecting against optic nerve head damage although robust evidence supporting the use of such agents is presently lacking; RCTs designed to measure the efficacy of neuroprotective agents would require long-term follow up in order to draw clinically meaningful conclusions (8)

#### **1.1.6.1 Topical therapy**

A typical first line treatment would be topical monotherapy with a prostaglandin analogue such as latanoprost, travoprost or bimatoprost which works by increasing uveo-scleral outflow. These drops may need to be switched to, or supplemented by, other classes of IOP lowering drops such as beta-blockers, carbonic anhydrase

inhibitors or alpha-2 adrenergic agonists. The predominant mechanism of action of these other agents is reduction of aqueous production.

### **1.1.6.2 Laser trabeculoplasty**

If sufficient IOP lowering cannot be achieved with drops, then laser treatment may be offered.

#### **1.1.6.2.1 Argon laser trabeculoplasty**

Argon laser trabeculoplasty causes a thermal burn to the tissue causing tissue contraction and scar formation and this is thought to result in a mechanical stretching of the surrounding uveoscleral TM (9). A Cochrane review (10) of laser trabeculoplasty for OAG concluded that in newly diagnosed OAG participants, the risk of uncontrolled IOP at six months and two years of follow up is lower in patients treated with laser trabeculoplasty compared to those on medical treatment. The trials reviewed did not include newer classes of drops i.e. prostaglandin analogues, carbonic anhydrase inhibitors or alpha-2 agonists. For participants already on maximum medical therapy, the risk of uncontrolled IOP at six months was higher in patients treated by laser trabeculoplasty compared to surgery (trabeculectomy), however, the trials did not include trabeculectomy augmented by anti-metabolites and had these been included it is likely the difference between the modalities would have been even greater. The

American Academy of Ophthalmology published a review on laser trabeculoplasty (11) confirming the technique was effective at lowering IOP in patients with OAG.

#### **1.1.6.2.2 Selective laser trabeculoplasty**

There is considerable interest in selective laser trabeculoplasty (SLT), an alternative to argon, which uses a frequency-doubled short-pulsed (Q-switched) neodymium:yttrium–aluminium– garnet (YAG) laser. It has been suggested that SLT works by stimulating macrophage recruitment and inducing changes in cytokines which stimulate extracellular matrix remodeling leading to increased aqueous outflow (9). The laser in SLT is thought to be selectively taken up by the pigmented trabecular meshwork cells. The theoretical advantage of SLT over ALT is that there appears to be less coagulative and structural damage to the TM (12) and it may therefore be more suitable for repeat treatments.

#### **1.1.6.3 Surgery**

Surgery may be considered in patients at risk of sight loss despite treatment (6). Trabeculectomy lowers IOP by re-directing aqueous humour into the sub-conjunctival space, forming a bleb under the upper eyelid and creating an alternative pathway for aqueous humour outflow. Modern surgical techniques employ wound modulation with anti-metabolites (mitomycin C (MMC) or 5-fluorouracil (5-FU)) and placement of

releasable sutures which provide the option of increasing flow through the trabeculectomy in the post-operative period and reducing the risk of hypotony. Despite advances in surgical technique, excessive drainage can lead to hypotony, which may be associated with choroidal detachments and/or maculopathy, whilst excessive fibrosis can lead to bleb failure. There is a trend in some centres towards non-penetrating glaucoma surgery or procedures that enhance Schlemm's canal. Whilst non-penetrating techniques are accepted to have a better safety profile than trabeculectomy, post-operative IOP is not as low as that achieved by trabeculectomy (13-15) and the procedures have a longer learning curve (16).

In cases where trabeculectomy has failed or in certain glaucoma subtypes there may be a preference instead to insert a glaucoma drainage device or 'tube' which serves to lower IOP by draining aqueous from the anterior chamber to the sub-conjunctival space. Data from a 5-year multi-centre randomised clinical trial (17), reported that trabeculectomy with MMC had a greater surgical failure rate than tube surgery although both procedures had similar rates of vision loss and late post-operative and serious complications.

#### **1.1.6.4 Management of angle closure**

The initial management of angle closure glaucoma involves making a hole in the peripheral iris, commonly with a YAG laser, in order to bypass 'pupil block', the anatomical configuration which causes the peripheral iris to bow forwards and close

the angle between the cornea and the iris. When iridotomy fails to open the drainage angle, laser iridoplasty may be considered as a treatment option and works by causing localised areas of shrinkage in the peripheral iris, causing it to be pulled away from the TM. Topical therapy may also be required as adjunctive treatment. Lens extraction with insertion of an intra-ocular lens (IOL) also causes widening of a closed/narrow drainage angle and is increasingly recognised to have a role in the management of angle closure glaucoma (18-20).

## **1.2 Pigment dispersion syndrome**

Pigment dispersion syndrome (PDS) is an ocular condition predisposing to OHT. A proportion of patients with raised IOP will go on to develop a secondary OAG referred to as pigmentary glaucoma (PG). In 1949, Sugar and Barbour (21) reported 2 young, myopic men with Krukenberg spindles, iris transillumination defects and TM hyperpigmentation who developed raised IOP with mydriasis and decreased with pilocarpine, using the term 'pigmentary glaucoma' to describe the condition. More patients were subsequently reported, and in 1966 Sugar reviewed 147 cases in the world literature(22), describing additional features including association with myopia, greater incidence in men than in women and a relatively young age of onset.

### 1.2.1 Clinical features

PDS is characterised by the following triad:

1. Krukenberg spindle. This is a central vertical band seen on the corneal endothelium and occurs as a result of aqueous convection currents depositing dispersed pigment on the endothelium.
2. Mid-peripheral spoke-like iris transillumination defects, which can be seen by retro-illumination.
3. Hyperpigmentation of the trabecular meshwork. This is usually a dense homogeneous band in a wide-open angle. With time pigment may regress initially from the superior trabecular meshwork, a phenomenon known as the pigment reversal sign (23).

Other anterior segment features of the syndrome include: pigment particles on the anterior iris surface, anisocoria (larger pupil in eye with greater transillumination defect) (24), pigment at the insertion of lens zonular fibers into the posterior lens capsule (Zentmayer ring or Scheie stripe) (25), deeper anterior chamber depths than expected for age, sex and refractive error (26).

Patients with PDS have been reported to have an increased prevalence of lattice degeneration reported to be 33% in a PDS cohort and 20% in a mixed PDS/PG cohort; these percentages are greater than expected for the degree for the degree of myopia

(27, 28). Prevalence of retinal detachment has been reported between 4-6.6% in PDS (28, 29) and 7.6% in PG (29) and these percentages are also greater than expected for the degree of myopia (29, 30). Greenstein et al. conducted electro-oculograms on patients with PDS and PG and reported significantly lower mean Arden ratios compared to control subjects and POAG/OHT patients, implicating the retinal pigment epithelium/photoreceptor complex in the pathology. Fundus autofluorescence imaging in the subjects with reduced Arden ratios would have been of interest in order to further investigate abnormalities of the posterior segment.

### **1.2.2 Epidemiology**

PDS is more common in myopes (29, 31) with an approximately equal male to female ratio (23, 29) whilst PG is more common in men (29, 32, 33). Only one study has investigated the prevalence of PDS (34): a population glaucoma screening study of 654 white subjects reported that 2.45% had evidence of PDS.

### **1.2.3 Risk of conversion**

A study of 21 patients indicated that the probability of developing a significant IOP rise in PDS patients is 52% at 2 years (35) and 86% at 10 years (36). Several studies have investigated the risk of conversion from PDS to PG: Migliazzo et al.(33) conducted a retrospective study which included 37 PDS patients with OHT of whom 35 % eventually developed glaucomatous field defects (mean overall follow up period was 17 years).

Farrar et al. (30) conducted a similar retrospective study which included 18 patients with PDS. With regard to the latter group, 7 out of 18 (39%) converted to PG during the follow up period although this may be an underestimate as only 4 out of 18 had follow up of more than 6 months. Both of these studies included patients on treatment and were based on patients attending a specialist glaucoma service and as such are likely to include a disproportionate number of patients with OHT as referral from primary care of patients with PDS tends to be on the basis of high IOP. It is likely that there are many cases of PDS without OHT that are never referred to an ophthalmologist or glaucoma subspecialist. There has only been one community-based study looking at risk of conversion (32). The authors of this study conducted a retrospective review of 113 patients with newly diagnosed PDS over a 24-year period and determined the probability of converting to PG to be 10% at 5 years and 15% at 15 years.

#### **1.2.4 Economic cost of pigmentary glaucoma**

Detection, treatment and provision of state and family social care for patients with primary POAG and OHT was estimated to cost £944 per patient for the year 2010 (37). Per patient costs are likely to be similar for PG. There are no prevalence data on PG but the incidence in a predominantly Caucasian population has been estimated at 1.4 per 100,000. Using UK Census data for the size of the Caucasian population together the above estimates suggest the cost of newly diagnosed PG is £715,917 per year. The mean age of diagnosis is 42 years (compared to around 70 years in POAG) so the

lifetime costs after the first year of diagnosis are considerably more than POAG, not to mention the costs in lost productivity through visual disability in a population largely of working age.

### **1.2.5 Pathophysiology**

Campbell (38) was the first to propose that in PDS the posteriorly bowed iris led to frictional contact between packets of anterior zonular fibres and the posterior pigment epithelium resulting in pigment dispersion. The concept of the 'reverse pupillary block' mechanism was introduced by Karickhoff (39). Karickhoff proposed that abnormal irido-lenticular contact causes the iris to act like a flap valve permitting unidirectional flow of aqueous from the posterior to the anterior chamber, maintaining the posterior bowing. Dispersed pigment is deposited throughout the anterior segment including within the TM. In a proportion of patients pigment accumulation in the TM leads to impaired drainage of aqueous humour with a consequent increase in IOP.

Iris concavity in PDS/PG appears to be enhanced by accommodation and this has been quantified on studies using ultrasound biomicroscopy (UBM) (40) and AS-OCT (41). The degree of accommodation-induced concavity is inversely correlated with age (42). Accommodation is associated with miosis and forward movement of the anterior pole of the lens (43) which increases the area of irido-lenticular contact and potentiates the flap-valve effect. Accommodation-induced iris concavity appears, however, to be a

relatively transient response with reversal of concavity within 3 minutes despite continued accommodative effort (44).

#### **1.2.5.1 Damage to outflow**

Richardson et al. (45) conducted light and electron microscopy of TM from PDS patients and noted pigment granules entering TM undergo phagocytosis by endothelial cells. It was hypothesised that phagocytosis-induced damage to the endothelial cells led to denudation of the trabecular beams with subsequent collapse and sclerosis of TM. Alvarado et al. (46) determined that the majority of resistance to aqueous outflow occurs at the terminations of the aqueous channels (cul-de-sacs) and have shown the area of these terminations to be markedly reduced in TM specimens from PG and POAG patients compared to those from non-glaucomatous normal subjects.

#### **1.2.6 Management**

##### **1.2.6.1 Topical therapy**

Topical drugs can be used to manage raised IOP in OAG and the same classes of drug are also used to manage raised IOP secondary to pigment dispersion. Prostaglandin analogues, beta-blockers, carbonic anhydrase inhibitors and alpha-adrenergic agonists can all lower IOP. Pilocarpine, a parasympathomimetic acting on cholinergic receptors, reduces IOP by increasing outflow and has the additional advantage of reducing iris

concavity (41, 47). However in practice, high concentrations of pilocarpine are often poorly tolerated in young myopes on account of causing increased myopia and accommodative spasm. Furthermore, pigment dispersion subjects require a careful peripheral retinal examination prior to commencing miotic therapy as this class of drugs is associated with an increased risk of retinal detachment (48).

### **1.2.6.2 Laser trabeculoplasty**

ALT appears to be effective early on in PG with a subsequent increase in IOP after 3 months(49). Longer-term ALT success rates have been reported between 62-80 % at 8-12 months (50, 51) with younger patients and those with glaucoma of a shorter duration having greater success rates.

A study of 30 eyes with PG (52) reported success rates with SLT at 85% at 12 months but only 14% at 48 months. Criteria for classifying a treatment as failed were, however, quite stringent: <20% drop in IOP, subsequent change in medical treatment, performance of a further SLT treatment or the need for surgery. There are conflicting data on the safety of SLT in PDS/PG. In the above study (52), the authors reported 2 cases showing mild inflammation following laser and a further 2 cases developing IOP spikes 2 hours post laser, which normalised the following day. Kouchecki et al. (53) reported a mean reduction in IOP of 19% at 18 months although 26% needed either further SLT or trabeculectomy and 22% developed significant IOP spikes.

Harasymowycz et al. (54) noted significant IOP spikes following SLT in heavily pigmented eyes of 4 patients (3 of whom had features of pigment dispersion); 3 of these eyes went on to require trabeculectomy. The authors suggested that eyes with heavily pigmented TM, previous ALT and being on multiple topical medications are potential risk factors for IOP spikes.

### **1.2.6.3 Role of laser peripheral iridotomy**

Laser peripheral iridotomy (LPI) is a widely established procedure for primary angle closure and angle closure glaucoma. It is generally regarded as a safe procedure although there is a small short-term risk of bleeding, raised IOP and inflammation; such adverse effects are generally transient and can usually be managed without resulting in significant long-term sequelae. Diplopia or 'ghost images', lens opacity and corneal injury are rare complications and malignant glaucoma, retinal burns and lens-induced uveitis are extremely rare complications.

Performing LPI in PDS/PG patients provides a route by which aqueous humour can drain from the anterior to the posterior chamber, thereby overcoming reverse pupillary block and reducing or eliminating iris concavity. A reduction in iridolenticular contact and iris concavity following LPI have been reported in UBM studies (48-50). LPI may therefore reduce the amount of pigment dispersed and represents a one-off, relatively non-invasive intervention with the potential to reduce the risk of developing raised IOP and PG.

Gandolfi et al. (27) investigated the effect of LPI in eyes with normal IOP at baseline. The authors reported results on 21 PDS subjects (age range 18-60 years) who underwent unilateral LPI in a randomly selected eye whilst the fellow untreated eye served as the control. At 2 years, 52% of untreated eyes showed an elevation of 5mmHg or more compared with only 4.7% of treated eyes. LPI appeared less effective

in older patients. Scott et al. (55) conducted a prospective randomized control trial of 116 patients with PDS and ocular hypertension. Eight eyes (15%) in the laser group and 3 eyes (6%) in the control group converted to glaucoma in the study period (median follow up 3 years). Studies have also investigated the effect of LPI in PDS patients with raised pressure and PG: Reistad et al. (56) retrospectively analysed data contributed by members of the American Glaucoma Society on patients with bilateral PG receiving uni-ocular LPI. A greater decrease in IOP was observed in treated eyes compared with fellow eyes (among 46 patients observed for 2 years or more), however, linear model analysis indicated that the higher mean baseline IOP in the treated eyes accounted for the apparent treatment effect. Lagreze et al. (53) reported on IOP pre- and post-LPI in their cohort of 20 PDS (including some PG) eyes and found no significant difference at 9 months when compared with untreated fellow eyes. There is little data, therefore, to support the efficacy of LPI in eyes that have already developed an IOP rise or GON.

#### **1.2.6.4 Trabeculectomy**

Filtering surgery is required in cases of PG where topical or laser therapy has been insufficient to control IOP. PG patients tend to be young and are therefore at risk of bleb failure from excessive post-operative scarring and the use of anti-metabolite adjuncts such as MMC is particularly useful to modulate the post-operative course. A large clinical study suggested that a greater percentage of PG patients require trabeculectomy compared to a randomly selected control group with chronic simple

glaucoma and that men with PG required surgery at a younger age compared to women with PG (29).

### **1.2.7 Pigment dispersion as a heritable phenotype**

Becker(57) et al. originally proposed that PDS had a specific genetic pre-disposition when they noted an increased prevalence of HLA B13 or Bw17 in PDS subjects compared to those without PDS, although this finding was not replicated in a small subsequent study (58). Gramer et al. (59) report a family history of glaucoma in 39% of patients with PDS or PG, but such a family history was no more common in PG compared to PDS. There are several reports of families segregating for PDS/PG (60-62).

#### **1.2.7.1 Gene mapping in PDS/PG families**

Linkage analysis is the method of choice for gene mapping in large multigenerational families in which at least 4 individuals are affected. The approach identifies disease susceptibility loci by typing genetic markers across the genome in the most informative members of the family and studying which markers are linked with the disease of interest. Linkage analysis was used by Andersen et al. (63) who studied 4 families segregating for PDS/PG, all of whom had some degree of Irish ancestry, and reported significant linkage to the telomere of the long arm of human chromosome 7 (7q35-q36), a locus subsequently designated as *GPDS1* (glaucoma-related pigment dispersion syndrome 1, OMIM ID 600510). Based on this region, a homeobox gene involved in

forebrain development, a cholinergic receptor gene and a gene for nitric oxide synthetase were put forward as candidate genes. Mutations in nitric oxide synthetase could lead to the production of reactive nitrogen species, possible mediators of apoptotic cell death within iris tissue or cells of the RPE/photoreceptor complex. A 12 cM region located within 18q21 was subsequently identified as a second locus through linkage analysis on 4 further pedigrees (64) although no causative genes have so far been identified from either locus. Subsequently, polymorphisms of the GPDS1 locus have been shown to be associated with normal tension glaucoma in a Japanese population (65).

Ritch (23) highlighted that a causative gene would need to explain the increased prevalence of lattice degeneration and suggested the gene would affect development of the middle third of the eye early in the third trimester as this would be consistent with a condition that appears to affect the iris as well as the retina.

#### **1.2.7.2 DBA/2J mouse model**

John et al.(66) described pigment dispersion and iris atrophy in mice of the inbred strain DBA/2J. DBA denotes the parent strain, '2' denotes the sub-strain and 'J' refers to the Jackson Laboratory where the strain was developed. IOP was increased in this strain by around 9 months of age with subsequent retinal ganglion cell death, optic nerve atrophy and optic nerve cupping. There are, however, important differences between the clinical findings in DBA/2J mice and PG in humans: in the mouse model

there is accumulation of macrophages laden with pigment in the angle and a tendency to develop both anterior and posterior synechiae leading to secondary angle closure rather than the OAG seen in human PG. In addition, the presence of iris atrophy and anterior synechiae suggest a degree of overlap with the irido-corneal endothelial (ICE) syndrome. The pigment dispersion in this strain was subsequently found to be caused by a premature stop codon mutation in a gene known as *Gpnmb* (67), occurring only in strains homozygous for this change whilst stromal atrophy was caused by the recessive allele of *Tyrp1* (67).

Schraermeyer et al. (68) used light and electron microscopy and immunohistochemistry to study the ocular pigment abnormalities in the DBA/2J strain. The authors reported migration of macrophages from the iris into the TM where they block aqueous outflow. These macrophages are laden with immature melanosomes (melanin-containing granules within melanocytes) from the iris pigment epithelium and the authors commented that abnormal melanosomes were also present in the iris of some PDS patients.

### **1.2.7.3 Myocilin and pigmentary glaucoma**

The published literature on the genetics of PDS has thus far failed to separate out distinct genetic contributions to PDS and the glaucomatous optic neuropathy (GON) that may ensue. Some investigators have suggested that PG may be a variant of POAG

(69) and it may be that there are separate genetic components independently conferring susceptibility to PDS, and raised IOP/GON.

PDS and PG have been associated in several studies with mutations in the myocilin (*MYOC*) gene, one of the few genes whose causative role in glaucoma is well-established. *MYOC* was originally discovered by Stone et al.(70) who reported mutations in in this gene causing juvenile open angle glaucoma (JOAG); the gene mapped to the GLC1A region which had been previously identified by Sheffield et al.(71) through linkage analysis of large pedigree segregating for autosomal dominant JOAG.

*MYOC* encodes a 504-amino-acid glycoprotein, which contains an olfactomedin domain (residues 246–501), where the majority of the mutations documented have been identified, although the exact role of myocilin in the pathogenesis of OAG is unknown. Over 70 mutations in the *MYOC* gene have been implicated in POAG (72) and *MYOC* mutations are thought to be responsible for 2-4% of glaucoma worldwide (73). *MYOC* associated OAG is particularly associated with high IOP (74). Whilst *MYOC* mutations were initially associated with JOAG, the most common mutation, Gln368Stop, is associated with late-onset OAG (75, 76).

A small number of mutations in *MYOC* have been reported in associated with PDS/PG. Vincent et al. (77) have reported Thr293Lys mutation in a 31 year old with PG. The

proband had a family history of late onset POAG but this remained unconfirmed as family members were not available for examination. Faucher et al.(78) reported a 40 year with PG carrying the Ala445Val MYOC mutation and Alward et al. (79) reported a case of PG associated with Arg470Cys and a case of pigment dispersion (without glaucoma) carrying the Gln368Stop mutation. Conversely, Paglinauan et al. (80) have described 3 pigment dispersion pedigrees where linkage to the 1q21-q31 region (the locus subsequently found to contain MYOC) was excluded.

### **1.3 Aims**

Whether to perform LPI in patients with PDS/PG remains an area of controversy and depends, to a large extent, on whether iris concavity is the key abnormality driving the pathogenesis of the condition. As LPI represents a relatively non-invasive, one-off intervention with the potential to prevent the development of glaucoma (and thereby avoid the necessity of lifelong drops and possible filtering surgery) in a relatively young patient population, establishing the role of iris concavity in pigment dispersion syndrome remains a goal of considerable importance.

Establishing the genetic basis of PDS/PG is important for 2 main reasons: 1) it might allow screening of unaffected first degree relatives of patients, allowing those without genetic predisposition to be safely discharged to the care of their optometrist whilst focusing resources on those carrying high risk mutations in an effort to commence

treatment prior to the onset of significant visual loss, and, 2) understanding the molecular pathways underlying the pathogenesis could lead to the discovery of targets for novel therapies.

Within this context, the work has 3 principal aims:

- 1) To determine which anterior segment parameters, as quantified on AS-OCT, best distinguish PDS/PG eyes from age-, sex- and refraction-matched controls
- 2) To determine the prevalence of iris concavity in early adolescence and explore associations with refractive error
- 3) To identify disease susceptibility loci/genes for PDS/PG using 2 different approaches: linkage analysis in a pedigree segregating for PDS/PG and genome-wide analysis in a cohort of unrelated PDS/PG probands using an appropriate genotypic control dataset

2	<b>ANTERIOR SEGMENT BIOMETRY IN PIGMENT DISPERSION: BETWEEN- AND WITHIN-OBSERVER AGREEMENT AND COMPARISON WITH AGE-, SEX- AND REFRACTION- MATCHED CONTROLS</b>	
2.1	Introduction	42
2.1.1	Quantification of iris concavity and the role of accommodation	42
2.1.2	Iris concavity and blinking	43
2.1.3	Anterior segment biometry in PDS/PG compared to controls	43
2.1.4	Anterior segment optical coherence tomography in PDS/PG	44
2.1.5	Repeatability of iris curvature measurements	45
2.1.6	Case-control study	45
2.2	Methods	46
2.2.1	Image acquisition	47
2.2.2	Line construction for iris concavity	48
2.2.3	Between- and within-observer agreement	50
2.2.4	Anterior segment imaging case-control study	50
2.2.4.1	Control subjects	
2.2.4.2	Additional AS-OCT analysis	
2.2.4.3	Statistical analysis	

2.3	Results	54
2.3.1	Between- and within-observer agreement	54
2.3.2	Anterior segment imaging case-control study	57
2.4	Discussion	66

## **2.1 Introduction**

Iris concavity (IC) is considered to be the key anatomical abnormality in PDS and reversal of this concavity is the basis for offering patients laser peripheral iridotomy (LPI).

### **2.1.1 Quantification of iris concavity and the role of accommodation**

The role of IC in PDS has been studied with ultrasound biomicroscopy (UBM). Carassa et al. (81) have described a method for IC quantification by measuring the maximum deflection of the posterior iris pigment epithelium from a line constructed between the innermost point of the posterior pigment epithelium in contact with the lens and its outermost point at the iris root. The authors reported IC in 27 of 50 PDS eyes and in 2 out of 15 control subjects. Of the 23 eyes with PDS showing either a convex or planar configuration, 3 showed concavity on accommodation only. Studies that have specifically investigated the role of accommodation in iris concavity in PDS/PG have yielded conflicting results. Adam et al. (42) studied the changes in iris profile in 92 patients with PG and reported the accommodated state to be associated with significant posterior bowing. Balidis et al. (82) studied 49 eyes of 30 PDS/PG subjects and found the effect of accommodation on iris profile to be variable, reporting an increase in concavity in only 20% of subjects on accommodation. However, the mean age of the subjects in the latter study was 53 years, which was 11 years older than the

mean age of the study by Adam et al. which might account of the apparent difference in accommodation-induced concavity

### **2.1.2 Iris concavity and blinking**

Liebmann et al. (83) have demonstrated, using UBM, how prevention of blinking alters iris configuration. After a period of up to 15 minutes of continuous scanning, during which time blinking was prevented, the authors reported anterior iris movement in 10 out of 10 PDS eyes and 9 out 10 healthy controls. The mean change in iris position, from most concave to most convex was 0.32 mm for eyes with PDS and 0.09 mm for control eyes ( $P=0.0001$ ). It is thought that when blinking is prevented, aqueous humour accumulates in the posterior chamber. Normal blinking produces transient vector forces on the cornea which promote aqueous flow from the posterior to the anterior chamber leading to a more concave (or less convex) configuration.

### **2.1.3 Anterior segment biometry in PDS/PG compared to controls**

Investigators have reported greater anterior chamber depth in PDS/PG subjects compared with other forms of open angle glaucoma or glaucoma suspects (84) and a more posterior iris insertion (85) compared to matched controls. To identify the anatomical factors predictive of PDS, Mora et al. (86) conducted a study examining iris-lens contact, iridocorneal angle and iris concavity as measured by UBM comparing 24 PDS/PG subjects with 25 age-, sex- and refraction-matched controls. Receiver

operating characteristic (ROC) curves were constructed to assess the ability of UBM to discriminate between cases and controls. Irido-corneal angle in accommodation was found to be the most sensitive parameter, reaching a sensitivity and specificity of 0.875 with a cut off of 53°. Interestingly, IC in accommodation was the 2<sup>nd</sup> most sensitive parameter.

#### **2.1.4 Anterior segment optical coherence tomography in PDS/PG**

Whilst UBM has advanced our understanding of iris configuration in PDS, it does require physical contact with the globe with the patient in a supine position. Furthermore, the ultrasound probe in contact with the patient's eye is likely to reduce the blink rate and this may lead to underestimates of the degree of iris concavity; this departure from the physiological state gives rise to the potential for artefactual results. Anterior segment optical coherence tomography (AS-OCT) is a non-contact imaging device that images the eye with the patient sitting upright and may better reflect true iris anatomy. Laemmer et al. (87) reported iris concavity in 18 out of 22 PDS subjects but also mild iris concavity in 1 out of 10 control patients using AS-OCT. Liu et al. (41) used AS-OCT to study iris contour in 20 PDS subjects and their data corroborated the conclusions of Adam et al. (42) in supporting the role of accommodation in inducing iris concavity. However, in contrast to the UBM studies, they reported that the iris concavity diminished when blinking was allowed; even a subsequent phase of forced blinking did not restore iris concavity. One disadvantage of AS-OCT, however, is its

inability to image structures posterior to the iris (88) meaning it is unable to reliably quantify areas of irido-lenticular contact.

### **2.1.5 Repeatability of iris curvature measurements**

Balidis et al. (89) have investigated the repeatability of iris curvature measurements by UBM in PDS/PG and concluded that whilst there was good intra-observer agreement, the variability between observers was greater and suggested that when using their method of measuring iris concavity, measurements should preferably be taken by the same observer.

Although AS-OCT is now becoming more commonly used to image iris anatomy in PDS (74, 87), there are no published data investigating the repeatability of this modality in assessing iris concavity. The first part of this chapter describes a study assessing between- and within-observer agreement in measuring iris curvature in AS-OCT images of patients with PDS/PG.

### **2.1.6 Case-control study**

The majority of studies examining differences between PDS/PG subjects have used UBM to image the anterior segment (84-86). AS-OCT allows a more physiological record of anterior segment biometry to be obtained and in particular allows for assessment of features such as iris curvature, anterior chamber depth and relative iris

insertion, all of which are thought to be significantly different in PDS/PG subjects compared with matched controls. The second part of this chapter describes a case-control study where AS-OCT biometric parameters of 50 PDS/PG subjects and 50 age-, sex- and refraction-matched controls were compared. The purpose of this study was to determine the relative importance of each parameter in distinguishing PDS/PG from myopic control subjects and to validate findings of previous UBM-based studies. Differences in iris curvature between cases and controls is of particular interest as the intervention of LPI is thought to work by reducing iris concavity and eliminating the anatomical predisposition to pigment dispersion.

## **2.2 Methods**

Participants recruited into a genetic study into PDS/PG were enrolled between December 2008 and July 2011. Participants underwent detailed phenotyping comprising slit lamp biomicroscopy looking for the presence of Krukenberg spindle and iris transillumination defects and gonioscopy to document the presence and amount of trabecular meshwork hyperpigmentation. IOP was checked using Goldmann applanation tonometry and optic disc assessment was performed using indirect ophthalmoscopy. Automated perimetry was performed with the Humphrey Field Analyzer Mark II (or II-i) and the Swedish interactive threshold algorithm standard 24-2 program. Refractive error was determined by spectacle focimetry or autorefraction if current spectacles were not available. Ethics Committee approval was obtained and

the study adhered to the tenets of the Declaration of Helsinki, a statement of ethical principles for medical research involving human subjects, including research on identifiable human material and data.

As part of the phenotyping for this study participants underwent AS-OCT imaging and provided informed consent for the purposes of the imaging studies. Diagnostic criteria for PDS were a) at least 270° of confluent dark brown trabecular meshwork pigmentation plus either a Krukenberg spindle *or* mid-peripheral transillumination defects, or b) 180 dark brown trabecular meshwork pigmentation plus both Krukenberg spindle *and* mid-peripheral transillumination defects. A diagnosis of PG was made if, in addition, there was a glaucomatous visual field defect on automated 24-2 Humphrey perimetry with corresponding damage to the optic nerve head (cup-to-disc ratio  $\geq 0.07$ , focal narrowing of the neuroretinal rim, or both). Subjects with previous intra-ocular surgery, LPI or non-glaucomatous causes of field loss were excluded.

### **2.2.1 Image acquisition**

Anterior segment imaging was performed using the Visante AS-OCT (Carl-Zeiss-Meditec, Dublin, California, USA). Images were acquired using near and distance fixation targets in dim illumination with the room lights switched off and window blind pulled down prior to image acquisition. Fixation was monitored using the pupil-tracking screen and the appearance of a central interference flare was used to indicate good

centration. A scan of the temporal and nasal quadrants was taken using the 'horizontal scan' protocol; as the focimetry/autorefraction details had been entered during the registration process, this scan was deemed to represent distance fixation.

The "POWER" tab, which controls the focus of the fixation target and is set by default to zero, was gradually reduced while asking the subject if he could still see a clear and sharp image. The value at which the subject reported a blurred image was noted e.g. -3.00 dioptres. The subject was moved away and the power value determined above was exceeded e.g. -4.00 dioptres before placing the subject back onto the chin rest. The power value was then made gradually more positive, acquiring the image once the subject reported seeing a sharp image again. This second scan was deemed to represent near fixation.

### **2.2.2 Line construction for iris concavity**

A line was drawn from the innermost to the outermost extremity of the posterior pigment epithelium (figure 2.1a). At the point of maximal iris deflection, a second line was constructed starting from, and perpendicular to, the first line. This line was extended to the posterior iris pigment epithelium and its length was taken as the iris deflection measurement (figure 2.1b). Blinking was allowed during image acquisition and the iris deflection measurement was taken in the same way regardless of whether the accommodation has been induced.

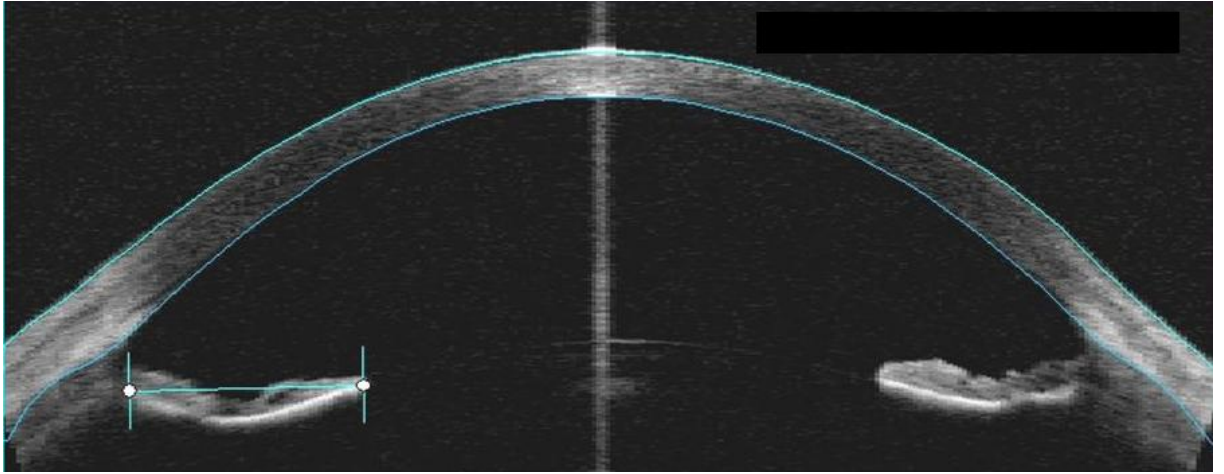


**Figure 2.1a** Line joining inner and outer extremities

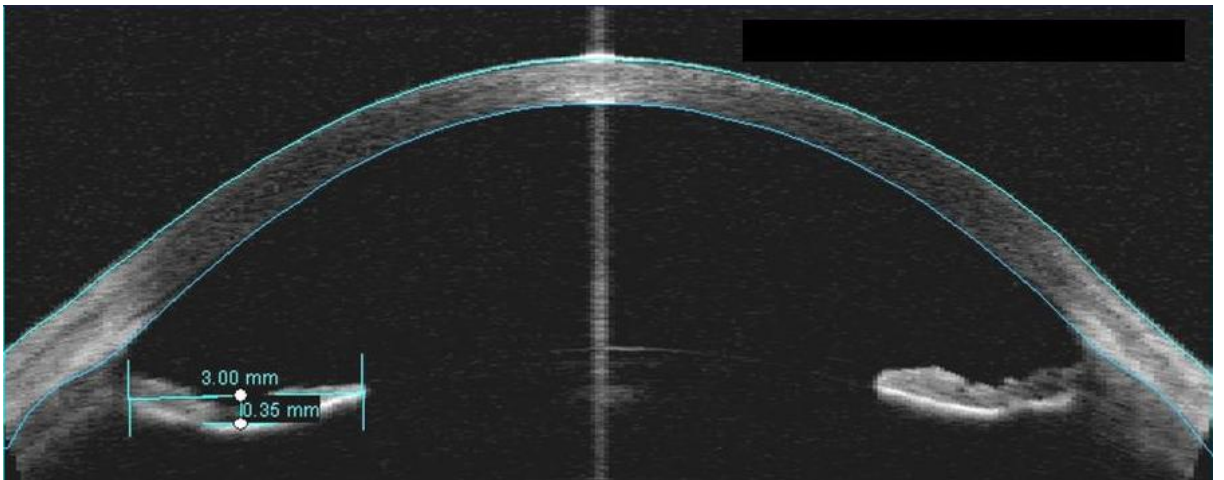


**Figure 2.1b** Measuring maximum deflection. In this example iris concavity was recorded as -0.35 mm.

### **2.2.3 Between- and within-observer agreement study**

AS-OCT images from the first 50 consecutive PDS/PG patients were used for this study. The eye with the least flat iris profile was selected from each eye pair to maximize the chance of finding disagreement between and within observers. Iris curvature was quantified independently by 2 observers for both temporal and nasal quadrants using AS-OCT software as described in section 2.2.2. A small number of examples were discussed amongst the observers with the aim of achieving uniformity in identifying the scleral spur. These examples were not included in the analysis. Observer 1 repeated the measurements on the same set of images 1 week later. Nasal and temporal quadrants were analysed separately. Bland-Altman plots were constructed. Average agreement (bias) was estimated by the mean of the differences between or within observers and limits of agreement (LoA) were calculated as the bias  $\pm$  (1.96 x standard deviation of the differences) (90).

In addition to quantitative measurements, iris profiles were categorised as planar ( $-1.0 \leq \text{deflection} \leq 1.0$ ), convex (deflection  $> 1.0$ ) or concave (deflection  $< -0.1$ ). Agreement was assessed using a weighted Kappa statistic ( $\kappa$ ). Statistical analyses were performed using MedCalc Version 11.2.1.0.

## **2.2.4 Anterior segment imaging case-control study**

### **2.2.4.1 Control subjects**

The 'case' group comprised 50 PDS/PG subjects recruited as part of the genetic study.

A 'control' cohort was recruited from members of staff at Moorfields Eye Hospital and patients without PDS who were attending the Glaucoma Service for management of primary open angle glaucoma, ocular hypertension or who were glaucoma suspects.

Control subjects underwent similar clinical examination and each subject was matched to a PDS/PG subject, based on: 1) sex, 2) age within 5 years and 3) spherical equivalent (SE) as judged by spectacle focimetry or autorefractometry within 1 dioptre. Cases and controls were both predominantly of Caucasian ancestry which minimised differences in ethnicity between the groups giving rise to bias.

### **2.2.4.2 Additional AS-OCT analysis**

In addition to iris curvature, the following additional analysis was performed on the non-accommodative and accommodative images from both the case and control cohort using the device's in-built software (Visante version 3.0). The scleral spur was identified by the operator and based on this landmark the software calculated the following parameters: anterior chamber depth (ACD), scleral-spur to scleral-spur distance, lens vault (LV, the perpendicular distance between the anterior pole of the

crystalline lens and a horizontal line joining the 2 scleral spurs (91)), angle opening distances at 500 and 750 microns from scleral spur (AOD500 and AOD750) (92) and trabecular-iris space area (TISA) at 500 and 750 microns from the scleral spur (TISA500 and TISA750) (93). These measurements are illustrated in figure 2.2.

The antero-posterior distance between the scleral spur and the iris root (abbreviated to 'root-to-spur' from this point forward) is an important metric as greater proximity of the iris root to the scleral spur implies the posterior iris pigment epithelium is anatomically closer to the lens zonules resulting in a greater likelihood of frictional contact. The root-to-spur distance was measured as follows (figure 2.3): the calliper tool was used to construct a straight line joining the nasal and temporal scleral spur. The posterior iris pigment epithelium is well defined on AS-OCT as a line of hyper-reflectivity and the iris root insertion was defined as the point where this line terminates peripherally. A second line was then constructed starting at the iris root insertion running parallel with the first line. The root-to-spur distance was deemed to be the perpendicular distance between these 2 parallel lines.

#### **2.2.4.3 Statistical analysis**

The means of the above parameters were compared between cases and controls using a paired Student t-test. Receiver operating characteristic (ROC) analysis was used to assess the ability of each of the measured parameters in distinguishing PDS/PG cases

from controls. Comparison of the areas under the ROC curves (AUC) was calculated according to DeLong et al. (94). Correlations between iris curvature and age were explored using Pearson's correlation coefficient. A previously published cut-off(86) was tested in the present cohort. Analyses were performed using MedCalc Version 11.3.1.0 and Prism version 6.0c for Mac OS X, GraphPad Software, La Jolla California USA, [www.graphpad.com](http://www.graphpad.com). A *P*-value < 0.05 was deemed significant.

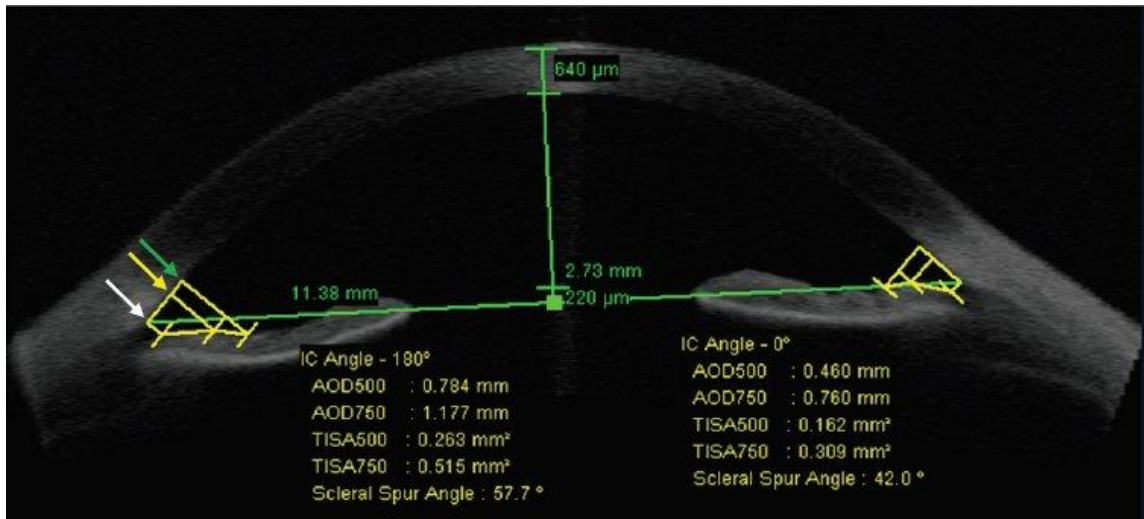


**Figure 2.2** Example AS-OCT screenshot illustrating semi-automated measurements. White arrow denotes scleral spur. Yellow and green arrows denote points 500  $\mu\text{m}$  and 750  $\mu\text{m}$  respectively anterior to scleral spur along corneal endothelium.

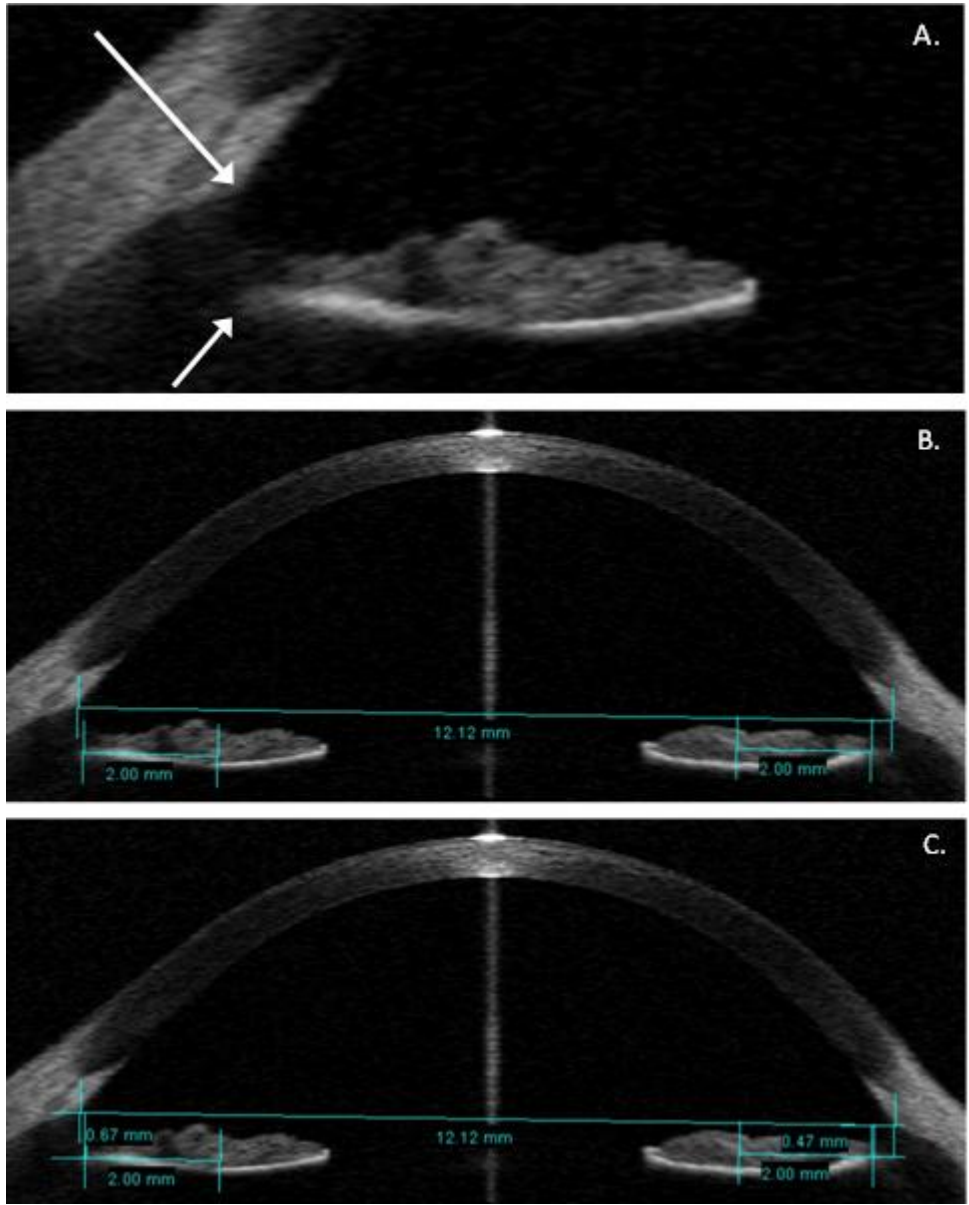


**Figure 2.3** Determination of posterior displacement of iris root from scleral spur. A. Identification of scleral spur (long arrow) and iris root (short arrow). B. Construction of horizontal line joining scleral spurs and parallel line originating at iris root. C. Displacement deemed to be perpendicular distance between horizontal lines measured at iris root. In this example displacement is 0.67 mm in the temporal quadrant and 0.47 in the nasal quadrant.

## 2.3 Results

### 2.3.1 Between- and within-observer agreement

Images from one subject were of insufficient quality to confidently measure iris curvature and these were excluded from the analysis. Tables 2.1 and 2.2 show results of within- and between-observer agreement for classifying temporal quadrant images as convex, flat or concave. Results for nasal quadrant were similar (data not shown).

		Observer 1(A)		
		Concave	Flat	Convex
Observer 1(B)	concave	20	1	0
	flat	1	11	0
	convex	0	1	15
<b>Weighted kappa statistic = 0.96</b>				

**Table 2.1** Within-observer agreement for classifying temporal quadrant

		Observer 1		
		Concave	Flat	Convex
Observer 2	concave	14	1	0
	flat	4	13	0
	convex	0	1	17
<b>Weighted kappa statistic = 0.89</b>				

**Table 2.2** Between-observer agreement for classifying temporal quadrant

Bland-Altman plots showing within- and between-observer agreement are shown in figures 2.4 and 2.5 respectively. Neither of these plots showed any relationship between the measurement difference and the magnitude of the measurement and it was therefore appropriate to calculate 95% limits of agreement (LoA) which are shown in table 2.3.

Difference	Bias (mm)	95% LoA (mm)
Between-observer temporal quadrant	-0.008	-0.056 to 0.040
Between-observer nasal quadrant	-0.009	-0.065 to 0.048
Within-observer temporal quadrant	0.005	-0.057 to 0.067
Within-observer nasal quadrant	-0.003	-0.039 to 0.034

**Table 2.3** Bias and 95% limits of agreement (LoA) for between- and within-observer difference in estimate of iris concavity

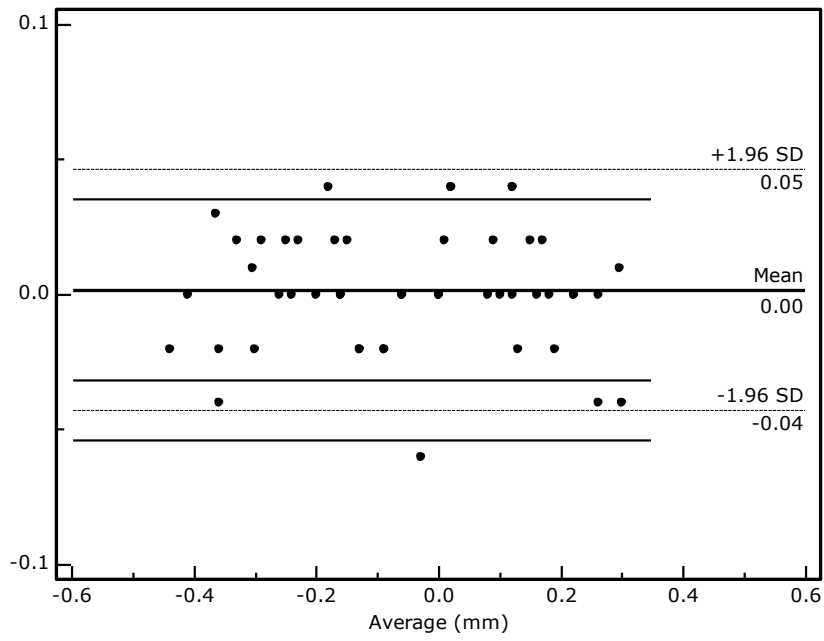


**Figure 2.4** Bland-Altman plot to show within-observer agreement in the temporal quadrant

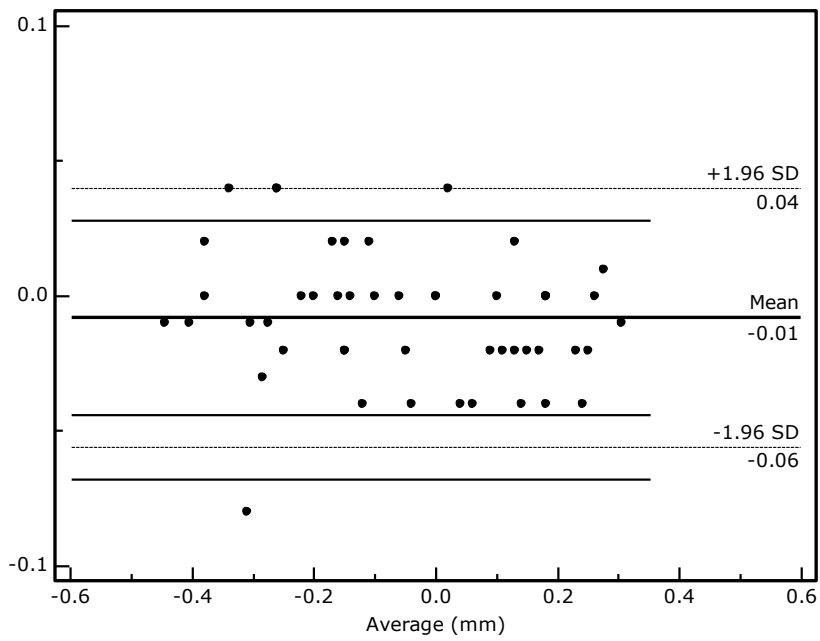


**Figure 2.5** Bland-Altman plot to show between-observer agreement in the temporal quadrant

### 2.3.2 Anterior segment imaging case-control study

Fifty eyes of 50 patients were imaged from each of the case and control group. The accommodative scan was not available for 1 PDS case. The posterior pigment epithelium was poorly visible in 1 control patient and the scleral spur could not be identified in another control patient.

The mean subject age was 41.9 years in both the case and the control group. The mean SE was -2.1 D in the case group and -2.25 D in the control group; this difference was not statistically significant ( $P = 0.36$ ). There was no statistically significant difference in spur-to-spur distance between the 2 groups. The mean anterior lens movement on accommodation was 76.1  $\mu\text{m}$  in the PDS group compared to 90.8  $\mu\text{m}$  in the control group ( $P = 0.143$ , paired Student t-test). Statistically significant differences between cases and controls were seen for all other AS-OCT parameters (table 2.4), data not shown for AOD750 and TISA750 but differences between cases and controls were similar to AOD500 and TISA500 respectively). The area under the ROC curve for these parameters is shown in table 2.5 (data not shown for AOD750 and TISA750 but AUC was similar to AOD500 and TISA500 respectively).

Parameter	Case (SD)	Control (SD)	Mean difference	Test statistic t	Two-tailed probability
Mean AC depth NA/mm	3.17(0.39)	2.94(0.51)	-0.23	-2.95	0.0049
Mean AC depth A/mm	3.07(0.33)	2.89(0.30)	-0.18	-3.09	0.0034
Mean lens vault NA/ $\mu$ m	-5.0(308.1)	176.2(252.6)	181.2	3.53	0.0009
Mean lens vault A/ $\mu$ m	77.96(244.17)	276.73(235.20)	198.8	4.320	0.0001
Mean AOD500 NA/mm	0.831(0.440)	0.485(0.233)	-0.346	-4.89	<0.0001
Mean AOD500 A/mm	0.823(0.426)	0.494(0.238)	-0.329	-4.756	<0.0001
Mean TISA500 NA/mm <sup>2</sup>	0.296(0.174)	0.170(0.091)	-0.127	-4.613	<0.0001
Mean TISA500 A/mm <sup>2</sup>	0.282(0.149)	0.494(0.238)	-0.212	5.398	<0.0001
Mean angle NA/ $^{\circ}$	54.5 (14.6)	41.3(13.3)	-13.2	-4.500	<0.0001
Mean angle A/ $^{\circ}$	53.1(16.4)	41.9(13.7)	-11.3	-3.475	0.0011
Mean spur-to-root distance NA/mm	0.570(0.135)	0.481(0.164)	-0.089	-2.788	0.0076
Mean spur-to-root distance A/mm	0.530(0.116)	0.416(0.164)	-0.114	-3.987	0.0003
Mean iris curvature NA/mm	-0.029(0.223)	0.149(0.119)	0.177	5.185	<0.0001
Mean iris curvature A/mm	-0.070(0.236)	0.113(0.415)	0.183	2.573	0.0133

**Table 2.4** Summary of anterior segment optical coherence tomography parameters in cases and controls. NA = non-accommodating, A = accommodating, AC = anterior chamber, AOD = angle-opening distance; TISA = trabecular-iris space area. In the case group, N=50 for non-accommodative measurements and N=49 for accommodative measurements. In the control group, N=49 for both accommodative and non-accommodative measurements.

Parameter	AUC	95% CI	<i>P value</i> *	Criterion	Sensitivity (%) at 90% specificity
AC depth NA/mm	0.613	0.511-0.709	0.0453	>2.68	28.0
AC depth A/mm	0.649	0.546-0.742	0.0072	>3.09	26.5
Lens vault NA/ $\mu$ m	0.675	0.574-0.765	0.0011	$\leq$ 30	30.0
Lens vault A/ $\mu$ m	0.742	0.645-0.825	0.0001	$\leq$ 100	22.5
AOD500 NA/mm	0.762	0.666- 0.841	0.0001	>0.6	45.0
AOD500 A/mm	0.743	0.645-0.826	0.0001	>0.637	32.7
TISA500 NA/mm	0.756	0.660-0.837	0.0001	>0.201	45.0
TISA500 A/mm	0.729	0.630-0.813	0.0001	>0.203	31.6
Angle NA/ $^{\circ}$	0.760	0.664-0.840	0.0001	>50.1	46.0
Angle A/ $^{\circ}$	0.724	0.625-0.809	0.0001	>49.3	30.6
Spur-to-iris root distance NA/mm	0.648	0.545-0.741	0.0085	>0.43	12.0
Spur-to-iris root distance A/mm	0.723	0.623-0.808	0.0001	>0.42	10.2
Iris curvature NA/mm	0.817	0.727-0.888	0.0001	$\leq$ 0.08	58.4
Iris curvature A/mm	0.700	0.599-0.789	0.0001	$\leq$ 0	30.6

**Table 2.5** Receiver Operating Characteristic analyses for anterior segment optical coherence tomography parameters in cases and controls. NA = non-accommodating, A = accommodating, AC = anterior chamber, AOD = angle-opening distance; TISA = trabecular-iris space area AUC = area under the curve. \*Testing the hypothesis that AUC = 0.5

The best performing parameter at distinguishing between cases and controls was iris curvature in non-accommodating eyes. The area under the ROC curve was 0.82 (95% CI 0.73-0.89,  $P = 0.0001$ ) and this area was significantly greater than the areas under the curve for non-accommodating AC depth, accommodating AC depth and accommodating iris curvature ( $P = 0.001, 0.004$  and  $0.01$  respectively). Comparison of the ROC curve for non-accommodating iris curvature with those for accommodating iris curvature and anterior chamber angle can be seen in figure 2.6 and comparison with LV and root-to-spur distance can be seen in figure 2.7.

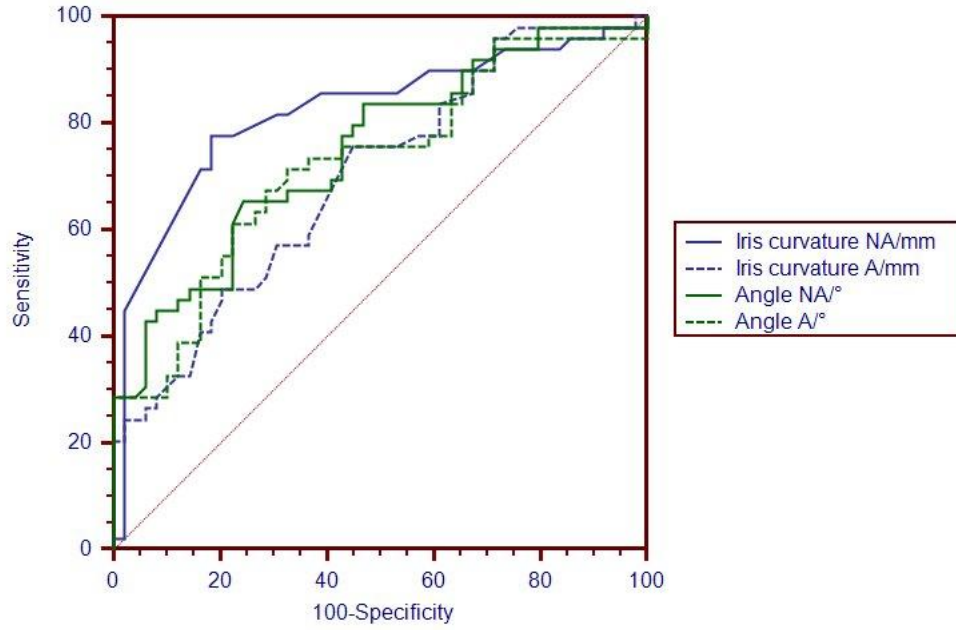


**Figure 2.6** Receiver operating characteristic curves for iris curvature and anterior chamber angle. NA = non-accommodating, A = accommodating.

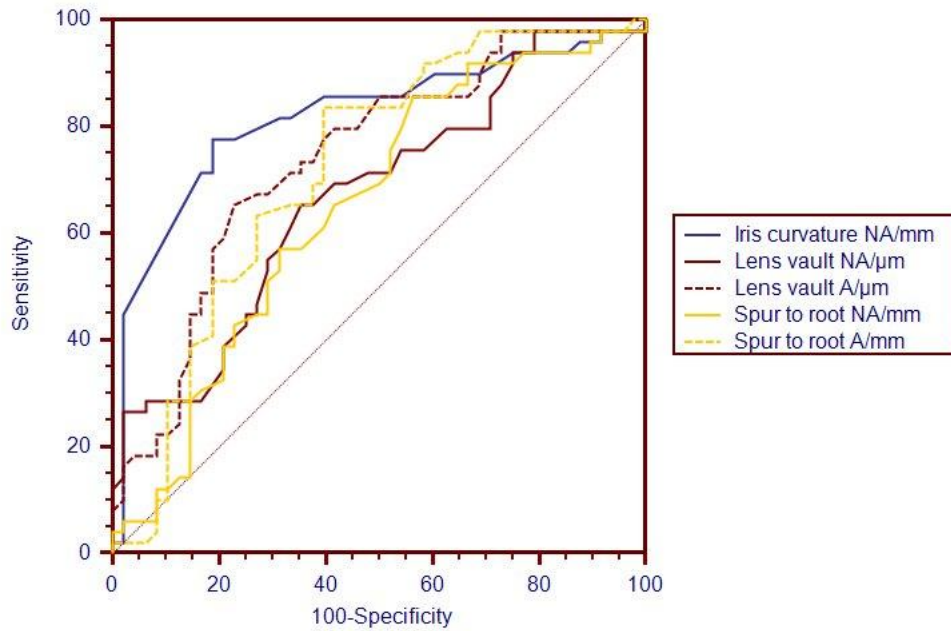


**Figure 2.7** Receiver operating characteristic curves for iris curvature, lens vault and spur-to-root distance. NA = non-accommodating, A = accommodating.

AUC was in fact similar for all parameters and a correlation matrix was constructed to investigate the relationship between the AS-OCT parameters (tables 2.6 and 2.7). The angle-derived parameters (angle, AOD500/750 and TISA500/750) were all strongly correlated with each other ( $r = 0.89 - 0.99$ ), LV and ACD were moderately correlated with angle-derived parameters ( $r = 0.36 - 0.60$ ) whilst iris curvature was the most weakly correlated ( $r = 0.26 - 0.42$ ). A scatter plot of age against accommodative iris curvature is shown in figure 2.8. Regression analysis was performed for iris curvature on age (table 2.8). Robust regression with outlier exclusion (95) revealed that age accounts for a significant amount of variation in accommodative iris curvature in both cohorts. The association remained significant but was weaker for non-accommodative iris curvature. A previously published cut-off to distinguish between PDS/PG and control eyes of  $53^\circ$  angle width, derived from UBM measurements, (86) was tested in our cohort and correctly classified 27 out of 50 cases of PDS/PG (54% sensitivity) and 38 out of 50 controls (76% specificity).

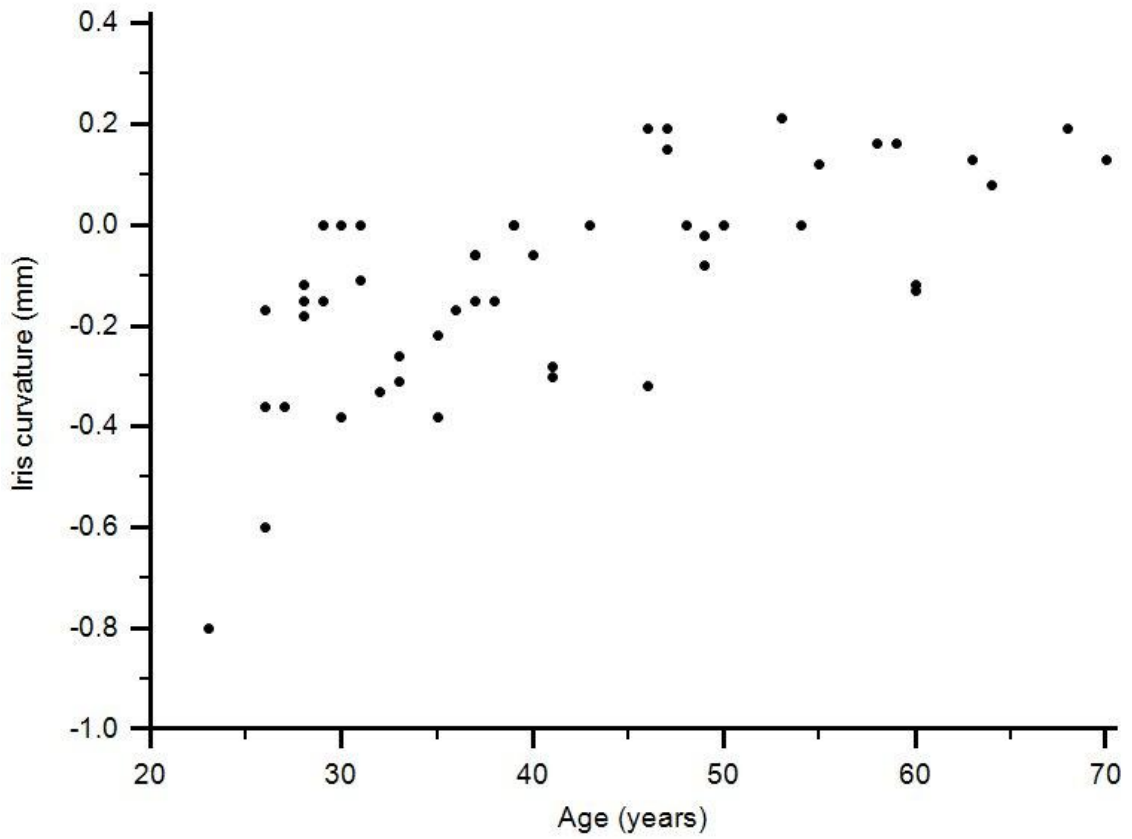


**Figure 2.8** Scatterplot of accommodative iris curvature against age in PDS/PG cohort

Group	Outlier exclusion	r <sup>2</sup>	P value
PDS/PG NA	no	0.25	0.002
PDS/PG NA	yes	0.16	0.003
PDS/PG A	no	0.29	<0.0001
PDS/PG A	yes	0.44	<0.0001
Controls NA	no	0.09	0.038
Controls NA	yes	0.10	0.026
Controls A	no	0.07	0.065
Controls A	yes	0.51	<0.0001

**Table 2.8** Results of robust regression of iris curvature on age with and without outlier exclusion. A = accommodating, NA = non-accommodating. PDS/PG = pigment dispersion syndrome/pigmentary glaucoma

	AC depth/mm	Lens vault / $\mu\text{m}$	AOD500/mm	AOD750/mm	TISA500/mm	TISA750/mm	Angle/ $^{\circ}$	Spur-to-iris root distance /mm	Iris curvature
AC depth/mm	1.0	-0.40	0.40	0.46	0.36	0.60	0.41	0.26	-0.37
Lens vault / $\mu\text{m}$	-0.40	1.0	-0.51	-0.51	-0.44	-0.54	-0.54	-0.25	0.25
AOD500/mm	0.40	-0.51	1.0	0.95	0.96	0.99	0.96	0.70	-0.33
AOD750/mm	0.46	-0.51	0.95	1.0	0.89	0.95	0.93	0.68	-0.38
TISA500 /mm	0.36	-0.44	0.96	0.89	1.0	0.98	0.89	0.74	-0.26
TISA750	0.60	-0.54	0.99	0.95	0.98	1.0	0.99	0.78	-0.42
Angle/ $^{\circ}$	0.41	-0.54	0.96	0.93	0.89	0.99	1.0	0.68	-0.37
Spur-to-iris root distance/mm	0.26	-0.25	0.70	0.68	0.74	0.78	0.68	1.0	-0.15
Iris curvature/mm	-0.37	0.25	-0.33	-0.38	-0.26	-0.42	-0.37	-0.15	1.0

**Table 2.6** Correlation matrix to show correlation between non-accommodating anterior segment optical coherence tomography parameters. All values represent Pearson correlation coefficient, apart from correlations between TISA750 and other parameters for which Spearman's rank correlation is shown. ACD, anterior chamber depth; AOD, angle-opening distance; TISA, trabecular-iris space area.

	AC depth/mm	Lens vault / $\mu\text{m}$	AOD500/mm	AOD750/mm	TISA500/mm	TISA750/mm	Angle/ $^{\circ}$	Spur-to-iris root distance /mm	Iris curvature
AC depth/mm	1.0	-0.16	0.25	0.23	0.26	0.63	0.22	0.1	-0.19
Lens vault / $\mu\text{m}$	-0.16	1.0	-0.58	-0.63	-0.53	-0.61	-0.66	-0.34	0.14
AOD500/mm	0.25	-0.58	1.0	0.97	0.97	0.99	0.89	0.58	-0.38
AOD750/mm	0.23	-0.63	0.97	1.0	0.94	0.97	0.89	0.58	-0.40
TISA500 /mm	0.26	-0.53	0.97	0.94	1.0	0.99	0.86	0.59	-0.33
TISA750	0.63	-0.61	0.99	0.97	0.99	1.0	0.96	0.65	-0.56
Angle/ $^{\circ}$	0.22	-0.66	0.89	0.89	0.86	0.96	1.0	0.53	-0.31
Spur-to-iris root distance/mm	0.1	-0.34	0.58	0.58	0.59	0.65	0.53	1.0	-0.11
Iris curvature/mm	-0.19	0.14	-0.38	-0.40	-0.33	-0.56	-0.31	-0.11	1.0

**Table 2.7** Correlation matrix to show correlation between accommodating anterior segment optical coherence tomography (AS-OCT) parameters. All values represent Pearson correlation coefficient, apart from correlations between TISA750 and other parameters for which Spearman's rank correlation is shown. ACD, anterior chamber depth; AOD, angle-opening distance; TISA, trabecular-iris space area

## 2.4 Discussion

The results of the agreement study indicated that there was very good within- and between-observer agreement in classifying iris curvature as convex, flat or concave. Reassuringly there were no cases where an image was classified as showing a concave profile by one observer but convex by another; this is noteworthy because the iris curvature is not uniform throughout its length and a particular segment of the iris may appear convex whilst a different section appears flat or concave. Agreement with regard to quantification of iris curvature was deemed reasonable as 95% LoA between -0.06 and 0.04 mm represent a relatively narrow interval when considered in the context of the normal range of iris curvature measurements. The method described therefore appeared to be reliable in quantifying iris curvature from AS-OCT images. Establishing that there was satisfactory agreement using AS-OCT in the measurement of iris curvature was important prior to planning the case-control section of this study. The current study focused on agreement on iris curvature measurements on individual AS-OCT images. A limitation of the study was that variability of iris curvature over time for an individual patient was not addressed. Future work should ideally look at repeat AS-OCT images taken several hours and several days apart in order to determine to what extent iris curvature measurements may fluctuate over time.

There is only one previously published study investigating between- and within-observer agreement on measurements of iris curvature: Balidis et al. (89) used UBM to derive a metric known as the 'R/D score' to represent iris curvature; their method

relied on identifying the outermost point of iridolenticular contact, referred to as point A, constructing a line from this point to the peripheral end of the iris pigment epithelium and measuring the angle between this line and a line tangent to the lens also originating from point A, an angle known as the reference angle, R. The point of maximum iris displacement was then identified, either anteriorly or posteriorly, usually in the mid-peripheral iris and a 3<sup>rd</sup> line was then constructed through this point also originating from point A. The angle between this line and the line tangent to the lens was known as the displacement angle, D. The authors stated that in an eye with a flat iris configuration, the ratio R/D will equal 1 and that the greater the ratio, the greater the concavity of the iris. Although there was substantial agreement between two of the observers there was only moderate agreement with a 3<sup>rd</sup> observer. The authors concluded that assessments should preferably be made by the same observer when using this technique. One of the strengths of their method is that only the peripheral segment of the iris not in contact with lens is used for the assessment of curvature which produces a measurement of iris curvature less dependent on the relative position of the lens. Inspection of the AS-OCT images suggests that the central iris may, to some extent, be conforming to the anterior lens surface. It might be preferable to exclude the segment of iris in direct contact with the lens when measuring iris curvature, as is the case with Balidis' method, to avoid the effect of relative lens position on iris curvature. It would not, however, be possible to apply this method to determine iris curvature on images from the present study as irido-lenticular contact is not well delineated on AS-OCT. Instead the method used was that described by Carassa

et al. (81) which assesses curvature along the whole length of the iris from the periphery to the pupil edge.

Accommodation was stimulated by de-focusing an internal fixation target and relied upon the participant reporting blurring of the target, an approach which differed from the method used by Liu et al. (41) who held a -3.0 D and -6.0 D lens in front of the eye to stimulate accommodation. However, using the internal fixation target allowed the subject to accommodate maximally thereby increasing the study's ability to detect accommodation-induced changes.

The method used for assessing iris root to scleral spur distance along the antero-posterior axis had the advantage of better reflecting the proximity of the posterior iris pigment epithelium to the lens zonules and may therefore be a more relevant metric to the pathophysiology of pigment dispersion. The method used in the present study differed to that used by Sokol et al. (85) which directly measured the distance between the 2 landmarks and is usually an oblique measurement.

This is the first report of AS-OCT parameters in PDS/PG and age-, sex- and refraction-matched controls. All parameters studied were significantly different between groups and the parameter that best distinguished between groups was iris curvature in non-accommodating eyes. Campbell (38) was the first to propose that in PDS the posteriorly bowed iris led to frictional contact between packets of anterior zonular

fibres and the posterior pigment epithelium resulting in pigment dispersion. The concept of the 'reverse pupillary block' mechanism was introduced by Karickhoff (39), who proposed that excessive irido-lenticular contact causes the iris to act like a flap valve permitting unidirectional flow of aqueous from the posterior to the anterior chamber, maintaining the posterior bowing.

More recently, Dorairaj et al. (44) studied the response of the iris to accommodation in eyes with narrow angles, PDS and controls (age and refraction matched to the PDS group) over time. The drop in curvature (i.e. change from a more convex to a more concave configuration) immediately after accommodation was greatest in the PDS group. Average curvature reduced from  $60 \pm 79 \mu\text{m}$  (mean  $\pm$  standard error of the mean (SEM) prior to accommodation to  $-3 \pm 83 \mu\text{m}$  immediately after, although this change was not statistically significant. Continued imaging of the iris over the following 3 minutes revealed that the concavity was not maintained and in fact reverted to a more convex configuration than was present at baseline ( $146 \pm 94 \mu\text{m}$ ). The curvature value at this point was significantly different to both baseline iris curvature and curvature immediately after accommodation. Furthermore, the subsequent reversal in iris curvature was faster in the PDS group than in the other 2 groups from which the authors inferred that the chronic posterior bowing of the iris in PDS is not the result of slow recovery from accommodation. In the present study the area under the ROC curve for baseline iris curvature was significantly greater than for accommodating iris curvature. Baseline iris curvature may therefore play a greater part in frictional irido-

lenticular contact than accommodation-induced changes in curvature. Prospective studies investigating the natural history of PDS should carefully assess baseline curvature in order to explore correlation with subsequent severity of the clinical phenotype and the risk of developing PG.

The present study found iris curvature best distinguished PDS/PG cases from controls. In contrast, the UBM-based study by Mora et al. reported irido-corneal angle in near vision to be the best performing parameter. AS-OCT imaging does not require contact or a supine subject position and it is possible the magnitude of concavity detected by UBM is reduced through prevention of blinking. A limitation of the study is that the observer was not blinded to whether the images were from cases or controls. If the study were to be repeated it would be important to blind the observer in order to eliminate this source of potential bias.

Age was moderately associated with accommodative iris curvature in both cohorts. The slope in figure 2.8 can be seen to level off after the age of 50 years and this may reflect loss of accommodation seen in presbyopia after this age. In retrospect, it would have been useful to record the amplitude of accommodation and plotted these data against age in order to compare the curve with that from figure 2.8. Accommodation is associated with anterior movement of the lens and pupillary constriction. The anterior lens movement was likely to account for some of the concavity detected in this study as the central iris is pushed anteriorly by the lens and conforms to its contour whilst

the peripheral iris remains fixed giving rise to a concave configuration overall. Anterior lens movement reduces with age and this may explain the reduction in concavity in older patients. A weaker association with age was also detected with non-accommodative iris curvature. Increasing age is associated with pupillary miosis and it may be the case that a smaller pupil stretches the iris resulting in a flatter iris configuration. The reduction in concavity with age may mean that older patients with PDS/PG will be less likely to benefit from LPI, which aims to reverse iris concavity; this lack of benefit is compounded by the fact that the TM has had a longer time to become overloaded with pigment in older patients and there may be a greater degree of TM dysfunction. Gandolfi et al. (35) reported that in older, normotensive PDS patients, LPI was less effective at preventing a subsequent IOP rise. However, Ritch argues for the existence of a 'burn-out' phase in older subjects (23) with PDS and this may mean there is less need for LPI in older patients. Whilst there appears to be a role for LPI in reducing/reversing iris concavity (81, 96), studies have not demonstrated that this necessarily translates into a reduction in the risk of PG (55, 56, 97). The data from this study suggest that excessive baseline iris concavity is a key feature in the pathophysiology of PDS. There is a need for further studies in PDS patients to clarify the role of LPI in reducing pigment dispersion and the subsequent risk of raised IOP and PG.

<b>3</b>	<b>IRIS CONCAVITY, CORNEAL BIOMECHANICS AND ASSOCIATIONS WITH OCULAR BIOMETRY IN A COHORT OF 10-12 YEAR OLD UK SCHOOL BOYS: A LONGITUDINAL STUDY</b>	
3.1	Introduction	74
3.1.1	Iris concavity in PDS and non-PDS eyes	74
3.1.2	Myopia in school age children	74
3.1.3	Corneal biomechanical parameters and axial length	75
3.1.4	Additional data collection	76
3.2	Methods	77
3.2.1	Eligibility and recruitment	77
3.2.2	Examination and imaging	78
3.2.2.1	Visual acuity	
3.2.2.2	Refractive error	
3.2.2.3	Ocular biometry	
3.2.2.4	Corneal biomechanical properties	
3.2.2.5	Anterior segment optical coherence tomography	
3.2.2.5.1	Image processing	
3.2.2.6	Non-ocular data collection (follow up study only)	
3.2.2.7	Statistical analysis	
3.3	Results	82
3.3.1	Baseline study (December 2009)	82
3.3.2	Follow up study (December 2011)	88



### **3.1 Introduction**

#### **3.1.1 Iris concavity in PDS and non-PDS eyes**

The role of iris concavity in the pathogenesis of PDS has been discussed in section 1.2.4. In brief, excessive irido-lenticular contact causes the iris to act like a flap valve, permitting unidirectional flow of aqueous from the posterior to the anterior chamber, potentiating a concave iris configuration (39). Iris concavity predisposes to frictional contact between packets of anterior zonular fibres and the posterior pigment epithelium resulted in pigment dispersion (38). The iris becomes more concave (or less convex) with accommodation but this may be a transient phenomenon, reverting back to the original configuration despite continued accommodative effort (44).

Physiological iris concavity has also been observed in normal subjects in the resting state (81) and following exercise (98) but its prevalence during eye growth in normal subjects is not well known. The tendency to iris concavity is more pronounced in myopic eyes (98) but its relationship with other ocular biometric parameters has not been studied to date.

#### **3.1.2 Myopia in school age children**

The incidence of myopia is increasing and several large studies from the USA and the Far East have provided data in school age children. The Singapore Cohort study Of the

Risk factors for Myopia (SCORM) (99) found that 34% of 7-9 year olds were myopic at baseline, whilst a large US study reported that only 10% of a slightly older cohort (mean age 10 years) were myopic (100). There are relatively little contemporary data on the UK prevalence/incidence of myopia in young people. Williams et al. (101) reported a prevalence of spherical equivalent (SE)  $< -1.5$  diopters of 1.5% in 7 year olds from auto-refraction data in a cohort of children in the Avon area, South West England; this figure increased to 3.6% when the same cohort was re-examined 3 years later.

Axial length (AL) is an easily measurable quantitative trait considered to be a component of refractive error (102). A study in Japanese 7-13 year old myopes demonstrated the ability of the IOLMaster (Carl Zeiss Meditec, Dublin, CA) to provide highly repeatable AL measurements in this age group (103).

### **3.1.3 Corneal biomechanical parameters and axial length**

There is some evidence that corneal biomechanical properties may be related to axial biometry. Corneal hysteresis (CH) is a parameter considered to represent the dampening or viscoelastic properties of the cornea (104). Song et al. (105) studied 1153 secondary school children in rural China and found CH to be lower in eyes with longer AL. However, a cross sectional study of 271 Singaporean children (106), reporting on CH and the 'corneal resistance factor' (CRF), did not show any association with refractive error or axial length.

### **3.1.4 Additional data collection**

The present study provided the opportunity to collect non-ocular data which had potential relevance to the development of myopia.

Birth weight has been associated with refractive error (107) and AL (108). There is evidence that control of eye growth differs between men and women (109). By collecting data on digit ratio, a putative marker for pre-natal androgen exposure (110-112), whether eye growth differs between boys with greater or lesser exposure to maternal levels of androgens was investigated. Bio-impedance analysis measures body composition, in particular the percentage of body fat. Height, weight, percentage body fat and waist circumference provide an indication of general metabolic status and may reflect long-term insulin levels. Epidemiological evidence implicates a role for chronic hyperinsulinaemia in juvenile-onset myopia (113). The above easily measured parameters were therefore investigated in this cohort.

### **3.1.5 Aims**

Prior to the advent of AS-OCT, imaging of the anterior segment in paediatric patients had been difficult owing to the relative invasive nature of UBM and as a result there are no normative data on iris curvature in paediatric populations.

The primary aims of the study were:

1. To estimate the prevalence of iris concavity in 10-12 year old UK school boys at baseline and during accommodation
2. To explore relationships between iris curvature and axial length/refractive error and between corneal biomechanical parameters and anterior segment/axial biometric measurements
3. To investigate changes in anterior segment/axial biometric and corneal biomechanical parameters over a 2-year period

The secondary aim of the study was to explore the influence of the following non-ocular parameters: birth weight, digit ratio, height, weight, waist circumference and bio-impedance on ocular biometric parameters.

## **3.2 Methods**

### **3.2.1 Eligibility and recruitment**

All students in 2 consecutive year groups at City of London School, an independent boys' school, were considered eligible for enrolment. The 10-12 year old age group was selected as participants were sufficiently mature to be fully co-operative with data collection. The study was approved by the Moorfields and Whittington Research Ethics

Committee and adhered to the tenets of the Declaration of Helsinki.

Following logistic arrangements with the school and an introductory lecture to the students, information sheets and consent forms were sent to all of the students and their parents.

One hundred and forty boys were invited to take part in the baseline study (December 2009). One eye of each participant was pre-selected at random using a web-based research randomization tool (114) and this eye was designated as the study eye.

Participants from the baseline study were invited to take part in a follow up study 2 years later. The methodology was identical for the follow up study with the additional collection of non-ocular data.

### **3.2.2 Examination and imaging**

#### **3.2.2.1 Visual Acuity**

Distance visual acuity was measured in each eye at 4 metres with their current spectacles if available (LogMAR Acuity Charts; Keeler, Ltd., Windsor, UK). Pinhole visual acuity was also measured if the initial visual acuity was logMAR 0.2 (Snellen equivalent 6/9.5) or worse.

### **3.2.2.2 Assessment of Ocular Refraction**

Non-cycloplegic ocular refraction was measured using an autorefractor (Nvision-K5001; Shin-Nippon Commerce Inc., Tokyo, Japan). Manual focimetry was performed where spectacles were worn.

### **3.2.2.3 Ocular Biometry**

The AL of the study eye was measured using laser interferometry (IOLMaster, Carl Zeiss Meditec Ltd, Welwyn Garden City, UK). The subject was asked to focus on the internal fixation target and the reflection of the alignment light was centred within the cross hairs on screen. A minimum of 5 measurements were taken and checked for consistency, paying attention to any software notifications indicating measurements required evaluation. Only measurements within 0.1 mm of each other were included in calculating mean AL. Readings with a signal-to-noise ratio < 2.0 were excluded.

### **3.2.2.4 Corneal biomechanical properties**

The Ocular Response Analyzer (ORA, Reichert Inc, Depew, New York, USA) measures the corneal response to indentation by a rapid air pulse and derives values for CH and CRF (104, 115). The ORA device also uses corneal biomechanical data to generate corneal-compensated IOP (cciOP), a measure of IOP that is less affected by corneal

properties (116). The ORA device was used to obtain at least 3 good quality measurements as determined by visual inspection of the waveform looking for sharp, well-defined raw signal peaks. ORA software generates a waveform score reflecting measurement quality. Only measurements with a waveform score  $\geq 4$  were included in the analysis.

### **3.2.2.5 Anterior Segment Optical Coherence Tomography**

Images of the anterior segment were obtained using the Visante AS-OCT (Carl-Zeiss-Meditec, Dublin, California, USA). The device uses an internal fixation device with the apparent viewing distance set to infinity by the instrument optics when the subject's refraction is entered. The operator can stimulate accommodation by adjusting the focus of the internal fixation target. AS-OCT imaging of the horizontal and nasal quadrant was performed at near and distance fixation under dim illumination as described in section 2.2.1.

#### **3.2.2.5.1 Image processing**

The AS-OCT images were analysed using the device's Visante 3.0 software by one investigator (AS); both accommodative and non-accommodative images were analysed. The following parameters were measured as described in section 2.2.4.2: central corneal thickness (CCT), anterior chamber depth (ACD), lens vault (LV), angle

opening distances at 500 and 750 microns from scleral spur (AOD500 and AOD750) and trabecular-iris space area at 500 and 750 microns from the scleral spur (TISA500 and TISA750).

Between-observer agreement of semi-automated anterior segment parameters was assessed by randomly selecting 20 subjects for assessment by an experienced investigator (Miss Sancy Low).

#### **3.2.2.6 Non-ocular data collection (follow up study only)**

Waist circumference was measured at the mid-point between the lower border of the rib cage and the iliac crest using a soft non-stretchable tape to the nearest 0.1 cm .

Standing height was measured using a stadiometer also to the nearest 0.1 cm. Weight and percentage body fat (derived from bio-impedance) were determined using the Tanita BC543 Body Composition Analyser (Tanita Corp., Tokyo, Japan). The subject was instructed to stand on the device after removing shoes and socks. Age and height were entered when prompted. Weight and percentage body fat were returned on a digital display.

Hand scans were taken using an Epson Perfection 1650 scanner. Right hand digit ratio was measured using Image J version 1.45s to measure the lengths of the index and ring fingers from the middle of the basal crease to the tip of the finger in pixels. Digit ratio

was obtained by dividing the length of the right hand index finger by the length of the right hand ring finger.

### **3.2.2.7 Statistical analysis**

To determine which variables were predictive of iris curvature, multiple regression analysis was performed using 6 variables (spur-to-spur distance, ACD, LV, mean scleral spur angle, SE, and AL). Linear regression analysis was used to investigate the relationship between AL/spur-to-spur distance and CH/CRF (dependent variable). Bland-Altman plots were constructed to assess between-observer agreement of AS-OCT parameters; the difference between observers and the magnitude of the parameter being measured was assessed for trend by linear regression analysis. 95 % limits of agreement (LoA) were calculated as appropriate. The relationship between ocular and non-ocular parameters was explored. Paired student t-test was used to compare measurements between the 2 time-points. Analyses were performed using Prism version 6.0c for Mac OS X, GraphPad Software, La Jolla California USA, [www.graphpad.com](http://www.graphpad.com) and MedCalc for Windows, version 12.2.1.0 (MedCalc Software, Mariakerke, Belgium).

### **3.3 Results**

#### **3.3.1 Baseline study (December 2009)**

One hundred and forty boys were invited to take part of whom 103 (73.6%) returned registration forms indicating a willingness to participate and 96 (68.6%) attended on the day. Mean (SD) age was 11.51 (0.5) years. Data on racial ancestry was not formally collected, although the approximate proportions were as follows: 79% Caucasian, 8% Indian, 5% Chinese, 5% mixed and 2% Japanese. Seven participants exited the testing circuit early in error and did not attend the AS-OCT station. The Visante image in accommodation from one participant showed marked ghosting and was excluded from the analysis. Seventy-nine subjects had at least 1 set of adequate quality ORA measurements.

Summary data for age, AL, SE, CH, CRF and IOPcc are shown in table 3.1. All parameters were distributed normally as determined by the Kolmogorov-Smirnov test except for SE. AS-OCT measurements at distance fixation and accommodation are shown in table 3.2. Figure 3.1 shows an example of an increase in iris concavity seen on accommodation.

Parameter	Mean	SD
Spherical equivalent (dioptres)	-0.33	1.7
Axial length (mm)	23.80	0.95
Corneal hysteresis (mmHg)	11.8	1.7
Corneal resistance factor (mmHg)	11.9	1.8
Corneal-compensated IOP (mmHg)	15.5	4.3

**Table 3.1** Baseline ocular characteristics of 2009 schoolboy cohort

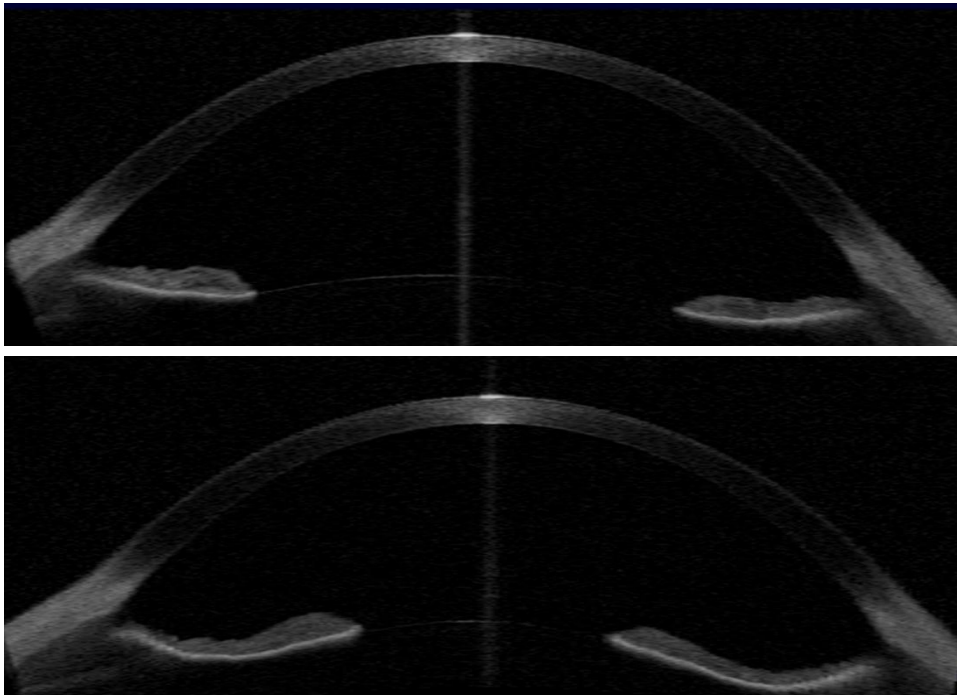


**Figure 3.1** Example AS-OCT image showing a slightly concave iris curvature on distance fixation (upper image) with a marked increase in iris concavity in the same eye on near fixation (lower picture)

Parameter	Non-accommodating (n=89)		Accommodating (n=88)		P*
	Mean	SD	Mean	SD	
Iris curvature (mm)	-0.002	0.12	-0.21	0.18	<0.0001
CCT (μm)	531.8	34.0	530.7	36.4	0.52
ACD (mm)	3.34	0.27	3.11	0.31	<0.0001
Lens vault (μm)	-171.5	190.9	46.9	259.0	<0.0001
Temporal AOD 500(μm)	851.0	312.1	933.0	331.6	0.0034
Temporal TISA 500(mm <sup>2</sup> )	0.303	0.117	0.321	0.124	0.24
Temporal scleral spur angle (°)	56.9	10.4	59.5	9.3	0.0023
Nasal AOD 500(μm)	806.6	295.4	895.7	334.3	0.0008
Nasal TISA 500(mm <sup>2</sup> )	0.275	0.099	0.294	0.108	0.03
Nasal scleral spur angle (°)	56.3	9.8	58.8	9.9	0.0043
Spur to spur distance (mm)	11.99	0.47	11.96	0.48	0.69

**Table 3.2** Summary for AS-OCT parameters in 2009 schoolboy cohort. \*Paired *t*-test. CCT, central corneal thickness; ACD, anterior chamber depth; AOD, angle-opening distance; TISA, trabecular-iris space area

The prevalence of iris concavity in the non-accommodative state was 24% and on accommodation this increased to 65%. Although not formally recorded, the accommodative amplitude as measured by the AS-OCT was approximately 10 D for this cohort. Multiple regression analysis revealed the only variable significantly associated with non-accommodating iris curvature was lens vault ( $R^2 = 0.23$ ,  $P = 0.028$ ). A scatterplot of lens vault against non-accommodating iris curvature is shown in figure 3.2. Variables significantly associated with accommodating iris curvature were ACD ( $t = 2.68$ ,  $P = 0.009$ ), lens vault ( $t = -2.01$ ,  $P = 0.047$ ) and scleral spur angle ( $t = -5.1$ ,  $P < 0.0001$ ). For these 3 variables acting jointly,  $R^2 = 0.33$ .

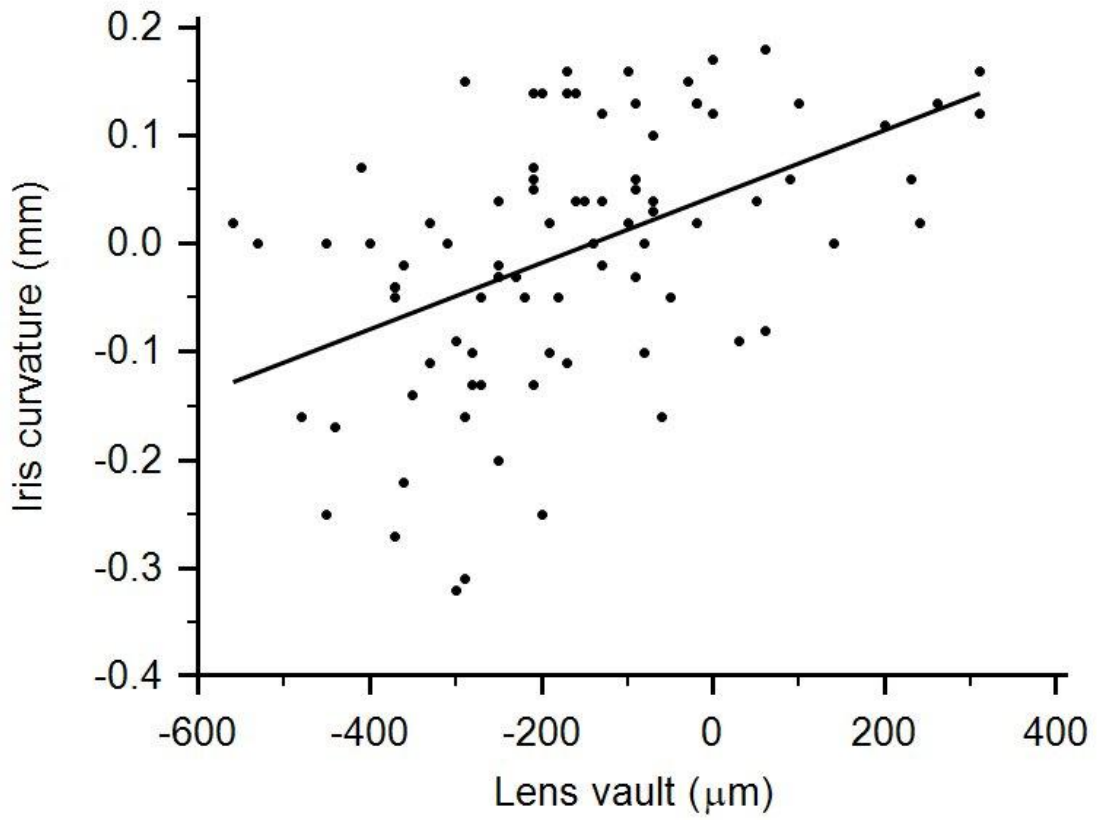


**Figure 3.2** Scatterplot of lens vault against non-accommodating iris curvature in 2009 schoolboy cohort. Regression equation:  $y = 0.0003x + 0.04$ .

CH and CRF were both associated with spur-to-spur distance in the non-accommodating state ( $R^2 = 0.07$  for both,  $P = 0.025$  and  $0.027$  respectively). CH (but not CRF) was associated with spur-to-spur distance in accommodation ( $R^2 = 0.11$ ,  $P = 0.005$ ). No significant association was found between CH/CRF and AL. Spur-to-spur distance and axial length were significantly correlated ( $r = 0.29$ ,  $P = 0.007$ ).

There were statistically significant differences between near and distance measurements for all angle metrics except temporal TISA500 ( $P = 0.09$ ). Mean anterior lens surface movement on accommodation was 0.23 mm (SD 0.17mm).

In the Bland Altman plots, the measurement difference between observers was unrelated to the magnitude of the measurement for all parameters. 95 % limits of agreement (LoA) together with the range of values in this cohort are shown in table 3.3. The criterion for minimum acceptable LoA is a clinical decision, judged against the range of values of the parameter being measured (90). CCT, ACD and spur-to-spur distance demonstrated reasonably good agreement whereas LV, scleral spur angle and all AOD and TISA measurements demonstrated moderate agreement when considering the range of values for these parameters. Interestingly, ACD and spur-to-spur distance were both operator-determined but showed better agreement than the angle metrics that were software-determined.

Parameter	Range	Mean difference	95 % Limits of agreement
CCT ( $\mu\text{m}$ )	440 to 650	-1.8	-18.3 to +14.8
ACD (mm)	2.44 to 4.00	0.01	-0.08 to +0.09
Lens vault ( $\mu\text{m}$ )	-560 to 770	41.5	-93.3 to +176.3
Temporal AOD 500 ( $\mu\text{m}$ )	0 to 2016	-120	-380 to +150
Temporal AOD 750 ( $\mu\text{m}$ )	0 to 2245	-120	-390 to +160
Temporal TISA 500 ( $\text{mm}^2$ )	0 to 0.837	-0.04	-0.13 to +0.05
Temporal TISA 750 ( $\text{mm}^2$ )	0 to 1.357	-0.07	-0.21 to +0.08
Temporal scleral spur angle ( $^\circ$ )	20.9 to 79.3	-3.9	-12.6 to +4.9
Spur-to-spur distance (mm)	10.29 to 13.10	0.07	-0.1 to +0.24
Nasal AOD 500 ( $\mu\text{m}$ )	0 to 1698	-80	-370 to +210
Nasal AOD 750 ( $\mu\text{m}$ )	0 to 2170	-80	-420 to +250
Nasal TISA 500 ( $\text{mm}^2$ )	0 to 0.568	-0.02	-0.13 to +0.08
Nasal TISA 750 ( $\text{mm}^2$ )	0 to 1.063	-0.05	-0.22 to +0.13
Nasal scleral spur angle ( $^\circ$ )	29.1 to 76.6	-2.7	-11.6 to +6.2

**Table 3.3** Between-observer agreement on AS-OCT parameters on 40 images (accommodative and non-accommodative scans) from 20 randomly selected subjects from 2009 schoolboy cohort

Fourteen participants had an uncorrected refractive error (defined as visual acuity of LogMAR 0.2 or worse which improved with pin-hole) and letters were written to the parents of these participants advising them of the need for an optometric assessment. One participant was subsequently diagnosed as having keratoconus. Ten participants had ORA IOPcc values of greater than 21 mmHg and were offered appointments in a Paediatric Ophthalmology clinic and of these, 1 participant was noted to have significant angle recession secondary to a prior ocular injury.

### 3.3.2 Follow up study (December 2011)

Out of 96 pupils invited to take part, 62 (64.6%) agreed and took part. Near and distance scans from 1 student and the near scan from another were excluded due to

poor image quality. Iris curvature measurements were not possible in an additional 3 accommodative scans and 2 non-accommodative scans, due to difficulty identifying the posterior iris pigment epithelium. ORA measurements from 4 subjects were excluded, as waveform scores were consistently less than 4. Summary data are shown in table 3.4. All parameters were normally distributed based on the Kolmogorov-Smirnov test, except for iris curvature in distance fixation, which showed a longer tail at lower values of iris curvature. There was no significant difference in refractive error between those who participated 2 years later and those who did not (mean SE -0.44 D and -0.37D respectively,  $P = 0.86$ ).

Parameter	N	Mean	SD
Axial length (mm)	62	24.01	1.04
Spherical equivalent (dioptres)	62	-1.09	1.91
Iris curvature A (mm)	57	-0.25	0.17
Iris curvature NA (mm)	59	-0.02	0.14
Spur-to-spur distance A (mm)	60	12.1	0.48
Spur-to-spur distance NA (mm)	61	12.1	0.47
Mean digit ratio	62	0.95	0.033
Height (cm)	62	164.45	8.58
Corneal hysteresis (mmHg)	59	11.4	1.64
Corneal resistance factor (mmHg)	59	11.5	1.98
Weight (kg)	62	53.7	11.38
Waist circumference (cm)	62	72.3	7.93
Percentage body fat	62	16.2	6.24
Birth weight (kg)	61	3.34	0.78

**Table 3.4** Ocular and non-ocular characteristics of 2011 schoolboy cohort

For the purposes of this study, iris concavity was defined as iris curvature  $\leq -0.1$ mm.

The prevalence of iris concavity was 19/59 (32%) at distance fixation and 49/58 (84%)

at near fixation. The distributions of non-accommodative and accommodative iris

curvature are shown in figures 3.3 and 3.4 respectively.

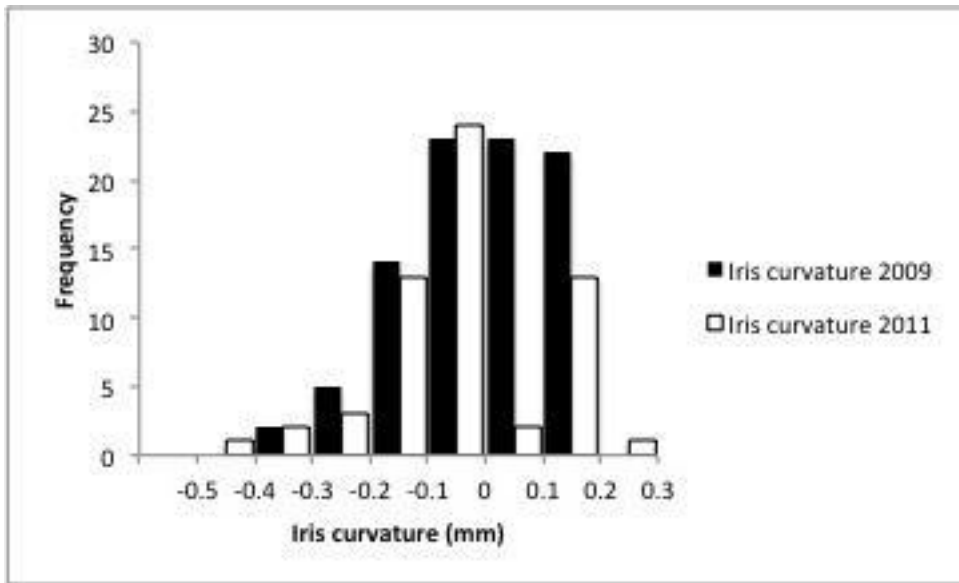


**Figure 3.3** Histogram to show distribution of non-accommodating iris curvature in 2009 and 2011

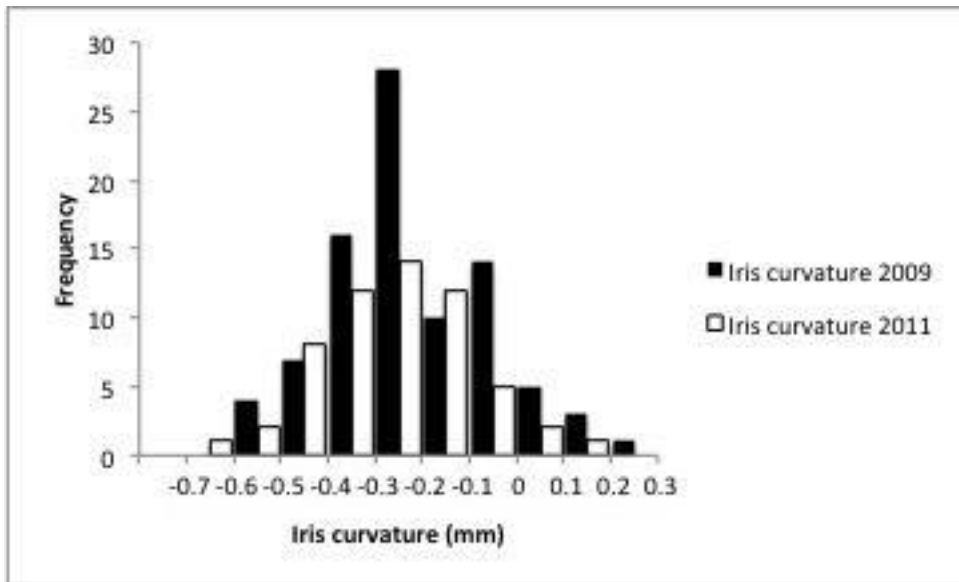


**Figure 3.4** Histogram to show distribution of accommodating iris curvature in 2009 and 2011

Variables significantly associated with non-accommodating iris curvature were ACD ( $t = 2.25, P = 0.029$ ) and mean scleral spur angle ( $t = -4.11, P = 0.0001$ ). For both variables acting jointly,  $R^2$ -adjusted = 0.59. Variables significantly associated with accommodating iris curvature were ACD ( $t = 2.34, P = 0.02$ ), lens vault ( $t = -2.01, P = 0.047$ ) and scleral spur angle ( $t = -7.30, P < 0.0001$ ). For both variables acting jointly,  $R^2$ -adjusted = 0.62.

Significant association was found between CH and non-accommodating spur-to-spur distance ( $R^2 = 0.07, P = 0.047$ ) as well as CH and accommodating spur-to-spur distance ( $R^2 = 0.13, P = 0.0067$ ) (figure 3.5).

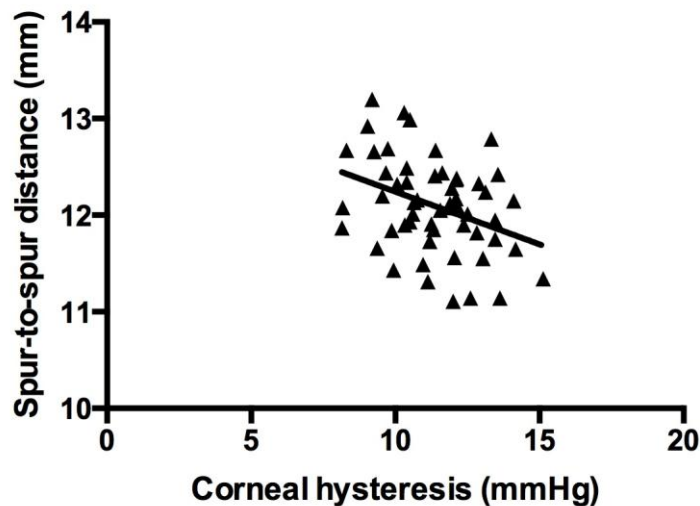


**Figure 3.5** Scatterplot of corneal hysteresis against spur-to-spur distance on accommodation for 2011 schoolboy cohort. Regression line:  $y = -0.11x + 13.3$

There was a mean increase in AL of 0.22mm (paired t-test,  $P < 0.0001$ ) and mean decrease in SE of 0.70 D compared to 2009 (paired t-test,  $P < 0.0001$ ). Mean iris curvature at distance fixation reduced from -0.002 mm in 2009 to -0.02 in 2011 ( $P = 0.40$ ) and at near fixation reduced from -0.21 in 2009 to -0.25 in 2011 ( $P = 0.19$ ). A comparison of parameters between baseline and follow up is shown in table 3.5.

Parameter	2009	2011	Difference	<i>P</i>
Axial length (mm)	23.79	24.01	0.22	<0.0001
Spherical equivalent (dioptries)	-0.39	-1.09	-0.7	<0.0001
Corneal hysteresis (mmHg)	11.6	11.4	-0.2	0.35
Corneal resistance factor (mmHg)	11.7	11.5	-0.2	0.25
Iris curvature NA (mm)	-0.016	-0.019	-0.003	0.77
Iris curvature A (mm)	-0.198	-0.246	-0.048	0.11
Anterior chamber depth NA (mm)	3.37	3.39	0.02	0.17
Anterior chamber depth A (mm)	3.14	3.15	0.01	0.61
Scleral spur angle NA (°)	58.4	56.6	-1.8	0.02
Scleral spur angle A (°)	60.4	58.4	-2	0.11
Lens vault NA (µm)	-165.6	-179.2	-13.6	0.52
Lens vault A (µm)	64.3	58	-6.3	0.8
Spur-to-spur distance NA (mm)	12.06	12.13	0.07	0.13
Spur-to-spur distance A (mm)	12.05	12.12	0.07	0.08

**Table 3.5** Comparison of ocular biometric parameters between 2009 and 2011 schoolboy cohorts. \*Paired *t*-test. ACD= anterior chamber depth, AOD= angle-opening distance, TISA= trabecular-iris space area. Values shown for scleral spur angle represent temporal quadrant. Values for nasal angle were similar.

Angle-opening distance (AOD), trabecular-iris space area (TISA), LV and scleral spur angle all show significant increases on accommodation (table 3.6), a finding that was also noted in the 2009 cohort.

	Non-accommodating (n=61)		Accommodating (n=60)		P*
	Mean	SD	Mean	SD	
Iris curvature (mm)	-0.02	0.14	-0.25	0.17	<0.0001
CCT ( $\mu\text{m}$ )	531.7	30.1	528.5	32.1	0.07
ACD (mm)	3.38	0.28	3.14	0.31	<0.0001
Lens vault ( $\mu\text{m}$ )	-176.2	217.6	59.3	223.4	<0.0001
Temporal AOD 500( $\mu\text{m}$ )	822.4	318.4	907.8	379.0	0.0016
Temporal AOD 750( $\mu\text{m}$ )	1084.5	366.8	1185.5	398.7	0.0006
Temporal TISA 500( $\text{mm}^2$ )	0.295	0.122	0.315	0.136	0.036
Temporal TISA 750( $\text{mm}^2$ )	0.536	0.210	0.580	0.237	0.006
Temporal scleral spur angle ( $^\circ$ )	55.8	10.5	57.6	11.5	0.03
Nasal AOD 500( $\mu\text{m}$ )	794.3	312.2	946.1	330.0	<0.0001
Nasal AOD 750( $\mu\text{m}$ )	1069.1	362.6	1233.3	392.1	<0.0001
Nasal TISA 500( $\text{mm}^2$ )	0.277	0.112	0.312	0.115	0.0014
Nasal TISA 750( $\text{mm}^2$ )	0.512	0.199	0.591	0.203	<0.0001
Nasal scleral spur angle ( $^\circ$ )	55.5	11.0	60.4	9.4	<0.0001
Spur to spur distance (mm)	12.17	0.48	12.10	0.48	0.78

**Table 3.6** Summary data for AS-OCT parameters in 2011 schoolboy cohort. \*Paired *t*-test. CCT= central corneal thickness, ACD= anterior chamber depth, AOD= angle-opening distance, TISA= trabecular-iris space area

No significant association was found between any ocular and non-ocular measurements. There was no statistically significant difference between CH/CRF values in 2009 and 2011. No significant association was detected between baseline CH, baseline CRF or non-ocular measurements and change in AL, SE and spur-to-spur distance.

### 3.4 Discussion

Iris concavity in PDS leads to increased frictional contact between the posterior iris surface and the lens zonules, thereby predisposing to PG. Iris concavity in the absence of PDS has been described (81, 87) but its prevalence has not been reported. As PG is a condition that often affects young males, this study was designed to look at the

prevalence of iris concavity in a cohort of males before the age at which PDS is typically identified.

Iris concavity was significantly more prevalent during accommodation than with distance fixation. The most widely accepted theory of accommodation is that put forward by Helmholtz (117) which states that contraction of the ciliary muscle relaxes the tension in the lens zonules which allows the lens to revert to a thicker and more convex form. Drexler et al. (43) studied changes in lens position in 10 healthy eyes in subjects whose mean age was 30 years and whose refractive error ranged from emmetropia to -5 dioptres using partial coherence interferometry. During accommodation the mean forward movement  $\pm$  standard deviation (SD) of the anterior pole of the lens was  $185 \pm 89 \mu\text{m}$  whilst the backwards movement of the posterior pole was  $69 \pm 39 \mu\text{m}$ . The mean forward movement of the anterior pole in the present study was  $230 \mu\text{m}$  and it is likely the greater value in the present study reflects the larger accommodative amplitude (approximately 10 D) found in the school-age cohort. Sheppard et al. (118) demonstrated a decrease in anterior and posterior radius of curvature during accommodation in 15 young (19-29 years) emmetropes using magnetic resonance imaging as well as an increase in lens thickness and decrease in AC depth. Visual inspection of the images from our cohort suggests that the central iris may be conforming to the curvature of the lens as it moves anteriorly (figure 3.1). The most important determinant of iris concavity in accommodation was a smaller ACD. This would also support the hypothesis of anterior lens movement causing increased

iris concavity. However, if miosis and forward movement of the anterior lens pole are the only conformational change, this would cause a reduction in the anterior chamber angle, AOD and TISA on accommodation, rather than the increase observed (table 3.2). As there appeared to be accommodation-induced changes in the peripheral iris, it is unlikely that the changes seen in iris curvature could be explained solely by anterior lens movement acting on the central iris. Accommodation-induced change in lens position and miosis are likely to increase the area of contact between the iris and lens and this may result in a reverse pupillary block effect, similar to that seen in PDS, permitting mainly unidirectional flow from the posterior to the anterior chamber. The consequent increase in pressure in the anterior chamber relative to the posterior chamber may result in posterior displacement of the peripheral iris and this represents a possible explanation for the increase in angle parameters seen on accommodation. It should be mentioned that accommodation-induced miosis may confound the assessment of iris configuration; future studies should address this by varying the ambient light intensity in order to achieve equal pupil sizes in the accommodative and non-accommodative states.

24% of eyes exhibited iris concavity in the non-accommodative state. As the prevalence of PDS in a white population is reportedly 2.5% (34), the vast majority of these eyes are unlikely to develop PDS. It may be that iris concavity and the associated irido-lenticular contact must persist into adulthood for the development of PDS or other features need

to be present to induce pigment dispersion, such as factors intrinsic to the iris of PDS patients causing susceptibility to zonular abrasion or pigment shedding.

Good between- and within-observer agreement of the iris concavity measurements used in this study has previously been shown in a cohort of adult PDS patients (119). Between-observer agreement was investigated for the semi-automated AS-OCT parameters. Liu et al.(120) reported that scleral spur identification was more difficult in eyes with narrow angles. In general, scleral spur visibility was good in the vast majority of images in the present study; this was supported by better agreement for scleral spur angle and spur-to-spur distance whereas agreement for the automated readings for AOD and TISA were less good. Agreement for AOD and TISA may have been poorer as calculation of these parameters is dependent on the software correctly detecting the iris and corneal endothelial surfaces.

CH, CRF and IOP measured by the ORA have previously been described (104). Kirwan et al. (121) reported non-contact tonometry with the ORA to be an accurate method of determining IOP and found children cooperated better with this technique than with Goldmann applanation tonometry. Lower CH has been associated with longer AL in Chinese school children (105, 122) although Lim et al.(106) did not find any association with AL or refractive error in their study of 271 Singaporean (68.6% Chinese) children. Chang et al.(123) studied 126 eyes of 63 Taiwanese (predominantly Han Chinese) children and found that the difference in CH between the two eyes of each patient

correlated significantly with the difference in the AL between the two eyes. There was no relationship between ORA measurements and AL in the present study. The fact that CH and spur-to-spur distance were consistently associated at both time points in a relatively small sample is noteworthy and suggests that corneal biomechanical properties, as measured by the ORA, are associated with anterior segment geometry. No association was detected between CH/CRF and AL, although no AL and spur-to-spur distance were significantly correlated, raising the possibility that an underlying association between CH/CRF and AL may still exist despite not reaching statistical significance in the present study. No association was detected between baseline CH/CRF and changes in AL or spur-to-spur distance over the 2-year interval. Thus, the study did not find evidence that baseline corneal biomechanical parameters predict ocular growth, although the study was not powered to answer this question.

The prevalence of iris concavity in this cohort was greater in 2011 (32% at distance fixation and 84% at near fixation) compared to 2009 (24% and 65% respectively), although there was no statistically significant difference in iris curvature measurements over the 2-year period for boys with data available from both visits. The higher prevalence might have reflected a selection bias, whereby myopes may have been more interested (either through parental encouragement or independently) in taking part in the second visit compared to non-myopes. However, analyzing the 2009 cohort revealed no significant difference in refractive error between those who participated 2 years later and those who did not and so such selection bias appears unlikely. Figures

3.2 and 3.3 demonstrate a similar distribution of iris curvature in 2009 and 2011, supporting the view that selection bias was unlikely. Significant association was found between iris curvature and ACD in both accommodative and non-accommodative states, indicating that relative lens position may be an important determinant of iris curvature. However, there was no significant increase in ACD between 2009 and 2011 suggesting that increased ACD did not account for the observed increase in concavity. A possible explanation is that an increase in iris size between iris root and pupil margin creates 'redundant' iris tissue which positions posteriorly in a concave configuration.

The study presented an opportunity to collect additional data that were potentially relevant to ocular growth. Rahi et al. (107) found that myopia was positively associated with low birth weight for gestational age, whilst Saw et al. (108) reported that across the normal birth weight range, longer AL was associated with greater birth weight. However, Dirani et al.(124) analysed data from 1,224 twins from the Genes in Myopia twin study and found no significant association between birth weight and myopia.

The digit ratio is the ratio of the lengths of different digits or fingers typically measured from the bottom crease, where the finger joins the hand, to the tip of the finger. It has been suggested that the ratio of two digits (D) in particular, the 2nd (index finger; 2D) and 4th (ring finger; 4D), is affected by exposure to androgens e.g. testosterone while in the uterus and that this 2D:4D ratio can be considered a putative marker for prenatal androgen exposure, with lower 2D:4D ratios pointing to higher androgen

exposure (110-112). Interestingly, the differences are more pronounced in the right hand (125-127). There is evidence that control of eye growth differs between men and women (109) and by collecting data on digit ratio we aimed to explore whether eye growth differs between boys with greater or lesser exposure to maternal levels of androgens. Including a cohort of girls would have been of interest as this would have resulted in a greater range of values for exposure to maternal androgens but it was decided to use the limited resources to obtain a reasonable sized cohort of boys rather than a small cohort of boys and girls.

Birth weight and digit ratio are both markers of intra-uterine experience and Barker's theory (128) suggests that intrauterine experiences have a lifelong impact on health.

Bio-impedance monitors have been developed that can distinguish between lean and fat tissue based on differences in their conductance and impedance characteristics; furthermore, they are simple to use, cost-effective, portable and non-invasive.

Excellent correlation has been shown between bio-impedance and fat-free mass as measured by hydrodensitometry (129) and its use has been validated in children (130, 131). Height, weight, percentage body fat and waist circumference provide an indication of general metabolic status and may reflect long-term insulin levels.

Epidemiological evidence implicates a role for chronic hyperinsulinaemia, secondary to the refined sugars and starch in western diets, in juvenile-onset myopia because of its interaction with hormonal regulation of vitreal chamber growth (113).

No significant correlation was demonstrated between any of the above non-ocular parameters and AL, SE, CH, CRF (nor change in these parameters over the 2 years). The study was not powered to detect such associations, so this part of the study was considered exploratory, given the clinical importance of identifying risk factors for myopia.

The school at which this study was conducted has a strong focus on academic achievement. Participants in the present study may not be representative of the wider cross-section of this age group and a limitation of the present study is that the findings may not be widely generalizable. Another limitation is the relatively small sample size.

Iris concavity appears to be a frequent finding in this cohort at both time points. It is likely that the prevalence of iris concavity will fall as the cohort approaches adulthood on the basis that iris concavity in adults appears to be uncommon (81). Iris curvature was associated with LV, ACD scleral spur angle. It remains unclear whether there may be anatomical differences between the type of iris concavity found in our cohort and that found in PDS and this remains an area for further study. The data support the hypothesis that physiological iris concavity, which is more prominent during accommodation, may be related to a reverse pupil block mechanism. The anterior movement of the central iris alone did not explain the wider angle metrics and observed changes in iris curvature. The data also suggests there may be significant

associations between corneal biomechanical parameters and ocular size (determined by spur-to-spur distance but not AL in this dataset).

<b>4</b>	<b>LINKAGE ANALYSIS IN A PEDIGREE SEGREGATING FOR PIGMENT DISPERSION SYNDROME</b>	
4.1	Introduction	103
4.1.1	Concepts underlying linkage analysis	103
4.1.1.1	Genetic markers and recombination fraction	
4.1.1.2	Haplotype blocks	
4.1.1.3	Single nucleotide polymorphisms	
4.1.1.4	Calculating the logarithm of the odds (LOD score)	
4.1.1.5	Threshold for significant linkage	
4.1.2	Examples of glaucoma genes identified through linkage analysis	107
4.1.2.1	Myocilin	
4.1.2.2	Optineurin	
4.1.3	Linkage analysis in modern glaucoma gene mapping	108
4.1.4	Linkage analysis to map PDS susceptibility loci	109
4.2	Methods	109
4.2.1	Phenotyping	109
4.2.2	Genotyping	111
4.2.3	Analysis of genotypic data	111
4.2.4	Candidate gene sequencing	112
4.3	Results	112
4.3.1	Clinical findings	112
4.3.1.1	Assignment of affected/unaffected status	

4.3.2	Testing known PDS disease susceptibility loci	118
4.3.3	Linkage analysis	118
4.3.3.1	LOD scores and haplotype analysis	
4.3.4	Sequencing candidate genes	125
4.4	Discussion	125

## 4.1 Introduction

Evidence for a genetic basis to PDS comes from the existence of families with multiple affected members (63,64). A genetic abnormality affecting the middle third of the eye during the third trimester has been proposed in order to explain the association with lattice degeneration, retinal tears and retinal detachment (23). Linkage analysis is a powerful tool for gene mapping in multigenerational families with clear Mendelian inheritance; this approach has been used in families with PDS demonstrating an autosomal dominant pattern of inheritance (63, 64). Data from screening first degree relatives of patients attending the PDS clinic at Moorfields Eye Hospital suggest that the majority of patients with PDS are not from autosomal dominant pedigrees and it may be that these cases represent either recessive inheritance or sporadic mutations. Identification of genes for PDS may provide information about molecular mechanisms underlying the pathogenesis and may uncover targets for novel therapeutic interventions. This chapter describes the results of linkage analysis in a pedigree segregating for PDS/PG showing an autosomal dominant mode of inheritance.

## **4.1.1 Concepts underlying linkage analysis**

### **4.1.1.1 Genetic markers and recombination fraction**

Gene mapping in linkage studies is achieved by determining which genetic markers (whose chromosomal locations are already known) segregate with the disease of interest. The chromosomal region defined by these markers is likely to contain the disease susceptibility locus/gene. Recombination of homologous chromosomes occurs as a normal part of meiotic cell division. During prophase of meiosis I, pairs of homologous chromosomes exchange segments between individual chromatids, the point of crossover being known as a chiasma. If the gene of interest (location unknown) and a particular genetic marker (location known) are close together on a chromosome, the interval between these two loci is less likely to undergo recombination compared to a larger interval where the gene and marker are further apart. A central concept to linkage analysis is that of the 'recombination fraction' (denoted by  $\theta$ ): for an individual heterozygous for 2 loci A and B, If alleles A1 and B1 are inherited from the mother and alleles A2 and B2 are inherited from the father, the individuals gametes may be recombinant i.e. A1 B2 or A2 B1 or non-recombinants i.e. A1 B1 or A2 B2. The recombination fraction is the proportion of gametes that are recombinant. Recombination is unlikely to separate 2 loci that are close together and the recombination fraction is therefore a measure of the distance between 2 loci. The recombination fraction ranges from  $\theta=0$  for loci immediately adjacent to one another

to 0.5 for widely separated loci (or loci on different chromosomes). Genetic distances are measured in centimorgans (cM) where 1cM is approximately equal to a recombination fraction of 1%. This relationship is less true over larger distances because of the existence of multiple crossovers (132). A mathematical relationship between recombination fraction and genetic map distance is given by a mapping function. A widely used mapping function is Kosambi's function:

$$w = \frac{1}{4} \ln \left[ \frac{(1+2\theta)}{(1-2\theta)} \right]$$

where  $w$  = map distance and  $\theta$  = recombination fraction

Using Kosambi's function, a recombination fraction of 0.27 translates into a genetic distance of 30cM (133).

#### **4.1.1.2 Haplotype blocks**

The majority of recombination occurs over short discrete regions of the chromosome known as recombination hotspots whilst the intervening regions form relatively stable 'haplotype blocks' with low crossover rates. Sets of alleles close together in a chromosomal region tend to be inherited together in these haplotype blocks and can be tracked through pedigrees providing a useful way of confirming that a particular chromosomal locus segregates with the disease (132).

#### **4.1.1.3 Single nucleotide polymorphisms**

Single nucleotide polymorphisms (SNPs) are the most common type of genetic variation amongst individuals. An SNP represents a variation in a single nucleotide and occurs, on average, every 300 nucleotides. There are approximately 10 million SNPs spread over the human genome. They normally have only 2 alleles but due to their dense distribution across the genome and the ability of microarrays to assay over 500,000 SNPs at a time they are presently the genetic marker of choice.

#### **4.1.1.4 Calculating the logarithm of the odds (LOD score)**

Once a pedigree has been collected and genotyped (i.e. their SNPs assayed), the first step in determining whether there is significant linkage to any SNPs is to work out the recombination fraction. For an affected individual whose children (considered to be his meiosis) need to be scored as recombinant or non-recombinant, this can only be done if a number of conditions are met: a) the individual is heterozygous at the marker in question, b) the individual's parents' affected status and genotype is known, and c) it can be determined which alleles were inherited from each of the individual's parents. In a large number of cases, these conditions will not be met and computer software has been developed to deal with the inherent uncertainty in working out the recombination fraction. The probability that a marker is linked to the disease of

interest is given by the ratio of the overall likelihood given linkage: overall likelihood given no linkage. This is known as the likelihood ratio and is equal to:

$$\frac{(1-\theta)^m \times \theta^n}{0.5^{n+m}}$$

where  $\theta$  is the recombination fraction,  $n$  is the number of recombinants and  $m$  the number of non-recombinants. The logarithm of this ratio is termed the LOD (logarithm of the odds) score, symbolised by  $Z$ . LOD scores are calculated over a range of  $\theta$  values with the most likely value of  $\theta$  being that with the highest LOD score (132).

#### **4.1.1.5 Threshold for significant linkage**

For a single test, the threshold for statistical significance is  $Z=3$ . As  $\log_{10}1000=3$ ,  $Z=3$  corresponds to a 1000:1 odds. Using Bayesian statistics with a 1 in 50 prior probability of linkage, 1000:1 odds corresponds to a joint probability (prior x conditional) of 1 in 20 which equates to the conventional  $p = 0.05$  test for statistical significance (134). In gene mapping studies, pedigrees are genotyped over thousands of markers, with a test for linkage being conducted at each marker. As this is an extreme case of multiple testing, it could be argued that a Bonferroni correction should be applied. However, this results in an overly stringent LOD score threshold as linkage data are not independent (if one location is excluded, the pre-test probability that another location is linked increases) (132). Empirical LOD score thresholds have been proposed: a LOD

score of 1 at the initial screening stage would be considered 'interesting', a LOD score of 2 would be considered 'very interesting' and LOD score of 3 would be indicative of 'provisional linkage', awaiting confirmation from an independent dataset in order to be considered highly significant (135).

#### **4.1.2 Examples of glaucoma genes identified through linkage analysis**

Linkage analysis has been used to identify several loci in primary open angle glaucoma (POAG); *myocilin* and *optineurin* are both well-established glaucoma-causing genes identified through this approach.

##### **4.1.2.1 *Myocilin***

A disease susceptibility locus for juvenile open-angle glaucoma, known as GLC1A, was originally mapped to 1q21-q31 by genetic linkage analysis of a 37-member pedigree segregating for JOAG in an autosomal dominant pattern (71). Mutation screening of candidate genes within this region identified 13 glaucoma patients with mutations in the *TIGR* (TM-induced glucocorticoid response protein) gene, subsequently renamed *myocilin* (*MYOC*) (70).

#### **4.1.2.2      *Optineurin***

Sarafarazi et al.(136) mapped a locus for normal tension glaucoma, GLC1E, to 10p15-p14 through linkage analysis of a large British family demonstrating autosomal dominant inheritance. Subsequent work identified a missense mutation [Glu<sup>50</sup> → Lys (E50K)] in the *optineurin* (*OPTN*) gene located within this region. Sequence alterations in this gene were identified in 16.7% of 54 families with hereditary POAG (137).

#### **4.1.3              Linkage analysis in modern glaucoma gene mapping**

A novel POAG locus was more recently identified by Porter et al. (138). Linkage analysis was used to investigate a large 4-generation family with an autosomal dominant mode of inheritance. Ten affected members and 1 unaffected family member were genotyped and a significant LOD score of 3.1 centred at 4q35.1-q35.2 was found. Mutation analysis of 3 candidate genes *LRP2BP*, *CYP4V2* and *UFSP2* did not identify any mutations.

#### **4.1.4              Linkage analysis to map PDS susceptibility loci**

To date there have been 2 published loci, 7q31-36 and 18q21, identified through linkage analysis in autosomal dominant PDS pedigrees. The study presented here describes a linkage analysis on a British family with autosomal dominant PDS/PG with the aim of discovering novel PDS susceptibility loci.

## **4.2 Methods**

Ethical approval for the study was obtained from the Moorfields and Whittington Research Ethics Committee. The study was carried out according to the principles set out in the Declaration of Helsinki. Members of a 3-generation family with PDS/PG were enrolled into the study following informed consent. Family members were reviewed at Moorfields Eye Hospital (London, UK), Moorfields Eye Hospital Outreach Clinic at Northwick Park Hospital, Harrow (Greater London, UK) and Lincoln County Hospital (Lincolnshire, UK).

### **4.2.1 Phenotyping**

A total of 15 family members were enrolled into the study. DNA from 2 members of generation II (subjects II:3 and II:4, figure 4.1) had previously been taken with informed consent although the clinical notes were no longer available. The proband stated that subject II:3 (proband's father) had significant visual loss from glaucoma whilst subject II:4 (proband's mother) had no known ophthalmic problems. All living members enrolled into the study were examined by a single ophthalmologist (AS). Where they existed, previous ophthalmic medical notes were reviewed. Participants were asked about their ophthalmic and medical history, including their medications and allergies. Detailed ophthalmic examination was performed on all subjects with particular emphasis on looking for the clinical signs of PDS/PG, including hyperpigmentation of

the drainage angle by performing gonioscopy with an Ocular Magna View Gonio Lens (Ocular Instruments Inc., Washington, USA). Applanation tonometry was performed with a Goldmann applanation tonometer using Tonosafe™ disposable prisms. Dilated stereoscopic optic disc examination was performed in subjects with open angles. Visual fields were recorded using Humphrey 24-2 automated perimetry (Carl Zeiss Meditec, Dublin, CA). Glaucomatous optic neuropathy (GON) was defined as reproducible glaucomatous visual field (VF) defects with corresponding damage to the optic nerve head (cup disc ratio  $\geq$  0.7 and/or focal narrowing of the neural rim) and the absence of retinal or neurological condition that may account for the VF loss.

A glaucomatous VF was defined as a reproducible defect (in at least 2 consecutive reliable post-screening VFs) of two or more contiguous points with  $P < 0.01$  loss or greater, or three or more contiguous points with  $P < 0.05$  loss or greater, or a 10-dB difference across the nasal horizontal midline at two or more adjacent points in the total deviation plot (definition used in the UK Glaucoma Treatment Study (139)).

#### **4.2.2 Genotyping**

Participants' DNA was extracted using the Nucleon™ BACC2 DNA Extraction Kit (Tepnel Life Sciences, Manchester, UK) by Miss Beverley Scott, BMRC technician. DNA was prepared according to the protocol set out in Appendix 1. Prepared DNA was sent to the Wolfson Institute for Biomedical Research (WIBR) for hybridisation,

washing/staining and scanning. Genotyping was performed on an Affymetrix 50K Genechip.

#### **4.2.3 Analysis of genotypic data**

Genotype data from 15 individuals from this family were generated using the 50K Array Xba 240 Assay Kit from the GeneChip Human Mapping 100k Set (Affymetrix, High Wycombe, UK). Initial checks of the results were performed with GeneChip Command Console Viewer (v1.1.0.845). Genotyping Console (v3.0.2) was used to assign individual genotypes. Alohomora version 0.30 (Max Delbrück Center for Molecular Medicine, Berlin, Germany) was used to prepare the raw genotype data for total linkage analysis. PedCheck (version 1.1, Jeff O'Connell; University of Pittsburgh, Pittsburgh, PA, USA) was used to detect and remove Mendelian errors from the data. Genehunter (version 2.1\_r5 beta) was used to perform the subsequent parametric linkage analysis. The genetic model was specified as dominant and fully penetrant with a disease allele frequency of 0.0001. Merlin (80) was used to generate LOD scores.

Regions showing promising LOD scores were refined using markers from Marshfield genetic maps (<http://research.marshfieldclinic.org>), the GDB Human genome database and Ensemble database (<http://www.ensembl.org>). Phenotype and genotype data were stored using Progeny software version 7.6.04 (Progeny Software, Florida, USA).

#### **4.2.4 Candidate gene sequencing**

Candidate genes were selected from the regions identified by linkage analysis based on biological plausibility. Direct sequencing of the exonic regions of *SERTAD4*, *TGF $\beta$*  and *ENTACTIN* was performed in subjects III:9 (affected) and III:1 (unaffected). PCR primers were chosen to include the exonic sequence as well as a short section of adjacent intronic sequence. Amplicons were purified prior to sequencing using a purification kit (Qiagen Genclean Kit, Qiagen, Crawley, UK). Sequencing was performed using Big Dye 3.1 terminator chemistry (Applied Biosystems, Warrington, UK) and run on an ABI 3730 DNA sequencer (Applied Biosystems). Analysis of sequencing data was performed on Sequencher Version 4.1.4 (140).

### **4.3 Results**

#### **4.3.1 Clinical findings**

A clinical diagnosis of PDS or PG was made in 7 members of a 3-generation family of British ancestry with an autosomal dominant inheritance pattern (figure 4.1). There were no living members from generation I or II. Nine members from generation III and 6 members from generation IV agreed to clinical phenotyping for the purposes of the study. Four members of generation III met the diagnostic criteria for pigment dispersion (III:2, III:5, III:7 and III:9). Three of these 4 subjects had GON (vertical cup to

disc ratio of 0.9 and previous trabeculectomy in at least one eye in 2 subjects and in the 3<sup>rd</sup> subject a vertical cup to disc ratio of 0.3 right eye and 0.6 left eye with previous trabeculectomy). The 4<sup>th</sup> pigment dispersion subject was classified as a glaucoma suspect on the basis of disc asymmetry (vertical cup to disc ratio 0.6 right eye, 0.4 left eye) in the absence of a significant visual field defect. Subjects 4 and 8 from generation III had glaucomatous optic neuropathy requiring trabeculectomy in at least one eye although clinical features at the time of examination were insufficient to meet diagnostic criteria for pigment dispersion. Subject III:1 had occludable angles without glaucomatous optic neuropathy and was referred to her local eye clinic with a recommendation for urgent YAG laser peripheral iridotomies. No subjects from generation IV met diagnostic criteria for pigment dispersion nor had definite glaucomatous optic neuropathy. Clinical characteristics of generations III and IV are presented in tables 4.1 and 4.2 respectively.

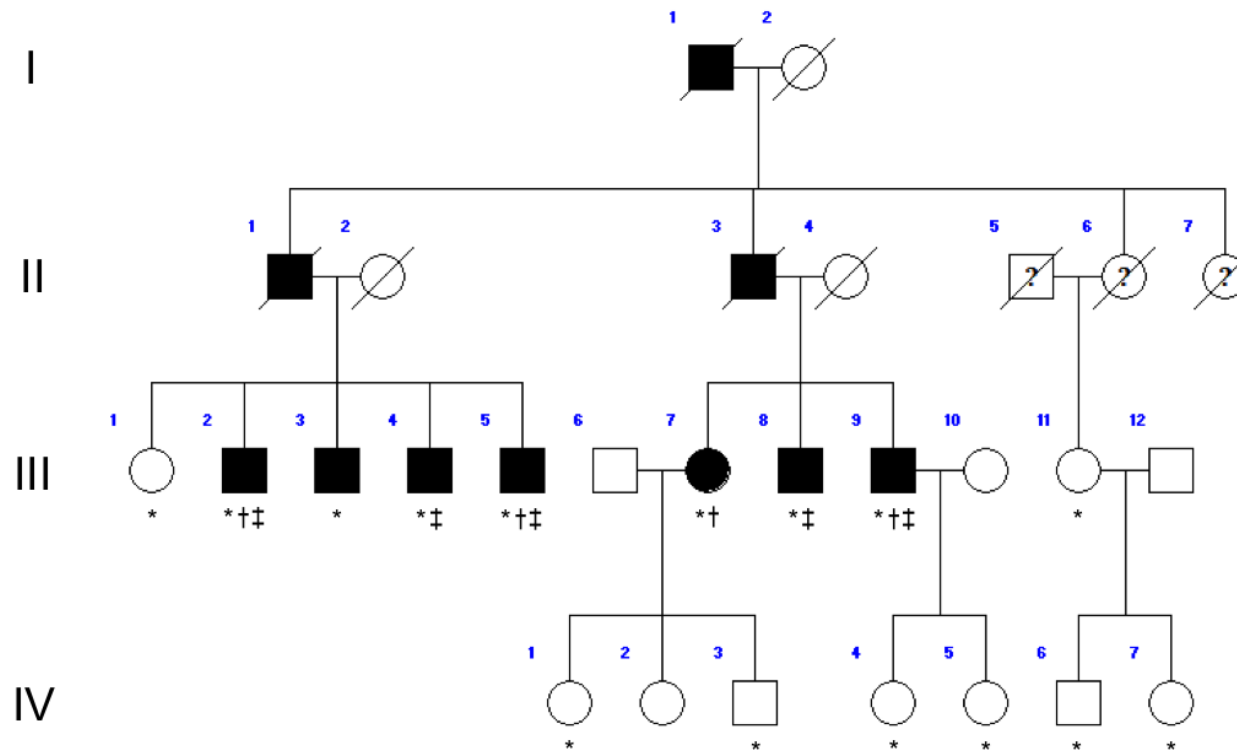


**Figure 4.1** Autosomal dominant pigment dispersion pedigree. \*Family members who attended for phenotyping.† Individual deemed to have definite pigment dispersion syndrome.‡ Individual deemed to have definite glaucomatous optic neuropathy

#### **4.3.1.1 Assignment of affected/unaffected status**

Whilst 4 subjects (III:2, III:5 and III:7) had clear evidence of pigment dispersion, the existence of 2 additional subjects (III:4 and III:8) with clear GON without features of pigment dispersion raises uncertainties in determining their affectation status. Subjects III:4 and III:8 were aged 60 and 73 at the time that they were examined. There is evidence of a regression phase in some patients with pigment dispersion such that the clinical signs may fade with increasing age (23, 38) sometimes to the extent that patients may be misdiagnosed as having POAG or low-tension glaucoma (141). Whilst it was possible that pigment dispersion and POAG were segregating as 2 separate conditions in this pedigree, it was considered more likely that the 2 subjects in question had pigment dispersion giving rise to glaucomatous optic neuropathy but that the signs had faded by the time that they were examined: an age-related reversal of iris trans-illumination defects has been documented as has an age-related reduction in degree of TM pigmentation (33, 38). The assumption was therefore made in the analysis that these 2 subjects would both be classified as 'affected'; this assumption extended to subject II:3 who had provided a blood sample for DNA analysis several years earlier to previous investigators but in whom no record of clinical examination could be found. The subject's daughter stated that he had significant visual problems that she attributed to glaucoma. For the purposes of the analysis, therefore, he was also classified as 'affected'.

Family member (age at presentation, y)	SE (D)	AL (mm)	Angle width (°)	KS		TID		TMP		Max. IOP (mmHg)	CCT (µm)	MD (dB)	CD ratio		Comments
				RE	LE	RE	LE	RE	LE						
III.1 (65)			5 RE 5 LE	0	0	0	0	0	0	18 BE			0.35	0.4	Occludable angles
III.2 (71)			35 RE 35 LE	+	+	+	+	++	++	16 RE 26 LE		-9.88RE -9.43LE	0.9	0.7	Right trab
III.3(62)		24.00 RE 23.97 LE	35 RE 35 LE	0	0	+/-	+/-	+	+	20 BE		-1.1RE -1.71LE	0.5	0.3	Right disc unchanged since 1999
III.4(72)	-0.88 RE -0.33 LE	24.94 LE		0	0	0	0	0	0	3 RE 18LE		-30.29RE -25.52LE	0.9	0.9	Bilateral trab, right RD, right chronic iritis
III.5(80)			35 RE 35 LE	0	++	0	+	++	++	21 RE 17 LE	553 RE 568 LE	-4.04 RE -27.5 LE	0.6	0.9	Left trab
III.7(52)	-2.38 RE -2.00 LE	24.23 RE 24.37 LE	35 RE 35 LE	+	++	0	+	+	++	23 RE 20 LE	541 RE 538 LE	1.04 RE 0.43 LE	0.6	0.4	Right disc suspicious
III.8 (61)	-2.25 RE	24.91 RE	35 RE 35 LE	0	-	0	-	+	-	21 RE	490 RE	-	0.9	-	Left eye enucleation following cactus injury
III.9 (56)	-1.88 RE -3.13 LE	25.70 RE 27.10 LE	40 RE 40 LE	+++	++	++	++	+++	++ +	32 RE 27 LE	542 RE 539 LE	-5.5 RE -5.2 LE	0.3	0.6	Right trab 2003. Equal disc size.
III.11 (67)	1.38 RE 1.38 LE	- -	25 RE 25 LE	0	0	0	0	+	++	16 RE 18 LE		1.56 RE 1.36 LE	0.4	0.3	Disc height 1.3 RE, 1.1 LE

**Table 4.1** Clinical characteristics of generation III of PDS/PG family. SE = spherical equivalent, D = diopters, RE = right eye, LE = left eye, trab = trabeculectomy, RD = retinal detachment

Family member (age at presentation,y)	SE (D)	AL (mm)	Angle width (°)	KS		TID		TMP		Max. IOP (mmHg )	CCT (µm)	MD (dB)	CD ratio		Comments
				RE LE	RE LE	RE LE	RE LE	RE LE	RE LE						
IV.1(27)										19RE 17LE	560BE				
IV.3(25)	-1.75 RE -1.75 LE	24.91 RE 24.94 LE	35 RE 35 LE	+/ -	+/-	0	0	+	+		498 RE 517 LE	0.27 RE -0.1 LE			
IV.4(23)	-0.375 RE -0.375 LE	23.83 RE 24.00 LE	35 RE 35 LE	0	0	0	0	+	+	14 BE	535 RE 546 LE	-2.39 RE -2.36 LE	0.3	0.3	Left Adie's pupil
IV.5(24)	-1.0 RE -0.375 LE	23.02 RE 23.03 LE	- -	0	0	0	0	-	-	-	-	-	0.3	0.3	Mild learning difficulties. Limited phenotyping possible
IV.6(37)	0 RE 0 LE	- -	35 RE 35 LE	0	0	0	0	+/-	+/-	16 RE 17LE	581 RE 580 LE	-	0.3	0.3	
IV.7(27)	0 RE 0 LE	- -	- -	0	0	0	0	0	0	12 RE 16 LE	582 RE 584 LE	0.22 RE 0.39 LE	0.3	0.4	Disc height 1.3mm RE, 1.1mm LE

**Table 4.2** Clinical characteristics of generation IV of PDS/PG family. SE = spherical equivalent, D = diopters, RE = right eye, LE = left eye

### **4.3.2 Testing known PDS disease susceptibility loci**

Microsatellite markers were used to investigate 7q31-36 and 18q21 in III:9 (affected) and III:1 (unaffected) and both of these loci were excluded.

### **4.3.3 Linkage analysis**

Haplotype analysis was performed by Dr N Waseem, Senior Post-doctoral fellow, Department of Genetics, UCL Institute of Ophthalmology.

#### **4.3.3.1 LOD scores and haplotype analysis**

Three chromosomal locations demonstrated promising LOD scores and were considered worthy of further investigation.

- 1) A 20.0-Mb region with a maximum parametric LOD score of 2.12 was identified on chromosome 1q41-42.2 (figure 4.2). The maximum non-parametric LOD score was 4.57. Haplotype analysis showed all affected family members sharing a common haplotype between D1S2703 and D1S2800 (figure 4.5).
- 2) A 23.0-Mb region with a maximum parametric LOD score of 1.96 was identified on chromosome 10q25.1-q26.3 (figure 4.3). The maximum non-parametric LOD score was 5.29. Haplotype analysis showed all affected

family members sharing a common haplotype between D10S597 and D10S1651 (figure 4.6).

- 3) An 11-Mb region with a maximum parametric LOD score of 1.97 was identified on chromosome 22q13.1-q13.31 (figure 4.4). The maximum non-parametric LOD score was 3.07. Haplotype analysis showed all affected family members sharing a common haplotype between D22S423 and D22S1149 (figure 4.7).

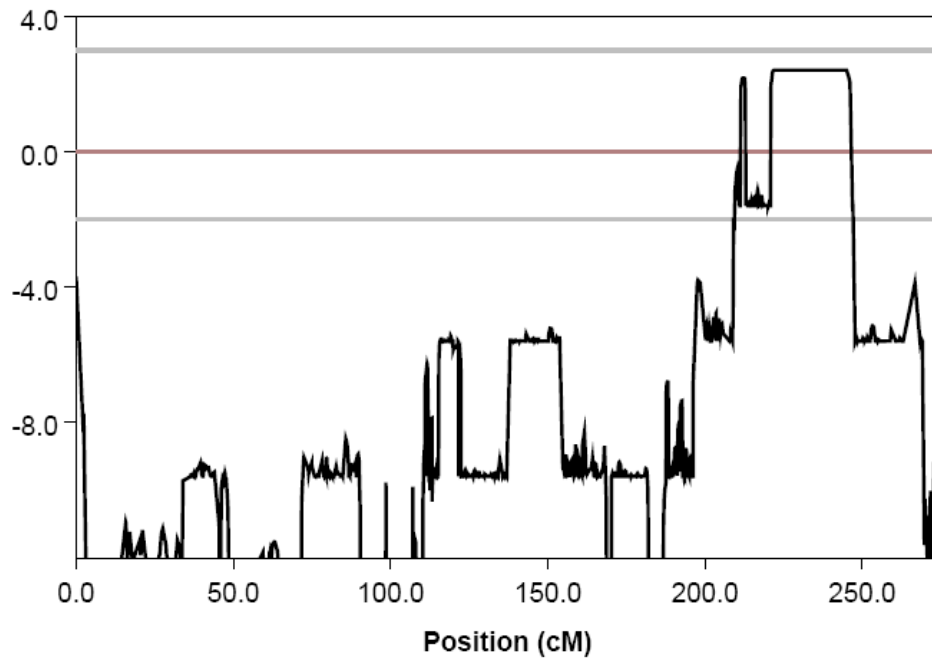


**Figure 4.2** Parametric genome-wide LOD scores for chromosome 1. Physical chromosome position shown on x-axis and LOD score shown on y-axis

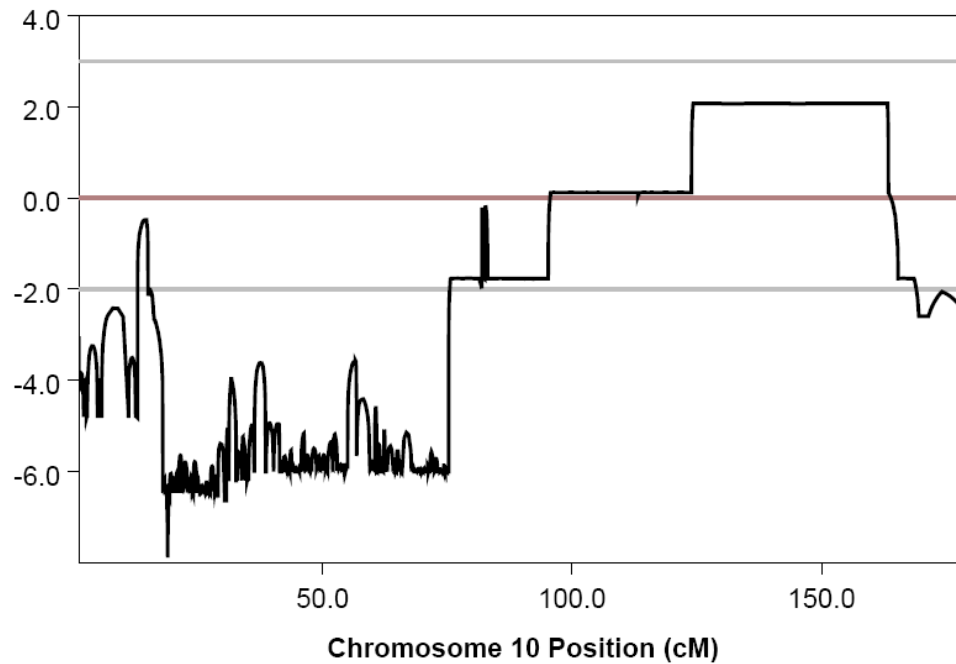


**Figure 4.3** Parametric genome-wide LOD scores for chromosome 10. Physical chromosome position shown on x-axis and LOD score shown on y-axis

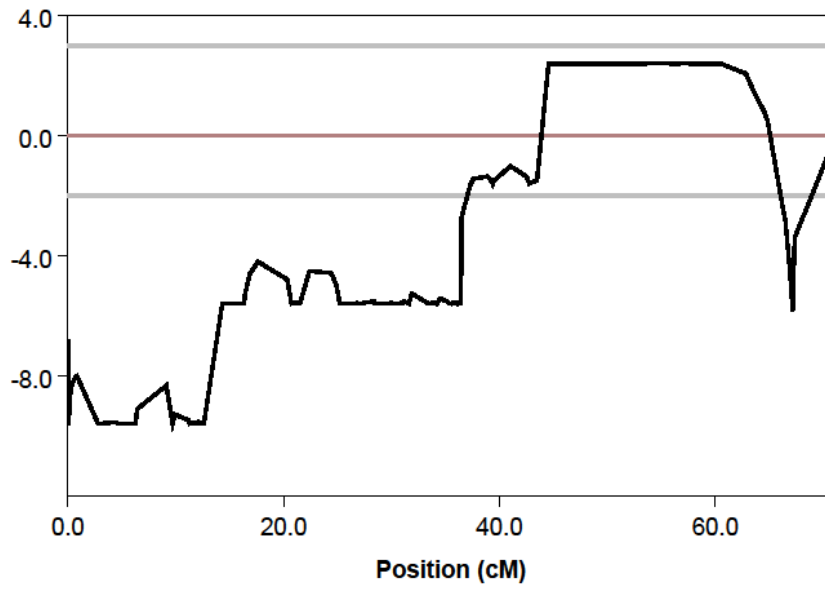


**Figure 4.4** Parametric genome-wide LOD scores for chromosome 22. Physical chromosome position shown on x-axis and LOD score shown on y-axis

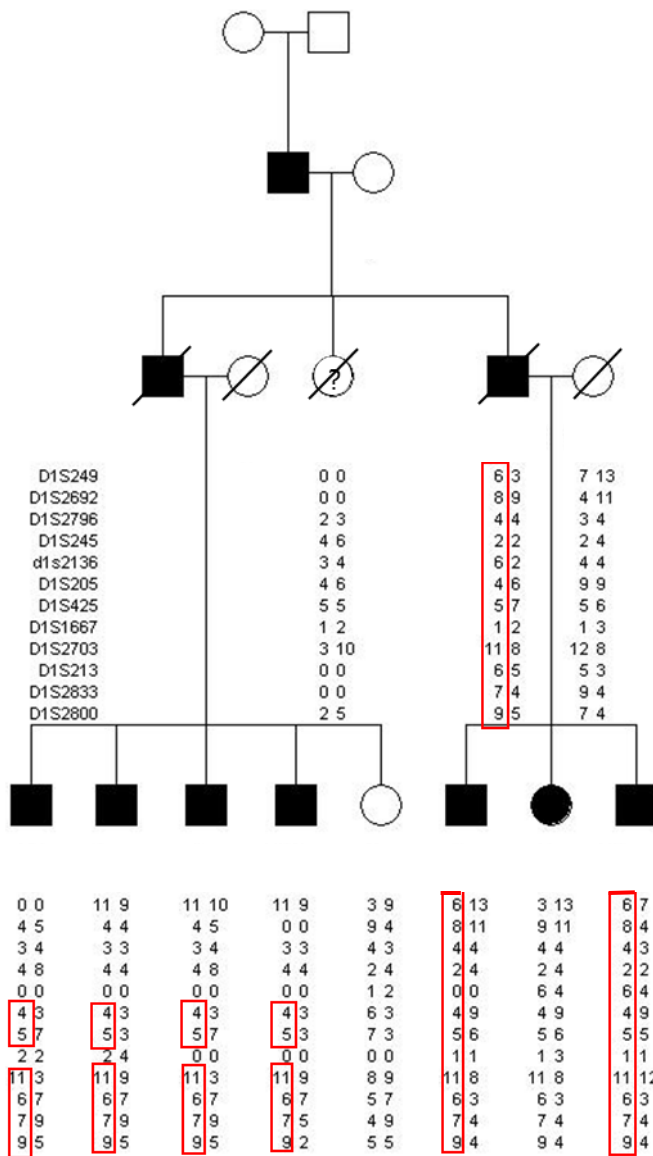


**Figure 4.5** Haplotype analysis for region of interest on chromosome 1





#### 4.3.4 Sequencing candidate genes

The following candidate genes from the region of interest on chromosome 1 were considered the best candidate genes based on biological plausibility: *SERTAD 4*, *TGF $\beta$ 2* and *ENTACTIN 1*. *SERTAD 4* is the human homologue of the murine *Cdca4* expressed in the optic eminence of mouse embryos. TGF signalling has a role in the normal development of cornea, lens and retina in transgenic mice. *ENTACTIN* codes for a basement membrane protein, aberrations in which could render iris tissue more fragile. Sequencing of the coding regions in individuals III:9 (affected) and III:1 (unaffected) revealed no missense or nonsense sequence changes that could have resulted in potentially pathogenic mutations.

#### 4.4 Discussion

This chapter has described the phenotypic features of 2 generations of a family with what appeared to be an autosomal dominant form of PDS/PG. Linkage to known PDS loci were excluded and genome-wide linkage analysis was performed which demonstrated 3 chromosomal regions of interest each with parametric LOD scores close to 2.

The family was identified after screening 297 PDS probands and their relatives in an effort to find families that might be suitable for linkage analysis. The family in the present study was the largest of those identified and was considered to be the most

suitable for linkage analysis. A number of assumptions were made in the analysis: it was assumed that individuals II:3 and II:4 (figure 4.1) were affected and unaffected respectively (based on the probands recollection of her parents' ocular morbidity) and that GON seen in subjects III:4 and III:8 (figure 4.1) was secondary to pigment dispersion. It was also assumed that the gene was fully penetrant. In fact, there may be other disease modifying genetic or environmental factors that affect whether the PDS phenotype is manifest. For example, as PDS has a predilection for myopic eyes it might be that emmetropic or hyperopic individuals with the PDS-causing genotype do not manifest the phenotype because their refractive state in some way is protective. Non-myopic eyes might not exhibit the iris concavity required for frictional contact with lens zonules thereby preventing pigment dispersion. Subject IV(4) was noted to have Adie's pupil and may develop a miosed pupil in the long term; in theory, this may offer some protection against pigment dispersion as the miosed pupil is 'on stretch' and therefore less prone to iris concavity.

No individuals in generation IV showed any of the 3 cardinal signs of PDS. As all were below 25 years of age, it was not possible to classify them confidently as unaffected and this generation was therefore excluded from the linkage analysis. Nevertheless, this family still represents a valuable resource for the identification of a disease susceptibility locus and it would be feasible to re-visit members of generation IV in 5 years time when it is likely that some members of the generation may be exhibiting the clinical features. Entering genotypic data from affected members of generation IV may narrow the region of interest and/or increase the LOD score.

Of the 3 regions identified, the region on chromosome 1 was considered to show the strongest evidence for linkage. As laboratory time and resources were limited, efforts to screen candidate genes were therefore focussed on this region. *SERTAD 4*, *TGFβ2* and *ENTACTIN* were considered the best candidate genes based on their known functions and expression patterns.

*SERTAD4* was identified as a result of work by Bennetts et al. (142) who isolated the murine *Cdca4* gene (cell division cycle associated 4) whilst conducting a genomic expression-based screen for genes involved in mammalian craniofacial development. Expression was demonstrated, amongst other regions, in sectioned mouse embryos in the optic eminence at day 13.5. The predicted CDCA4 protein contains a novel SERTA (*SEI-1*, *RBT1* ((Replication Protein A Binding Trans-activator 1) and *TARA* (mammalian counterpart of *Drosophila tara* gene, a gene related to *Cdca4*) motif. High conservation between CDCA4 and previously characterised SERTA domain proteins, indicates a potential role for CDCA4 in cell cycle regulation and control of gene expression. Sequence homology searches identified a further evolutionarily conserved uncharacterised human member of the SERTA domain family; this sequence has been annotated as a predicted 356 amino acid peptide sequence and named SERTAD4.

Ittner et al. (143) investigated the effect of neural crest cell specific inactivation of TGF signalling in transgenic mice; this was achieved by deletion of exon 4 of the TGFβ receptor type 2 (RT2), which leads to loss of TGFβ<sub>2</sub> protein expression in neural crest

stem cells. The cornea in TGF $\beta$  (RT2)-knockout embryos lacked an endothelial layer and the cornea and lens failed to separate whilst the retina showed diffuse patterning as opposed to clear structuring into anterior and posterior layers seen in controls. PDS eyes are likely to have some retinal involvement as the prevalence of lattice degeneration in these eyes has been reported to be 20-33% (27, 28). Normal formation of the TM and the ciliary body, indicated by a wrinkle in the iris primordium in control eyes, was not seen in TGF $\beta$ 2-mutant eyes. The changes in the eyes of TGF $\beta$ 2-mutant embryos were similar to those seen in human Axenfeld-Rieger's anomaly, a condition characterised by posterior embryotoxon, iris stromal hypoplasia, corectopia, pseudopolyopia and ectropion uveae. Iwao et al.(144) also described a similar transgenic mouse strain: heparan sulphate is required for TGF $\beta$  signalling which the authors were able to impair by disrupting the gene encoding exostosin 1, an enzyme required for heparan sulphate synthesis. The resulting phenotype displayed irido-corneal angle dysgenesis and raised IOP. Finally, David et al.(145) reported a family with a balanced translocation t(1;7) (q41;p21) associated with Peter's anomaly, a condition characterised by iridocorneal adhesions or keratolenticular apposition; the authors reporting this family considered *TGF $\beta$ 2*, located 500kb proximal to the breakpoint on chromosome 1, to be the main candidate gene.

Entactin is an integral and ubiquitous component of the basement membrane and could serve as a bridge between laminin and type IV collagen. Evidence for this comes from work on human choriocarcinoma cells which synthesize laminin and type IV collagen but not entactin. Chung and Durkin (146) observed that transfection of

entactin into these cells stimulated incorporation of laminin and type IV collagen along with entactin into the extracellular matrix and into structures resembling focal contacts. *ENTACTIN* was considered a candidate gene on the basis that the absence of a basement membrane component might cause fragility of the posterior iris pigment epithelium making it prone to dispersing pigment.

The regions identified through the linkage analysis were relatively broad, in the range of 10-20-Mb, compared to a 1.9-Mb region identified by linkage analysis in a family with autosomal dominant POAG (138). The region of interest on chromosome 1, for example, contains hundreds of genes and it may not be justified to spend the considerable time and resources on screening the remaining genes within the region given the LOD score was considerably less than 3. Sanger sequencing, also known as the chain-termination method, was the standard method for gene sequencing used worldwide up until the end of the 20<sup>th</sup> century. The subsequent period has seen the development of next generation sequencing (NGS), a technology that is capable of massive parallel sequencing, during which millions of DNA segments are sequenced simultaneously with the result that an entire genome can be sequenced in less than 24 hours. NGS involves fragmenting the DNA sample and attaching short adapter sequences onto the ends prior to amplifying. The fragments are then washed and nucleotides added in a pre-determined order. The addition of each nucleotide is recorded as the DNA segment is extended (147). Different platforms use different methods to record the sequence. The Illumina MiSeq platform works by detecting fluorescence emitted by pre-labelled nucleotides as the DNA fragment is extended

(148). Whilst linkage analysis has identified potential chromosomal regions of interest in this family, identification of the causative sequence change is difficult because the region identified is relatively wide. It is feasible to combine the linkage analysis described in this chapter with NGS technology in an effort to identify the responsible sequence variant. For example, Sobreira et al. (149) combined linkage information for metachondromatosis, a skeletal disorder affecting bone growth, leading to multiple enchondromas and osteochondromas with whole-genome DNA sequence in a single proband to identify a frameshift in *PTPN11* that alters the reading frame and co-segregates with the disease. Confirmation of this result was provided when a different mutation in the same gene was found to segregate with the disease in a different family.

Another application of NGS technology is whole-exome sequencing. Whilst it is possible to sequence the entire genome on NGS platforms, disease causing mutations are much more likely to be found in the coding regions (exons) of the genome and it is therefore more efficient to focus resources on these regions, which comprise around 1% of the total genome. Whole-exome sequencing may be useful in some of the smaller families that have been enrolled, with a view to identifying sequence variants that segregate with the disease; these smaller families would also be useful to validate any putative mutations that may be found in the family described in this chapter.

**5 GENOME-WIDE ASSOCIATION STUDY OF PIGMENT DISPERSION SYNDROME  
AND MUTATION SCREENING OF *GPNMB* IN A PANEL OF PDS SUBJECTS**

5.1	Introduction	134
5.1.1	Genome-wide association study into PDS/PG	134
5.1.1.1	Rationale	
5.1.1.2	Association analysis is based on linkage disequilibrium	
5.1.1.3	Examples of successful GWAS in ophthalmology	
5.1.1.3.1	Complement factor H in age-related macula degeneration	
5.1.1.3.2	E2-2 protein in Fuchs's corneal dystrophy	
5.1.1.4	Examples of successful GWAS in glaucoma	
5.1.1.4.1	LOXL1 in pseudoexfoliative glaucoma	
5.1.1.4.2	CAV1 and 2, TMCO1 and CDKN2B-AS1 in POAG	
5.1.1.5	Study design considerations	
5.1.2	Screening for <i>GPNMB</i> sequence variants	140
5.2	Methods	142
5.2.1	Genome-wide association study	142
5.2.1.1	Case and control cohorts	
5.2.1.2	Sample size	
5.2.1.3	DNA extraction and genotyping	
5.2.1.4	Quality control	
5.2.2	Screening for <i>GPNMB</i> sequence variants	145

5.3	Results	146
5.3.1	Genome-wide association study	146
5.3.1.1	Genotyping	
5.3.1.2	Quality Control	
5.3.1.2.1	Per-individual and per-marker missing genotypes	
5.3.1.2.2	Sex check	
5.3.1.2.3	Racial/ethnic ancestry	
5.3.1.2.4	Principal component analysis	
5.3.1.2.5	Hardy-Weinberg Equilibrium	
5.3.1.2.6	Heterozygosity	
5.3.1.2.7	Relatedness	
5.3.2	Screening for <i>GPNMB</i> sequence variants	155
5.4	Discussion	157
5.4.1	Genome-wide association study	157
5.4.1.1	Quality Control	
5.4.1.1.1	Per-individual and per-marker missing genotypes	
5.4.1.1.2	Sex check	
5.4.1.1.3	Racial/ethnic ancestry	
5.4.1.1.4	Principal component analysis	
5.4.1.1.5	Hardy-Weinberg Equilibrium	
5.4.1.1.6	Heterozygosity	
5.4.1.1.7	Relatedness	
5.4.1.2	Conclusion	



## **5.1 Introduction**

Patients with PDS/PG and their first-degree relatives were enrolled in an effort to find families suitable for linkage analysis (chapter 4). All participants had been carefully phenotyped and had provided blood samples for genetic studies into PDS/PG. Whilst most of these families were ultimately unsuitable for linkage analysis due to insufficient affected members, the project resulted in a DNA biobank for 130 PDS/PG probands. The DNA biobank was used in 2 ways: 1) a panel of 100 unrelated samples were used for a genome-wide association study (section 5.1.1), and, 2) a panel of 96 unrelated samples was screened for mutations in *GPNMB*, the human homologue of the gene which causes a pigment dispersion phenotype in the DBA/2J mouse strain (section 5.1.2).

### **5.1.1 Genome-wide association study**

#### **5.1.1.1 Rationale**

Whilst linkage analysis has had some success in identifying chromosomal loci for PDS (63, 64), this approach has relied upon the assumption that PDS is a monogenic Mendelian condition, at least within the pedigrees that have been investigated. The following features of PDS, however, are more in keeping with a 'complex' (150) rather than a Mendelian genetic model: phenotypic heterogeneity, likely polygenic inheritance (as evidence by the existence of at least 2 genetic loci), phenocopies

(pigment dispersion as a result of surgery, trauma) and possible incomplete penetrance (subject III:3, table 4.1). Genetic factors in complex disease are likely to be relatively weak and/or heterogeneous compared to genes responsible for Mendelian disorders and, as such, linkage analysis is not as powerful a technique in the former compared to the latter. An alternative approach is to use association analysis, a method of investigating association across a population between a disease and a genetic marker. Weak effects are more readily detected by association rather than linkage (151). Lander put forward the hypothesis that common SNPs (minor allele frequency of at least 5%) are likely to account for at least some of the genetic contribution to common diseases (152). Genome-wide association studies (GWAS) typically type thousands or millions of SNPs across the whole genome across a cohort of cases and controls. Association analysis is conducted by determining the prevalence of each allele in cases and controls and then testing for statistically significant differences.

#### **5.1.1.2 Association analysis is based on linkage disequilibrium**

SNP variants that are situated close together on a chromosome tend to be inherited together, more so than would be predicted by their individual allele frequencies, in groups known as haplotype blocks; this non-random association of alleles is referred to as linkage disequilibrium (LD). Whilst GWAS can identify genetic regions that harbour risk-conferring SNPs, they will rarely identify the functional variant, which usually requires further genotyping of the region of interest as well as functional studies (153).

There have been two key developments which have made GWA studies feasible: 1) The International HapMap Project (<http://hapmap.ncbi.nlm.nih.gov/>) (154) typed several million SNPs in four human populations and provided detailed data on LD across the genome. Sets of 500,000 SNPs can act as ‘tags’ or proxys for approximately 80% of common SNPs (155). Interrogating these ‘tag’ SNPs on commercially available genotyping platforms allows efficient capture of variation across the whole genome.

### **5.1.1.3 Examples of successful GWAS in ophthalmology**

#### **5.1.1.3.1 Complement factor H in age-related macula degeneration**

The first successful application of the GWAS approach in ophthalmology was the discovery of the role of complement factor H gene in age-related macula degeneration (AMD) (156); this study reported results of a genome-wide scan of 96 cases and 50 controls and identified association with the Y402H polymorphism at rs1061170 where a tyrosine is substituted by a histidine. The Y402H change has been replicated in other independent studies and has been associated with both early and late AMD, as well as dry (geographic atrophy) and wet (choroidal neovascular membrane) forms of the disease (reviewed in (157)).

#### **5.1.1.3.2 E2-2 protein in Fuchs's corneal dystrophy**

Baratz et al. (158) conducted a GWA study investigating Fuchs' endothelial dystrophy (FED), a condition in which patients develop visual loss as a result of bilateral corneal endothelial failure. The GWA study included 130 FED subjects in the discovery cohort and an additional 150 subjects in a replication cohort; the strongest association was found at rs613872 in intron 3 of the transcription factor 4 (*TCF4*) gene ( $P = 1.01 \times 10^{-12}$  in the discovery cohort and  $1.79 \times 10^{-13}$  in the replication cohort), located on chromosome 18. *TCF4* codes for the E2-2 protein, a member of a family of transcription factors involved in cellular growth and differentiation.

#### **5.1.1.4 Examples of successful GWAS in glaucoma**

##### **5.1.1.4.1 LOXL1 in pseudoexfoliative glaucoma**

This study enrolled 195 glaucoma patients and 14474 controls and identified 2 coding variants at the LOXL1 loci rs1048661 and rs3825942 (159). Sub-group analysis determined that the signal was driven entirely by 75 patients with pseudoexfoliative glaucoma. These associations have subsequently been replicated in multiple studies across different populations (160). The G allele of rs3825942 has been consistently reported as the risk allele in multiple populations, however, a study of the LOXL1 coding region in XFG subjects from South Africa found a strong association with the

opposite (A) allele (161). Williams et al. concluded that other, as yet unknown, causal variants of LOXL1 contribute to the genetic risk of XFG.

No significant differences have been found in the risk of LOXL1 polymorphisms of developing PEX syndrome versus PEX glaucoma, which would implicate separate genetic or environmental factors in determining risk of raised IOP/GON (160). The present study has made a similar assumption regarding the genetic risk of raised IOP/PG in PDS and as such has classified all PDS subjects as 'cases' regardless of the presence or absence of PG.

#### **5.1.1.4.2 CAV1 and 2, TMCO1 and CDKN2B-AS1 in POAG**

The caveolin locus for POAG was discovered through a GWAS of 1,263 cases and 34,877 controls from Iceland (162). A common sequence variant was identified at 7q31 (rs4236601[A], odds ratio (OR) = 1.36,  $P = 5.0 \times 10^{-10}$ ). The association with the caveolin locus was replicated in independent samples from Sweden, UK, Australia, Hong Kong and China and also in a further independent American cohort (163). The associated SNPs reside in a haplotype block which harbour the CAV1 and CAV2 genes which encode proteins involved in caveolae, small invaginations of the cell membrane involved in cell signalling and endocytosis.

An Australian GWAS enrolling 615 subjects with advanced POAG and 3946 controls reported significant and replicated association at 2 loci: rs4656461 at 1q24 (OR = 1.68,

$P = 6.1 \times 10^{-10}$ ) and rs4977756 at 9p21 (OR = 1.50,  $P = 4.7 \times 10^{-9}$ ); these loci implicate the *TMCO1* gene and a long non-coding RNA called CDKN2B-AS1 respectively (164).

#### **5.1.1.5 Study design considerations**

Subjects for both the case and control group should ideally be from the same ancestry because SNP frequencies will vary across populations (165). Robust quality control of the genotypic data is required to detect problems with the SNP assay or DNA quality as well as to detect previously unknown relatedness amongst subjects and differences in ancestry between cases and controls. An appropriately matched control population must be selected. In the case of PDS, the control group should be matched for myopia, in order to avoid erroneously identifying SNPs for myopia rather than PDS.

Correction must be made for multiple testing. GWAS typically test for association across at least 500,000 SNPs. Using a  $P$ -value of 0.05 in this context would result in 25,000 SNPs being erroneously taken forward for replication studies as a result of false-positive association. A more appropriate  $P$ -value can be obtained by dividing the threshold  $P$ -value by the number of tests (Bonferroni correction) although this value is overly stringent when the number of tests is large (132).

Finally, any associations detected in the 'discovery cohort' would require replication in an independent cohort.

### 5.1.2 Screening for *GPNMB* sequence variants

The DBA/2J mouse strain represents a mouse model for PG. The phenotype is attributed to mutations in *Gpnmb* and *Tyrp1*, which have been shown to cause iris pigment dispersion (IPD) and iris stromal atrophy (ISA) respectively (66, 166).

The features of IPD are similar to PDS in man and comprise deterioration of the posterior iris pigment epithelium, slit-like iris transillumination defects and pronounced pigment dispersion. IPD is caused by a premature stop codon mutation in *Gpnmb* (R150X) (67). Transcription of *Gpnmb* is regulated by microphthalmia transcription factor (MITF). A MITF-binding site has been identified in the in the *Gpnmb* promoter and is conserved in different mammalian species (167). Bachner et al. (168) investigated *Gpnmb* mRNA in murine embryonic development. High levels were initially detected in the outer retina whereas in subsequent stages in development mRNA expression is restricted to the retinal pigment epithelium and iris. Bachner et al. concluded that *Gpnmb* was important in melanin biosynthesis and in retinal pigment epithelium and iris development; this is significant because human PDS involves retinal (28) as well as iris pathology.

ISA is associated with a loss of iris stromal complexity and build up of iris stromal pigment and cellular debris in the drainage angle. ISA is caused by the recessive *Tyrp1*<sup>b</sup> mutant allele encoding a mutant protein containing two amino-acid substitutions. Mice

homozygous for mutations causing IPD and ISA have a more severe phenotype with an earlier age of onset and more aggressive GON than either mutation on its own (166).

The relationship between levels of ocular pigmentation and the development of the ISA and IPD phenotypes is demonstrated in DBA/2J-*pe* mice, a strain bearing the pearl (*pe*) mutation in which the homozygous genotype causes hypopigmentation of coats and eyes. Despite homozygosity for *Gpnmb*<sup>R150X</sup> and *Tyrp1*<sup>b</sup>, DBA/2J-*pe* mice homozygous for the *pe* mutations did not show the IPD or ISA phenotypes and also prevented the development of GON (67). Thus IPD and ISA phenotypes appear to be dependent upon the level of pigment production occurring in the adult eye.

Mutations in human *TYRP1* mutations cause OCA3 (169), a form of oculocutaneous albinism, with no reported increased risk of PG. Tyrosinase is an enzyme that catalyses the initial step in pigment production and TYRP1 forms part of a complex required for stabilisation of this enzyme. Mutant TYRP1 may fail to stabilize tyrosinase resulting in reduced pigment production and OCA3 may therefore be 'self-rescuing' with regard to the development of PG. Lynch et al. (170) sequenced the *TYRP1* gene in probands from families segregating for PDS/PG. Lynch et al. identified 3 novel synonymous SNPs in 2 PDS/PG subjects but report that these SNPs did not define a haplotype that segregated with the disease. No variants causing changes in the amino acid sequence were identified.

*GPNMB* codes for a highly glycosylated type I transmembrane protein and shows significant structural homology to the melanosomal structural protein, Pmel17 (171). The gene was first cloned when it was noted to show preferential expression levels in low-metastatic melanoma cell lines (172). Anderson et al. (67) sequenced the *GPNMB* coding region from 8 affected individuals in 4 families with autosomal dominant PDS and detected no mutations.

As laboratory time was limited it was decided to sequence *GPNMB* in the panel of PDS/PG patients in preference to *TYRP1*. The IPD phenotype in DBA/2J mouse strain more closely resembled human pigment dispersion than the ISA phenotype and *Gpnmb* mRNA expression had been demonstrated in the retinal pigment epithelium as well as the iris of embryonic mice. For these reasons *GPNMB* was considered the better candidate gene for human pigment dispersion.

## **5.2 Methods**

### **5.2.1 Genome-wide association study**

#### **5.2.1.1 Case and control cohorts**

Patients with PDS or PG had been recruited from Moorfields Eye Hospital from December 2008 and July 2011. Patients were invited to attend for phenotyping and to provide a blood sample for DNA extraction. All participants had been phenotyped by

one investigator (AS) and had consented for their blood samples to be used for the purposes of genetic investigation into PDS. Diagnostic criteria for PDS have been stated in section 2.1. One hundred unrelated probands were selected to form the 'case' cohort. Patients with clear non-Caucasian ancestry were excluded from selection. The study was approved by the South East London Research Ethics Committee.

The UK Twins Registry have a large cohort of patients with ophthalmic phenotypic data including refractive error, half of whom had been genotyped on the Illumina 317k platform, and half on the Illumina 610 Quad chip (550k plus 60k CNV SNPs). Agreement was obtained from the UK Twins Registry for access to genotypic data from a myopic cohort to serve as the control dataset.

#### **5.2.1.2 Sample size**

The OR of AMD prevalence in first-degree relatives of AMD probands has been estimated at 2.4-19.8 (173, 174); these estimates represent age- and sex- adjusted OR determined by comparing the prevalence of AMD in first-degree relatives of AMD probands with first-degree relatives of normal controls. There are no published data on the prevalence of PDS in first-degree relatives of probands. During efforts to identify PDS families suitable for linkage analysis, the prevalence of PDS in first-degree relatives of PDS probands was found to be approximately 20%. Although no similar study was conducted in relatives of control subjects, a crude estimate for this value is that of the published prevalence of 2.5% found during a screening study of New York office

workers (34). Using these values, the corresponding OR of PDS prevalence in first degree relatives can be estimated to be  $20/2.5=8$ . This approximation falls in the middle of the range for the OR for AMD quoted above, suggesting that a similar proposed sample size may be sufficient. Because the clinical signs of PDS fade with age, there is a risk that parents of probands may have been misclassified as unaffected whereas had they been examined in their 30s or 40s, may have been found to be affected. The prevalence figure of PDS in first-degree relatives might therefore be an underestimate and if this were the case, the OR would be even higher.

### **5.2.1.3 DNA extraction and genotyping**

DNA was extraction from frozen samples was performed by Miss Beverley Scott, BMRC Technician, Department of Genetics, UCL Institute of Ophthalmology. Extracted DNA was assessed for protein contamination using a spectrophotometer (Nanodrop ND-1000; Thermo Fisher Scientific Inc., Wilmington, USA). Samples with 260/230 values < 1.8 were deemed to be contaminated and underwent ethanol precipitation. All samples were electrophoresed on a 1% agarose gel to ensure they were within the 10-15 kbp range. Samples were frozen and shipped to a commercial service (Aros Applied Biotechnology, Denmark) for genotyping on the Illumina 660w Quad beadchip.

#### **5.2.1.4 Quality control**

Quality control (QC) was performed by Miss Cristina Venturini and Dr Pirro Hysi, King's College London, using Plink (175, 176) and 'R' (177). Genotype calling was performed on Illumina GenomeStudio software version 2011.1 (Illumina, San Diego, USA). QC was conducted according to a protocol published by Anderson et al. (178).

#### **5.2.2 Screening for *GPNMB* sequence variants**

Ninety-six unrelated patients were selected from the PDS probands who were originally enrolled when families suitable for linkage analysis were being sought. DNA was extracted from peripheral blood lymphocytes. All 11 exons of *GPNMB* (including the promotor region) were amplified and sequenced on a 3730 DNA Analyser. Results were analysed using Sequence Analysis 5.2 and Sequencher 4.1.4. Potentially significant changes were screened for in a panel of normal DNAs. Variants resulting in amino acid changes were submitted to the following 3 web-based applications to estimate their functional significance: SIFT (179), PolyPhen-2 (180) and PMut (181, 182).

### 5.3 Results

#### 5.3.1 Genome-wide association study

##### 5.3.1.1 Genotyping

A pilot batch of 8 samples was initially genotyped to check call rates (table 5.1).

0.9621
0.9931
0.9959
0.9962
0.9971
0.9973
0.9974
0.9977

**Table 5.1** Illumina 660w Quad beadchip genotyping call rates for 8 ‘pilot’ samples from PDS cohort

On the basis of the above result the remaining 92 samples were genotyped (table 5.2).

0.597	0.829	0.954	0.987	0.995	0.995	0.996	0.996	0.996	0.997	0.997	0.998
0.732	0.900	0.954	0.989	0.995	0.995	0.996	0.996	0.996	0.997	0.997	0.998
0.737	0.917	0.963	0.990	0.995	0.995	0.996	0.996	0.997	0.997	0.997	0.998
0.737	0.925	0.964	0.993	0.995	0.995	0.996	0.996	0.997	0.997	0.997	0.998
0.747	0.933	0.971	0.994	0.995	0.996	0.996	0.996	0.997	0.997	0.997	
0.763	0.933	0.977	0.994	0.995	0.996	0.996	0.996	0.997	0.997	0.997	
0.767	0.948	0.980	0.994	0.995	0.996	0.996	0.996	0.997	0.997	0.998	
0.808	0.951	0.986	0.995	0.995	0.996	0.996	0.996	0.997	0.997	0.998	

**Table 5.2** Illumina 660w Quad beadchip genotyping call rates for remaining samples from PDS cohort

### 5.3.1.2 Quality control

#### 5.3.1.2.1 Per-individual and per-marker missing genotypes

The proportion of missing individuals and SNPs with missing genotypes is shown in figures 5.1 and 5.2 respectively.

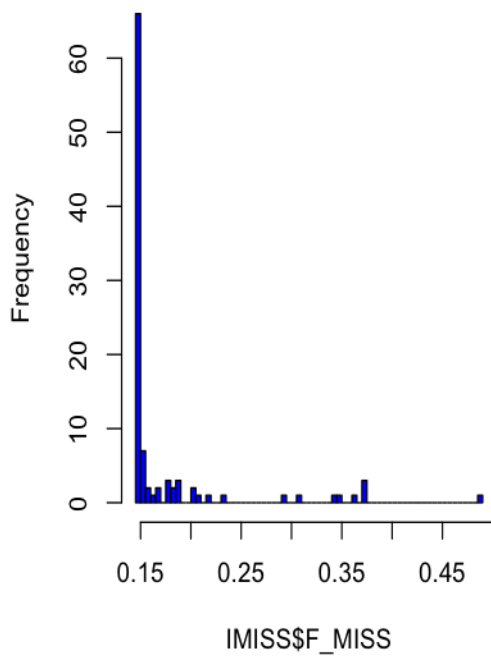


**Figure 5.1**

Proportion (shown on the x-axis) of individuals with missing genotypes

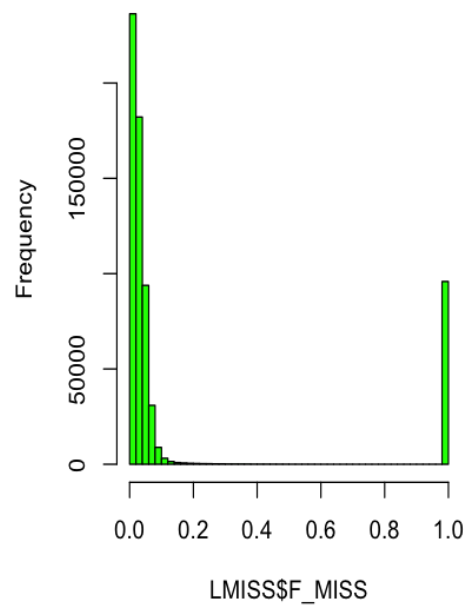


**Figure 5.2**

Proportion of SNPs (shown on the x-axis) with missing genotypes

### 5.3.1.2.2 Sex check

Homozygosity rates across all X-chromosome SNPs are shown figure 5.3. The data show 2 clusters: one around zero for females and another around 1 for males.

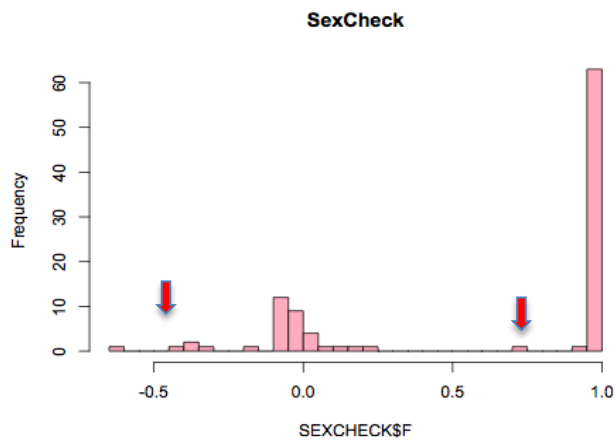


**Figure 5.3** X-chromosome homozygosity (on the x-axis) for PDS cohort. Red arrows indicate clusters away from expected values.

### **5.3.1.2.3 Racial /ethnic ancestry**

Reference population data from HapMap III (183) was used to find racial outliers.

Figures 5.4 and 5.5 show the location of the PDS subjects in comparison with HapMap III populations.

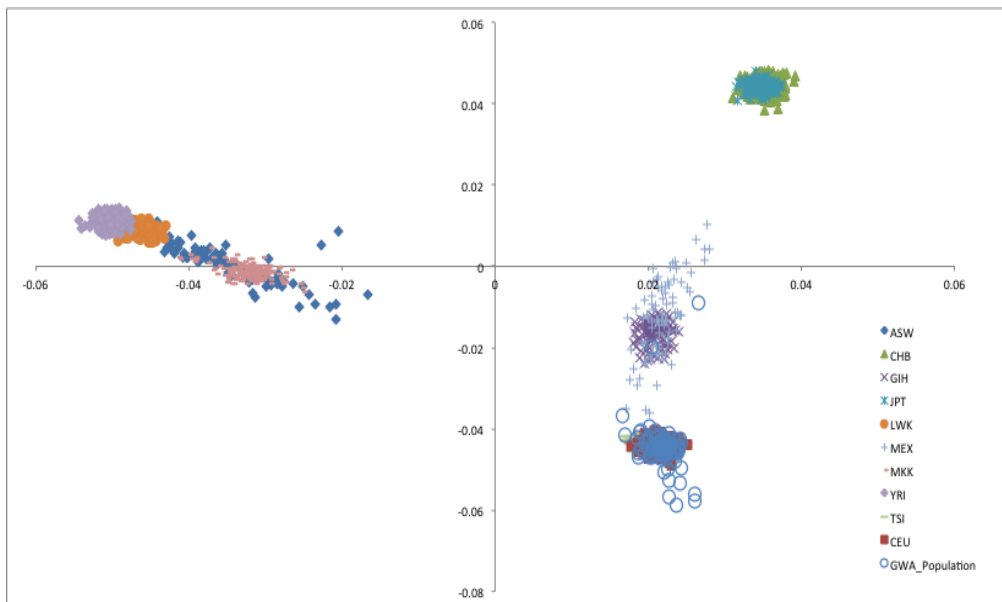


**Figure 5.4a**

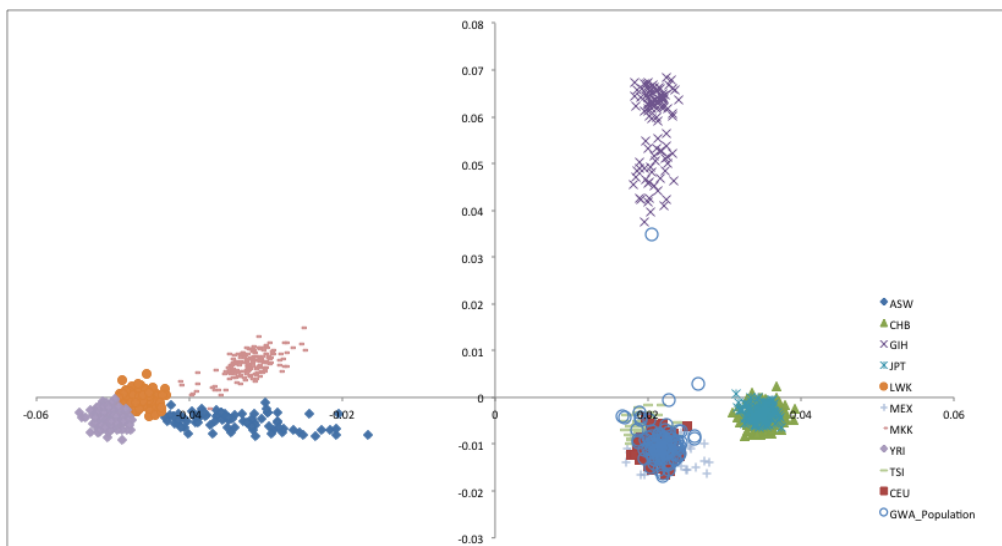


**Figure 5.4b**

**Figure 5.4** Clustering of PDS subjects (blue circles) in comparison with HapMap III populations. The majority of the PDS samples can be seen to cluster with individuals of known Northern and Western European ancestry, confirming that the PDS cohort is mostly genetically homogeneous. One individual can be seen to cluster with individuals of Mexican and Gujarati Indian ancestry and would need to be excluded from the genome-wide analysis. The 3-dimensional data is represented by two 2-dimensional graphs. ASW African ancestry in Southwest USA; CEU Utah residents with Northern and Western European ancestry from the Centre d'Etude du Polymorphisme Humain collection; CHB Han Chinese in Beijing, China; CHD Chinese in Metropolitan Denver, Colorado; GIH Gujarati Indians in Houston, Texas; JPT Japanese in Tokyo, Japan; LWK Luhya in Webuye, Kenya; MXL Mexican ancestry in Los Angeles, California; MKK Maasai in Kinyawa, Kenya; TSI Toscani in Italia; YRI Yoruba in Ibadan, Nigeria

### 5.3.1.2.4 Principal component analysis

Figures 5.5 and 5.6 show plots of principal components 1, 2 and 3. Plots for principal components 4 were similar (data not shown).

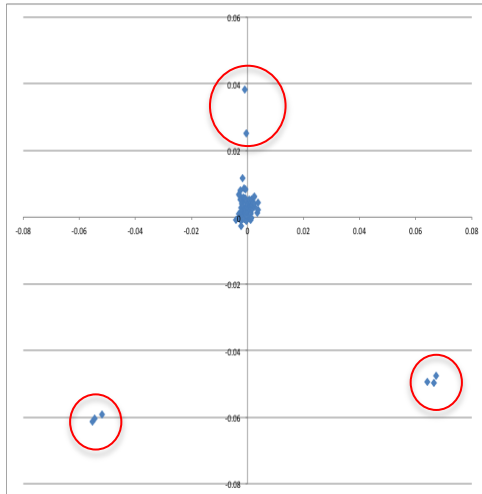


**Figure 5.5**

Plot of principal components 1 and 2 for genotypic data from PDS cohort. Outliers marked in red.

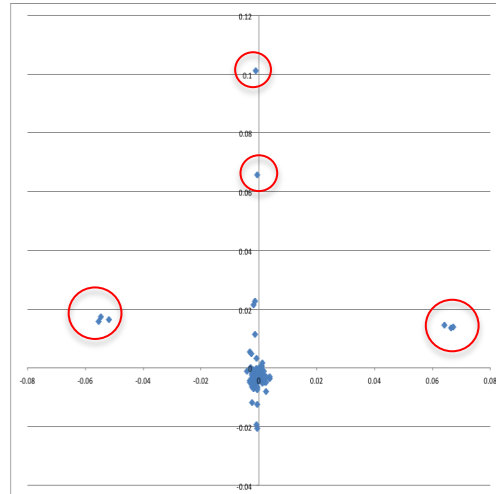


**Figure 5.6**

Plot of principal components 1 and 3 for genotypic data from PDS cohort. Outliers marked in red.

### 5.3.1.2.5 Hardy-Weinberg Equilibrium

A  $p$ -value for departure from Hardy-Weinberg Equilibrium (HWE) for each SNP was computed. The quantile-quantile plot is shown in figure 5.7. There is a departure from HWE after an expected chi-squared of approximately 7.

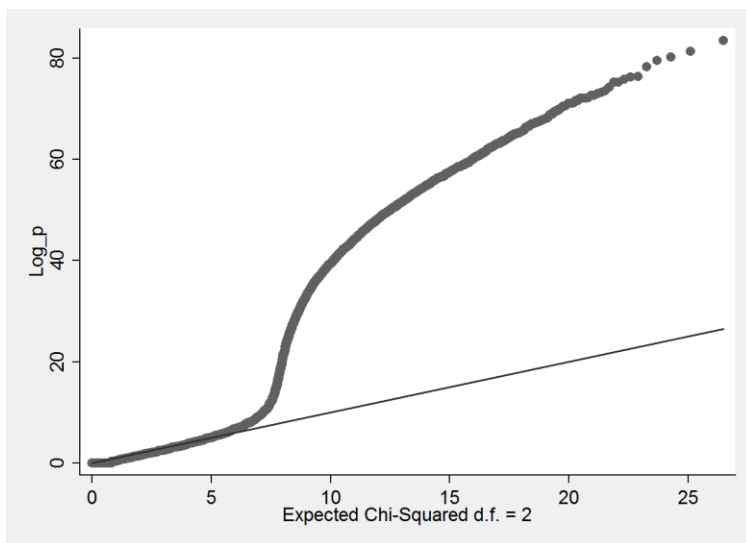


**Figure 5.7** Quantile-quantile plot showing the observed HWE Log  $p$ -values compared to the Log  $p$ -values expected from a theoretical uniform distribution of the HWE probabilities

### 5.3.1.2.6 Heterozygosity

Individual heterozygosity was determined by calculating the ratio between the observed and expected number of heterozygotes. These data are illustrated in figure 5.8.

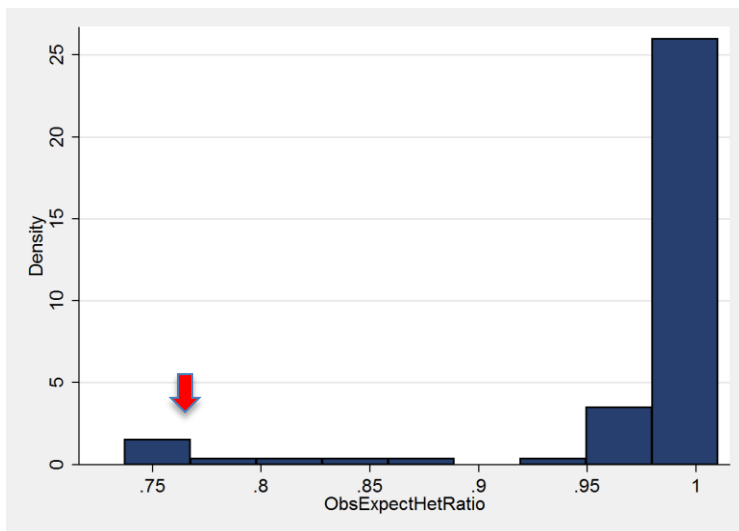


**Figure 5.8** Plot of observed to expected heterozygosity ratio (red arrow indicates the small peak at a ratio of 0.75)

### 5.3.1.2.7 Relatedness

Figure 5.9 depicts the frequency of different values of PI\_HAT, a measured of estimated relatedness between any two samples. There is an apparent excess of sample pairs sharing approximately 20% of their DNA and also a smaller portion of sample pairs sharing between 60 and 85% of their DNA.

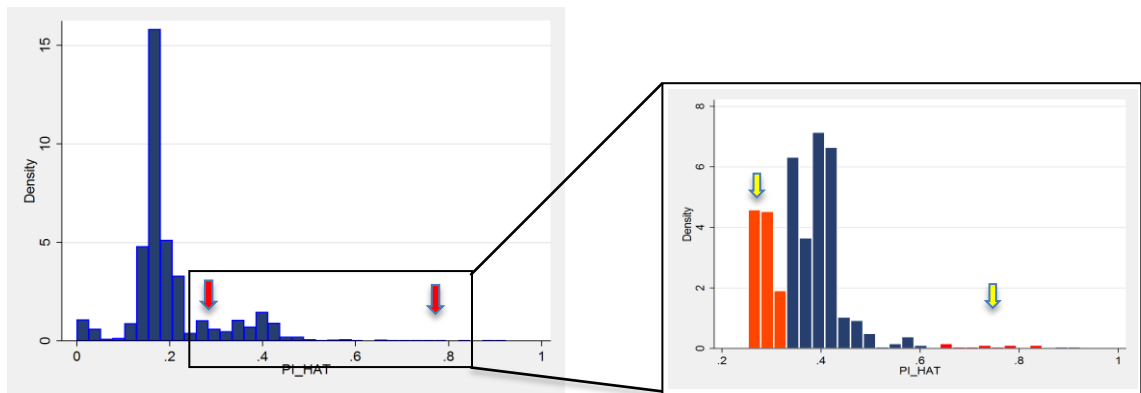


**Figure 5.9** Estimated relatedness (PI-HAT) between any 2 samples in the PDS cohort

### 5.3.2 Screening for *GNMB* sequence variants

One patient was found to have a missense change in exon 6 of *GNMB* (figure 5.10). This protein change, proline to leucine at codon 325, was not present in 182 Caucasian control samples and deemed to be ‘tolerated’, ‘possibly damaging’ and ‘pathological’ according to SIFT, PolyPhen-2 and pMut respectively. Two patients were found to have a c.-179insT in exon 1 proximal to the TATA-like element regulatory region (figure 5.11). The c.-179insT change was present in 1 out of 183 Caucasian control samples.

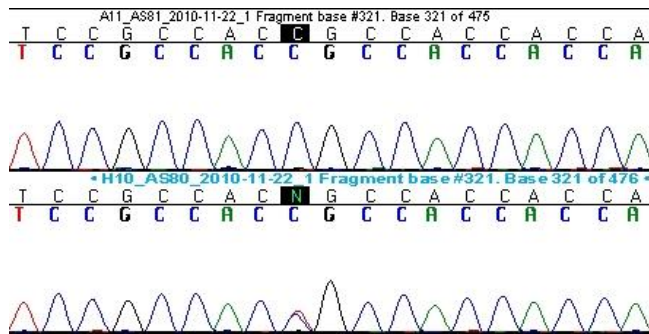


**Figure 5.10** Missense change in exon 6 of *GNMB*. Upper electropherogram shows region of exon 6 in patient with normal sequence. Lower electropherogram from patient showing c.325T missense change in the same region



The patient demonstrating the c.C325T change was a 26 year old white male with a maximum IOP of 32 mmHg right eye and 28 mmHg left eye with no evidence of GON.

Two patients demonstrated the c.-179insT change. The first was a 46 year old Somalian male with maximum IOP of 32 mmHg right eye and 35 mmHg left eye and evidence of bilateral GON. The second was a 55 year old white female with maximum IOP of 22 mmHg right eye and 23 mmHg left eye with no evidence of GON. All 3 patients were phenotypically similar to the rest of the cohort.

## **5.4 Discussion**

### **5.4.1 Genome-wide association study**

#### **5.4.1.1 Quality control**

##### **5.4.1.1.1 Per-individual and per-marker missing genotypes**

Genotypes are determined from probe intensity data by a genotype-calling algorithm within Illumina's proprietary software. The proportion of missing data was investigated for both individuals and SNPs. The QC protocol (178) recommends conducting QC on a 'per-individual' basis before doing so on a 'per-marker' basis to maximize the number of markers remaining in the study; this approach prevents markers from being erroneously removed because of a subset of poorly genotyped individuals, but

individuals may be falsely removed on the basis of a poorly genotyped subset of markers. When testing 550,000 markers, a 1% failure rate equates to 5,500 markers with the associated risk that a disease-associated SNP could be overlooked. For this reason, in a study with a large number of subjects it may be preferable to remove a few individuals rather than a small percentage of markers.

The results are shown in figures 5.1 and 5.2. Figure 5.1 shows that all individuals are missing at least 15% of their genotype information. The Illumina 660W-Quad Beadchip contains a total of 95,865 non-polymorphic probes used to fill in regions under-represented by SNPs. The percentage of missing genotypes seen in all individuals would correlate with the proportion of non-polymorphic probes. The total number of SNPs with missing genotypes was 31,371 and this represents 5.6% of all RS SNPs on the chip; this would appear to correlate with the 31,348 non-polymorphic probes on the chip assigned RS numbers.

#### **5.4.1.1.2 Sex check**

Males cannot be heterozygous for any markers that are on the X chromosome (that is not in the pseudo-autosomal region of the Y chromosome). The expected X-chromosome male homozygosity rate is therefore 1 and that for females is  $< 0.2$  (178). The X-chromosome homozygosity plot (figure 5.3) identifies a few individuals with atypical homozygosity ratios. The peak to the right may represent contamination or a

sex chromosome aberration and these individuals would need to be excluded prior to further analysis.

#### **5.4.1.1.3 Racial/ethnic ancestry**

The majority of samples cluster with HapMap III European-ancestry subjects, but there are clearly outliers who cluster with, for example, ethnic Indian subjects or who do not fall inside of any of the clusters, suggesting admixed individuals. Outliers would need to be excluded prior to further analysis.

#### **5.4.1.1.4 Principal component analysis**

GWA studies may be confounded by population stratification, whereby apparent differences in allele frequencies can arise as a result of divergent ancestry rather than the disease under study (184). Despite efforts to select cases and controls from the same genetically homogenous population, subtle genetic substructure may exist within that population and differences in this substructure between case and control cohorts may give rise to confounding. In the present study this was especially important because: 1) the PDS probands were ascertained retrospectively and formal ancestry history had not been taken, and 2) the PDS probands and myopic control group were recruited from centres in London and may therefore have had greater genetic heterogeneity than a similar group recruited from another part of the UK whose population had been more geographically stable.

Potential stratification was investigated by principal component analysis (PCA) (185, 186), a statistical technique used to produce several uncorrelated variables (or principal components) from a dataset containing potentially correlated variables. The computation is such that the first principal component accounts for the maximum amount of variation the data in a single component; this is followed by the second component and so on. In the context of GWAS, the SNPs are the potentially correlated variables. Genotypic data from populations of known ancestry e.g. HapMap populations, is used to build the PCA model, which can then be applied to a GWAS cohort to predict principal component scores for these samples. Ten subjects in total did not cluster well with the rest of the group and would need to have been removed prior to further analysis.

#### **5.4.1.1.5 Hardy-Weinberg Equilibrium**

At a locus where the only alleles are 'a' or 'A', with frequencies of  $p$  and  $q$  respectively, the Hardy-Weinberg theorem predicts genotype frequencies of AA, Aa and aa to be  $p^2$ ,  $2pq$  and  $q^2$ . SNPs demonstrating this distribution are said to be in Hardy-Weinberg equilibrium. Figure 5.7 shows the expected distribution of association test statistics (X-axis) across the million SNPs compared to the observed values (Y-axis). The departure from the X=Y line implies a bias as the large number of SNPs represented by this departure could not all truly be associated with PDS. As only individuals of clear

European ancestry were included in this analysis this raises questions about sample handling or DNA quality.

#### **5.4.1.1.6 Heterozygosity**

Figure 5.8 illustrates the ratio of observed to expected heterozygosity. There was a peak at 0.75, representing individuals with a low ratio, which may be indicative of inbreeding (178), although this would seem unlikely given the wide catchment area of the clinic from which these patients were recruited.

#### **5.4.1.1.7 Relatedness**

Duplicate or related individuals can be identified by calculating pairwise identity-by-state (IBS), a metric reflecting the proportion of loci at which a pair of individuals share the same alleles. Only independent SNPs are used in calculating IBS and this is achieved by excluding extended regions of linkage disequilibrium (LD) from the data set (187) and editing remaining regions so that only uncorrelated SNP pairs are included. Identity by descent (IBD), the proportion of alleles shared in common due to recent shared ancestry, can be estimated from the IBS data. (175, 176). PLINK calculates PI-HAT, a measure of relatedness derived from IBD. The expectation for an outbred, contamination-free population would be to have most PI-HAT values around 0. Peaks around 0.5 suggests two individuals are 1<sup>st</sup> degree relatives although this would be extremely unlikely as subjects were selected partly on the basis of being

unrelated to each other. Figure 5.9 shows an apparent excess of sample pairs sharing approximately 20% of their DNA and also a smaller portion of sample pairs sharing between 60 and 85% of their DNA; this degree of relatedness is uncharacteristic of contamination-free outbred populations.

#### **5.4.1.2 Conclusion**

The QC issues described above could be explained by low DNA quality and/or DNA contamination. DNA contamination could have arisen during pipetting of reagents: the laboratory work involves handling samples in 96-well plates using 'multi-pipettes' to add reagents to rows of samples at a time. Twenty-four individuals would need to be removed based on the QC analysis and it was felt that further analysis was precluded. Future efforts at conducting a GWA study into pigment dispersion syndrome would benefit from lessons learned from the present study: for any additional patients to be recruited, enquiry into ethnic ancestry should be made in order to exclude individuals known to be racially admixed. A 25% increase in sample size should be aimed for in order to allow for individuals being removed due to poor call rates and racial admixture. Meticulous laboratory technique should be adhered to in order to minimise the risk of sample contamination. Consideration should be given to involving other centres, ensuring uniform phenotyping across sites, in order to achieve the required sample size for the discovery and validation cohort.

#### 5.4.2 Screening for *GPNMB* sequence variants

One patient was found to have a missense change in exon 6 of *GPNMB* and this was not found to be present in 182 Caucasian control samples. This change was predicted to be 'tolerated', 'possibly damaging' and 'pathological' according to SIFT, PolyPhen-2 and pMut respectively. The sequence is evolutionarily conserved in mice and macaques but not in chickens. The subject in whom the c.C325T mutation was identified did not have any family members who were available for phenotyping and genotyping; this change would need to be found in other affected relatives whilst also being absent in unaffected relatives in order to be considered significant.

Two patients were found to have a c.-179insT in exon 1 between an M-box element and a regulatory TATA-like element. The M-box element is the binding site for microphthalmia transcription factor, a factor that has been shown to regulate *Gpnmb* expression in murine osteoclasts (167). The M-box element is the most evolutionarily conserved element in the *GPNMB* promotor, being conserved between at least 11 different species (167). The variant was close to, but did not fall within, any of the recognised regulatory elements and this finding, together with the detection of the change in 1 of the control samples, makes the c.-179insT change less likely to be significant.

Whilst mutations in *GPNMB* are not present in the vast majority of PDS/PG subjects, the detection of one non-synonymous variant indicated that the biochemical pathway

involving GPNMB may be relevant to the molecular basis of PDS/PG. Lu et al. (188) analysed gene expression in mouse strains based on the presence or absence of the R150X Gpnmb mutation and reported that the mutation radically alters the set of genes with which Gpnmb expression is correlated and have described different co-expression networks of genes associated with the mutant and wild-type transcripts. Human homologues of genes in both of these networks would be candidate genes for PDS/PG in man.

## 6 SUMMARY

AS-OCT provides a means to image iris curvature in a relatively physiological way and offers certain advantages over UBM. The results of the agreement study described in chapter 2 validated its use in the measurement of iris concavity. The main disadvantage of AS-OCT, however, is the inability to clearly identify areas of iridolenticular contact, an important parameter to consider when investigating the pathophysiology of pigment dispersion and the effect of LPI. The results of the case-control study indicated that non-accommodative iris concavity is the parameter that best distinguishes cases from controls and this corroborates published data indicating that the increase in iris concavity seen with accommodation is relatively transient and that the iris reverts to a more convex configuration despite accommodative effort being maintained.

LPI in PDS patients is a controversial intervention and robust evidence supporting its use is currently lacking. Ideally a longitudinal, prospective randomized control trial is needed to compare the effect of LPI on the risk of developing subsequent PG. Iris curvature assessments would form an important part of such a study as it would be useful to record any change in iris curvature pre- and post-LPI; whilst changes have been demonstrated in a cross-sectional study using UBM (81), longitudinal studies have not attempted to correlate imaging changes with the risk of developing raised IOP (35) or PG (55).

Although the results of the present study suggest good agreement with respect to measurements on individual AS-OCT images, whether curvature measurements taken on the same patient several hours or several days apart are repeatable has not been established. Future work should therefore assess the repeatability of these measurements over different time points. Fundus autofluorescence imaging represents an important tool to further investigate posterior segment changes in PDS/PG.

Age was significantly associated with iris curvature in both PDS/PG subjects and controls; this association was detected for non-accommodative as well as accommodative iris curvature and was stronger for the latter. The mechanism for the increased concavity on accommodation is not entirely clear; it is unlikely to be purely due to anterior lens movement as it is recognised that increased concavity is short-lived despite continued accommodation. The slope of the curve for age against accommodative iris curvature levels off after 50 years of age and this may well correspond to the reduction in accommodative amplitude associated with presbyopia.

Whilst iris concavity is a frequent finding in PDS, it can also occur in normal subjects and appears to be more common in younger, more myopic individuals. Chapter 3 described a study conducted primarily to investigate the prevalence of iris concavity in a cohort of 10-12 year old boys. Relationships between iris curvature and corneal biomechanical properties and anterior segment biometry were explored and the cohort was revisited 2 years later using an identical data collection protocol. In addition, reported birth weight and measures of height, weight, waist circumference,

digit ratio and percentage body fat were taken in order to explore relationships with myopia. Iris concavity was a common finding in this cohort at baseline and increased in prevalence at the 2-year follow up visit. At both time points iris curvature was related to lens vault, anterior chamber depth and scleral spur angle. Significant association was detected between corneal hysteresis, a parameter thought to represent corneal biomechanical properties, and spur-to-spur distance as measured on horizontal AS-OCT imaging. Screening children of PDS/PG patients for iris concavity on AS-OCT is unlikely to be a useful predictor for development of PDS/PG in adulthood.

Chapter 4 described the results of linkage analysis conducted on a multigenerational family segregating for autosomal dominant PDS/PG. Linkage to the 2 known PDS/PG loci was excluded. Three chromosomal regions of interest were identified and coding regions of candidate genes in the region identified on chromosome 1 were sequenced in one affected and one unaffected member of the pedigree. No pathological sequence variants were identified. Assumptions were made regarding the presumptive affected/unaffected status for deceased individuals that previously provided blood samples for genetic studies into PDS/PG as well as the likely aetiology of GON in older members of the family who did not at the time of examination meet diagnostic criteria for pigment dispersion. In addition, the genetic model underlying the linkage analysis made assumptions e.g. that the disease causing allele is fully penetrant, which cannot, prior to identifying a causative mutation, be verified. Whilst there is the possibility that the regions identified may represent false positives, the development of next generation sequencing, a technology that permits rapid, high

throughput sequencing provides an opportunity for the relatively wide regions of interest to be investigated for putative disease causing variants. In the course of searching for additional families that were suitable for linkage analysis, several smaller families have been recruited with between 1 and 3 affected members and these represents a valuable resource which could be screened for the purpose of attempting to validate any pathological sequence variants that might be identified in the future.

Whilst linkage analysis has been shown to be a powerful technique to identify rare variants with a large effect size, population based association studies are more appropriate for identifying more common alleles with a smaller effect size. High-density oligonucleotide microarrays have enabled the investigation of genome-wide association in more detail with smaller sample sizes than was previously possible. The first part of chapter 5 described efforts to conduct a pilot GWAS involving pigment dispersion samples from PDS/PG patients to identify associated genomic regions. DNA was extracted from these samples and sent to a commercial genotyping service. Genetic epidemiologists conducted the following quality control checks on the raw SNP calls according to a published protocol: missing SNP calls, gender checks, racial/ethnic ancestry checks, departure from Hardy-Weinberg equilibrium, heterozygosity and relatedness. Unfortunately the analysis identified significant problems with the genotypic data which implicated low quality DNA or sample contamination and this precluded taking the data forward to the association stage. Residual DNA from a number of subjects is still available and, providing the above issues could be addressed

and additional patients recruited to achieve the required sample size, it would still be possible to proceed with a genome-wide association study.

Murine *Gpnmb* codes for a transmembrane glycoprotein protein and a mutation in this gene giving rise to a premature stop codon causes the iris pigment dispersion phenotype in DBA/2J mice. The human homologue, located at chromosome 7p15, was considered an excellent candidate for pigment dispersion in man. The second part of chapter 5 reported on the sequencing of the promoter and coding regions of this gene in a panel of unrelated PDS/PG subjects. One patient was found to have a missense change in exon 6, not found to be present in a panel of 182 Caucasian control samples. Whilst this change gives rise to a change in the amino acid sequence, analyses on the significance of this change gave conflicting results. Two patients were found to have a c.-179insT in exon 1 proximal to the TATA-like element regulatory region; the identification of this change in 1 of the control samples suggests that it may not be significant. No other variants in *GPNMB* were detected in the remaining 93 samples.

There are a number of directions for future work building on the work described in the thesis. The key next studies would be:

1. Exploring the repeatability of iris curvature measurements with AS-OCT over multiple time points. This would be a key study in validating AS-OCT as a tool for quantifying iris curvature.

2. A prospective longitudinal RCT investigating the effect of LPI on the risk of developing raised IOP, using the fellow eye as a control eye. The results of the Gandolfi study (35) would be used in the power calculation to determine an appropriate sample size. PDS subjects without OHT or GON would need to be actively recruited from the community in an effort to minimise ascertainment bias that would arise from recruiting from a hospital-based glaucoma clinic. Following the untreated eye would provide valuable data on the natural history of PDS.
  
3. Analysis of the PDS pedigree described in Chapter 4 using exome sequencing, a technology that would provide sequencing data for coding regions across the whole genome for all family members. The results of the linkage analysis would be used to focus on those regions already found to have promising LOD scores in order to narrow down search for variants segregating with affected family members.
  
4. Further recruitment of PDS subjects for the GWA study. Rigorous testing of extracted DNA would need to be performed with meticulous attention to laboratory technique in order to minimise the risk of DNA contamination.

## **7 APPENDIX**

- 7.1 Protocol for DNA preparation prior to genotyping on Affymetrix 50K  
Genechip
  
- 7.2 Protocol for ethanol precipitation for extracted DNA samples not  
meeting QC criteria on spectrophotometry

**Appendix 1** Protocol for DNA preparation prior to genotyping on Affymetrix 50K  
Genechip

DNA was prepared according to the following protocol prior to sending samples to the Wolfson Institute for Biomedical Research (WIBR) for hybridisation, washing/staining and scanning. The volumes of reagent indicated are per sample of DNA unless otherwise stated.

**Digestion**

The following digestion master mix was prepared in a DNA/amplicon free hood.

Nuclease-free H <sub>2</sub> O	12.3 µl
NE Buffer 2(10X)	2 µl
BSA (10X (1mg/ml))	0.2µl
XbaI (20U/ul)	0.5 µl
<b>Total</b>	<b>15 µl</b>

15 µl of master mix was added to 5 µl of the previously diluted DNA.

The samples were run in a thermal cycler at 37°C for 2 hours then 70°C for 20 mins.

**Ligation**

The following master mix was prepared on ice:

Adaptor Xba (5µM)	1.25 µl
T4 DNA ligase buffer (10x)	2.5 µl
T4 LIGASE (400U/µl)	0.625 µl
H <sub>2</sub> O	0.625 µl
<b>Total</b>	<b>5 µl</b>

5  $\mu\text{l}$  of the ligase mix was added to 20  $\mu\text{l}$  of digested DNA.

The samples were run in a thermal cycler at 16°C for 2 hours then 70°C for 20 mins.

75  $\mu\text{l}$  nuclease-free H<sub>2</sub>O was added to the 25  $\mu\text{l}$  ligated solution.

### **Polymerase chain reaction (PCR)**

The following master mix was prepared on ice:

H <sub>2</sub> O	132 $\mu\text{l}$
Pfx buffer	30 $\mu\text{l}$
PCR enhancer	30 $\mu\text{l}$
MgSO <sub>4</sub> (50mM)	6 $\mu\text{l}$
dNTP (2.5mM)	36 $\mu\text{l}$
PCR Primer (10 $\mu\text{M}$ )	30 $\mu\text{l}$
Pfx Polymerase	6 $\mu\text{l}$
<b>Total</b>	<b>270 <math>\mu\text{l}</math></b>

The total volume per sample of 270  $\mu\text{l}$  was aliquoted into 3 tubes of 90  $\mu\text{l}$  each. 10  $\mu\text{l}$  of diluted ligated DNA was mixed with 90  $\mu\text{l}$  of PCR master mix. Three batches per DNA sample were prepared. The samples were run in a thermal cycler as follows:

Initial denaturation	94°C for 3 min	1 cycle
Denaturation	94°C for 30 s	30 cycles
Annealing	60°C for 45 s	
Extension	68°C for 1 min	
Final extension	68°C for 7 min	1 cycle

4  $\mu\text{l}$  of each PCR product was mixed with 1  $\mu\text{l}$  loading dye on 2% tris-acetate-EDTA gel at 120V for 1 hour.

### **Purification, quantification and normalization**

The three PCR reactions for each sample were consolidated into one well of a MinElute plate. A vacuum of 800 mmHg was applied until the wells were completely dry. PCR products were washed by adding 50  $\mu$ l nuclease-free water and maintaining the vacuum until the wells were completely empty. This step was repeated 2 additional times for a total of 3 water washes. The vacuum source was then switched off and the MinElute plate was removed from the vacuum manifold. 40  $\mu$ l EB buffer was added to each well. A plastic plate sealer was applied and the plate was shaken for 5 minutes at moderate speed. The re-suspended samples were then pipetted into a clean plate. 2  $\mu$ l of sample was quantified on a Nanodrop™ spectrophotometer. Samples were normalized to 40  $\mu$ g/45  $\mu$ l using EB.

### **Fragmentation**

45  $\mu$ l purified PCR product was mixed with 5  $\mu$ l 10x Fragmentation Buffer (FB), vortexed for 2 seconds and placed back on ice. This mixture constitutes the Fragmentation PCR Mix (FPM).

Fragmentation reagent was diluted as follows:

REAGENTS	3U/ $\mu$ L
FR ( <i>DNase I</i> )	2 $\mu$ L
FB X10	15 $\mu$ L
H <sub>2</sub> O	133 $\mu$ L

This was vortexed for 2 seconds and placed back on ice. 5  $\mu$ l diluted FR was mixed with 50  $\mu$ l FPM, vortexed for 2 seconds and placed back on ice. The samples were run on a

thermal cycler as at 37°C for 30mins and then 95°C for 15 mins. 4 µL of product was run on a 4% tris-acetate-EDTA agarose gel at 120V.

### Labelling

Labelling master mix (LMM) was prepared on ice as follows:

5x TdT Buffer	14 µl
GeneChip DNA Labeling Reagent (7.5mM)	2 µl
TdT (30U/µL)	3.5 µl
TOTAL	19.5 µl

The mixture was vortexed for 2 seconds and placed back on ice. 19.5 µL LMM was added to 50.5 µl of fragmented sample on ice, vortexed for 2 seconds and placed back on ice. The samples were then run on a thermal cycler at 37°C for 2hours and then 95°C for 15 mins. Samples were then stored at -20°C.

**Appendix 2** Protocol for ethanol precipitation for extracted DNA samples not meeting QC criteria on spectrophotometry

50  $\mu$ l of DNA was mixed with 5  $\mu$ l of 3M sodium acetate and 125  $\mu$ l 100 % ethanol.

This was briefly vortexed and spun for 20 minutes in a centrifuge at 12000 rpm at 4°C.

The supernatant was carefully aspirated and discarded taking care not to aspirate the DNA pellet at the base of the tube.

1 mL of cold 70% ethanol was added. This was spun for 10 minutes at 12000 rpm at 4°C and the supernatant was carefully aspirated and discarded as above. The DNA pellet was left to air dry for 10 minutes at room temperature and dissolved in 40  $\mu$ l Elution Buffer (EB) (10 mM Tris-HCl pH 7.5). The optical density of the eluted DNA was measured using a NanoDrop spectrophotometer. The ratio of absorbance at 260 nm and 280 nm of approximately 1.8 was considered acceptable and a ratio of absorbance at 260 nm and 230 nm between 1.8 and 2.2 was considered acceptable. DNA was diluted to a concentration of 50 ng/ $\mu$ l.

## 8 REFERENCES

1. Foster PJ, Buhrmann R, Quigley HA, Johnson GJ. The definition and classification of glaucoma in prevalence surveys. *Br J Ophthalmol*. 2002;86(2):238-42. Epub 2002/01/30.
2. Resnikoff S, Pascolini D, Etya'ale D, Kocur I, Pararajasegaram R, Pokharel GP, et al. Global data on visual impairment in the year 2002. *Bulletin of the World Health Organization*. 2004;82(11):844-51. Epub 2005/01/11.
3. Quigley HA, Broman AT. The number of people with glaucoma worldwide in 2010 and 2020. *Br J Ophthalmol*. 2006;90(3):262-7. Epub 2006/02/21.
4. In Cantor L, Fechtner RD, Michael AJ, Simmons ST, Wilson MR, Brown SVL. *Basic and Clinical Science Course, Section 10 Glaucoma: The Foundation of the American Academy of Ophthalmology*.; 2002.
5. The effectiveness of intraocular pressure reduction in the treatment of normal-tension glaucoma. Collaborative Normal-Tension Glaucoma Study Group. *Am J Ophthalmol*. 1998;126(4):498-505. Epub 1998/10/21.
6. National Institute for Health and Clinical Excellence Glaucoma. Diagnosis and management of chronic open angle glaucoma and ocular hypertension. CG85. 2009. <http://guidance.nice.org.uk/CG85>.

7. Leske MC. Ocular perfusion pressure and glaucoma: clinical trial and epidemiologic findings. *Current opinion in ophthalmology*. 2009;20(2):73-8. Epub 2009/02/26.
8. Sena DF, Lindsley K. Neuroprotection for treatment of glaucoma in adults. *The Cochrane database of systematic reviews*. 2013;2:CD006539. Epub 2013/03/02.
9. Stein JD, Challa P. Mechanisms of action and efficacy of argon laser trabeculoplasty and selective laser trabeculoplasty. *Current opinion in ophthalmology*. 2007;18(2):140-5. Epub 2007/02/16.
10. Rolim de Moura C, Paranhos A, Jr., Wormald R. Laser trabeculoplasty for open angle glaucoma. *The Cochrane database of systematic reviews*. 2007(4):CD003919. Epub 2007/10/19.
11. Samples JR, Singh K, Lin SC, Francis BA, Hodapp E, Jampel HD, et al. Laser trabeculoplasty for open-angle glaucoma: a report by the american academy of ophthalmology. *Ophthalmology*. 2011;118(11):2296-302. Epub 2011/08/19.
12. Kramer TR, Noecker RJ. Comparison of the morphologic changes after selective laser trabeculoplasty and argon laser trabeculoplasty in human eye bank eyes. *Ophthalmology*. 2001;108(4):773-9. Epub 2001/04/12.
13. O'Brart DP, Rowlands E, Islam N, Noury AM. A randomised, prospective study comparing trabeculectomy augmented with antimetabolites with a viscocanalostomy technique for the management of open angle glaucoma

- uncontrolled by medical therapy. Br J Ophthalmol. 2002;86(7):748-54. Epub 2002/06/27.
14. O'Brart DP, Shiew M, Edmunds B. A randomised, prospective study comparing trabeculectomy with viscocanalostomy with adjunctive antimetabolite usage for the management of open angle glaucoma uncontrolled by medical therapy. Br J Ophthalmol. 2004;88(8):1012-7. Epub 2004/07/20.
  15. Carassa RG, Bettin P, Fiori M, Brancato R. Viscocanalostomy versus trabeculectomy in white adults affected by open-angle glaucoma: a 2-year randomized, controlled trial. Ophthalmology. 2003;110(5):882-7. Epub 2003/05/17.
  16. Mendrinos E, Mermoud A, Shaarawy T. Nonpenetrating glaucoma surgery. Surv Ophthalmol. 2008;53(6):592-630. Epub 2008/11/26.
  17. Gedde SJ, Singh K, Schiffman JC, Feuer WJ. The Tube Versus Trabeculectomy Study: interpretation of results and application to clinical practice. Curr Opin Ophthalmol. 2012;23(2):118-26. Epub 2012/01/18.
  18. Azuara-Blanco A, Burr JM, Cochran C, Ramsay C, Vale L, Foster P, et al. The effectiveness of early lens extraction with intraocular lens implantation for the treatment of primary angle-closure glaucoma (EAGLE): study protocol for a randomized controlled trial. Trials. 2011;12:133. Epub 2011/05/25.
  19. Huang G, Gonzalez E, Peng PH, Lee R, Leeungurasatien T, He M, et al. Anterior chamber depth, iridocorneal angle width, and intraocular pressure changes

- after phacoemulsification: narrow vs open iridocorneal angles. Arch Ophthalmol. 2011;129(10):1283-90. Epub 2011/10/12.
20. Lam DS, Leung DY, Tham CC, Li FC, Kwong YY, Chiu TY, et al. Randomized trial of early phacoemulsification versus peripheral iridotomy to prevent intraocular pressure rise after acute primary angle closure. Ophthalmology. 2008;115(7):1134-40. Epub 2008/01/01.
  21. Sugar HS, Barbour FA. Pigmentary glaucoma; a rare clinical entity. Am J Ophthalmol. 1949;32(1):90-2. Epub 1949/01/01.
  22. Sugar HS. Pigmentary glaucoma. A 25-year review. Am J Ophthalmol. 1966;62(3):499-507. Epub 1966/09/01.
  23. Ritch R. A unification hypothesis of pigment dispersion syndrome. Trans Am Ophthalmol Soc. 1996;94:381-405; discussion -9. Epub 1996/01/01.
  24. Feibel RM, Perlmutter JC. Anisocoria in the pigmentary dispersion syndrome. Am J Ophthalmol. 1990;110(6):657-60. Epub 1990/12/15.
  25. Bellows JG. Krukenberg spindle and its relation to annular pigmented band on periphery of the lens. Arch Ophthalmol. 1944;32(6):480-2.
  26. Davidson JA, Brubaker RF, Ilstrup DM. Dimensions of the anterior chamber in pigment dispersion syndrome. Arch Ophthalmol. 1983;101(1):81-3. Epub 1983/01/01.

27. Weseley P, Liebmann J, Walsh JB, Ritch R. Lattice degeneration of the retina and the pigment dispersion syndrome. *Am J Ophthalmol.* 1992;114(5):539-43. Epub 1992/11/15.
28. Scuderi G, Papale A, Nucci C, Cerulli L. Retinal involvement in pigment dispersion syndrome. *Int Ophthalmol.* 1995;19(6):375-8. Epub 1995/01/01.
29. Scheie HG, Cameron JD. Pigment dispersion syndrome: a clinical study. *Br J Ophthalmol.* 1981;65(4):264-9. Epub 1981/04/01.
30. Farrar SM, Shields MB, Miller KN, Stoup CM. Risk factors for the development and severity of glaucoma in the pigment dispersion syndrome. *Am J Ophthalmol.* 1989;108(3):223-9. Epub 1989/09/15.
31. Farrar SM, Shields MB. Current concepts in pigmentary glaucoma. *Surv Ophthalmol.* 1993;37(4):233-52. Epub 1993/01/01.
32. Siddiqui Y, Ten Hulzen RD, Cameron JD, Hodge DO, Johnson DH. What is the risk of developing pigmentary glaucoma from pigment dispersion syndrome? *Am J Ophthalmol.* 2003;135(6):794-9. Epub 2003/06/06.
33. Migliazzo CV, Shaffer RN, Nykin R, Magee S. Long-term analysis of pigmentary dispersion syndrome and pigmentary glaucoma. *Ophthalmology.* 1986;93(12):1528-36. Epub 1986/12/01.
34. Ritch R, Steinberger D, Liebmann JM. Prevalence of pigment dispersion syndrome in a population undergoing glaucoma screening. *Am J Ophthalmol.* 1993;115(6):707-10. Epub 1993/06/15.

35. Gandolfi SA, Vecchi M. Effect of a YAG laser iridotomy on intraocular pressure in pigment dispersion syndrome. *Ophthalmology*. 1996;103(10):1693-5. Epub 1996/10/01.
36. Ungaro N SC, Vecchi M, Cimino L, Tardini L, Gandolfi SA. YAG-laser iridotomy in pigment dispersion syndrome:10 years later. *Invest Ophthalmol Vis Sci*. 2003;44(E-Abstract 4293).
37. Minassian D and Reidy A (2009). Future Sight Loss UK2: An epidemiological and economic model for sight loss in the decade 2010-2020. *Epivision and RNIB*.
38. Campbell DG. Pigmentary dispersion and glaucoma. A new theory. *Arch Ophthalmol*. 1979;97(9):1667-72. Epub 1979/09/01.
39. Karickhoff JR. Pigmentary dispersion syndrome and pigmentary glaucoma: a new mechanism concept, a new treatment, and a new technique. *Ophthalmic surgery*. 1992;23(4):269-77. Epub 1992/04/01.
40. Pavlin CJ, Macken P, Trope G, Feldman F, Harasiewicz K, Foster FS. Ultrasound biomicroscopic features of pigmentary glaucoma. *Can J Ophthalmol*. 1994;29(4):187-92. Epub 1994/08/01.
41. Liu L, Ong EL, Crowston J. The concave iris in pigment dispersion syndrome. *Ophthalmology*. 118(1):66-70. Epub 2010/08/31.
42. Adam RS, Pavlin CJ, Ulanski LJ. Ultrasound biomicroscopic analysis of iris profile changes with accommodation in pigmentary glaucoma and relationship to age. *Am J Ophthalmol*. 2004;138(4):652-4. Epub 2004/10/19.

43. Drexler W, Baumgartner A, Findl O, Hitzenberger CK, Fercher AF. Biometric investigation of changes in the anterior eye segment during accommodation. *Vision Res.* 1997;37(19):2789-800. Epub 1997/11/28.
44. Dorairaj S, Oliveira C, Fose AK, Liebmann JM, Tello C, Barocas VH, et al. Accommodation-induced changes in iris curvature. *Exp Eye Res.* 2008;86(2):220-5. Epub 2008/01/01.
45. Richardson TM, Hutchinson BT, Grant WM. The outflow tract in pigmentary glaucoma: a light and electron microscopic study. *Arch Ophthalmol.* 1977;95(6):1015-25. Epub 1977/06/01.
46. Alvarado JA, Murphy CG. Outflow obstruction in pigmentary and primary open angle glaucoma. *Arch Ophthalmol.* 1992;110(12):1769-78. Epub 1992/12/01.
47. Haynes WL, Thompson HS, Johnson AT, Alward WL. Comparison of the miotic effects of dapiprazole and dilute pilocarpine in patients with the pigment dispersion syndrome. *J Glaucoma.* 1995;4(6):379-85. Epub 1995/12/01.
48. Beasley H, Fraunfelder FT. Retinal detachments and topical ocular miotics. *Ophthalmology.* 1979;86(1):95-8. Epub 1979/01/01.
49. Lehto I. Long-term follow up of argon laser trabeculoplasty in pigmentary glaucoma. *Ophthalmic Surg.* 1992;23(9):614-7. Epub 1992/09/01.
50. Lunde MW. Argon laser trabeculoplasty in pigmentary dispersion syndrome with glaucoma. *Am J Ophthalmol.* 1983;96(6):721-5. Epub 1983/12/01.

51. Ritch R, Liebmann J, Robin A, Pollack IP, Harrison R, Levene RZ, et al. Argon laser trabeculoplasty in pigmentary glaucoma. *Ophthalmology*. 1993;100(6):909-13. Epub 1993/06/01.
52. Ayala M. Long-term outcomes of selective laser trabeculoplasty (SLT) treatment in pigmentary glaucoma patients. *J Glaucoma*. 2013. Epub 2013/02/23.
53. Kouchehi B, Hashemi H. Selective laser trabeculoplasty in the treatment of open-angle glaucoma. *J Glaucoma*. 2012;21(1):65-70. Epub 2011/02/01.
54. Harasymowycz PJ, Papamatheakis DG, Latina M, De Leon M, Lesk MR, Damji KF. Selective laser trabeculoplasty (SLT) complicated by intraocular pressure elevation in eyes with heavily pigmented trabecular meshworks. *Am J Ophthalmol*. 2005;139(6):1110-3. Epub 2005/06/15.
55. Scott A, Kotecha A, Bunce C, Balidis M, Garway-Heath DF, Miller MH, et al. YAG peripheral iridotomy for the prevention of pigment dispersion glaucoma: a prospective randomized controlled trial. *Ophthalmology*. 2011;118(3):468-73.
56. Reistad CE, Shields MB, Campbell DG, Ritch R, Wang JC, Wand M. The influence of peripheral iridotomy on the intraocular pressure course in patients with pigmentary glaucoma. *J Glaucoma*. 2005;14(4):255-9. Epub 2005/07/02.
57. Becker B, Shin DH, Cooper DG, Kass MA. The pigment dispersion syndrome. *Am J Ophthalmol*. 1977;83(2):161-6. Epub 1977/02/01.
58. Shin DH, Sugar HS. HLA in pigment dispersion and glaucoma. *Tissue antigens*. 1982;19(4):301-5. Epub 1982/04/01.

59. Gramer E, Thiele H, Ritch R. [Family history of glaucoma and risk factors in pigmentary glaucoma. A new clinical study]. *Klin Monbl Augenheilkd*. 1998;212(6):454-64. Epub 1998/08/26. Familienanamnese Glaukom und Risikofaktoren bei Pigmentglaukom. Eine klinische Studie.
60. Bovell AM, Damji KF, Dohadwala AA, Hodge WG, Allingham RR. Familial occurrence of pigment dispersion syndrome. *Can J Ophthalmol*. 2001;36(1):11-7. Epub 2001/03/03.
61. Kaiser-Kupfer MI, Kupfer C, McCain L. Asymmetric pigment dispersion syndrome. *Trans Am Ophthalmol Soc*. 1983;81:310-24. Epub 1983/01/01.
62. Mandelkorn RM, Hoffman ME, Olander KW, Zimmerman TJ, Harsha D. Inheritance and the pigmentary dispersion syndrome. *Ophthalmic Paediatr Genet*. 1985;6(1-2):325-31. Epub 1985/08/01.
63. Andersen JS, Pralea AM, DelBono EA, Haines JL, Gorin MB, Schuman JS, et al. A gene responsible for the pigment dispersion syndrome maps to chromosome 7q35-q36. *Arch Ophthalmol*. 1997;115(3):384-8. Epub 1997/03/01.
64. Wagner SH, DelBono E, Greenfield DS, Parrish RK, Haines JL, Wiggs JL. A second locus for pigment dispersion syndrome maps to chromosome 18q21. *Invest Ophthalmol Vis Sci*. 2005;46(E-Abstract 29.).
65. Nakamura K, Ota M, Meguro A, Nomura N, Kashiwagi K, Mabuchi F, et al. Association of microsatellite polymorphisms of the GPDS1 locus with normal

tension glaucoma in the Japanese population. *Clin Ophthalmol*. 2009;3:307-12. Epub 2009/08/12.

66. John SW, Smith RS, Savinova OV, Hawes NL, Chang B, Turnbull D, et al. Essential iris atrophy, pigment dispersion, and glaucoma in DBA/2J mice. *Invest Ophthalmol Vis Sci*. 1998;39(6):951-62. Epub 1998/05/14.
67. Anderson MG, Smith RS, Hawes NL, Zabaleta A, Chang B, Wiggs JL, et al. Mutations in genes encoding melanosomal proteins cause pigmentary glaucoma in DBA/2J mice. *Nat Genet*. 2002;30(1):81-5. Epub 2001/12/18.
68. Schraermeyer M, Schnichels S, Julien S, Heiduschka P, Bartz-Schmidt KU, Schraermeyer U. Ultrastructural analysis of the pigment dispersion syndrome in DBA/2J mice. *Graefes Arch Clin Exp Ophthalmol*. 2009;247(11):1493-504. Epub 2009/07/31.
69. Becker B, Podos SM. Krukenberg's spindles and primary open-angle glaucoma. *Trans Am Ophthalmol Soc*. 1966;64:135-47. Epub 1966/01/01.
70. Stone EM, Fingert JH, Alward WL, Nguyen TD, Polansky JR, Sunden SL, et al. Identification of a gene that causes primary open angle glaucoma. *Science*. 1997;275(5300):668-70. Epub 1997/01/31.
71. Sheffield VC, Stone EM, Alward WL, Drack AV, Johnson AT, Streb LM, et al. Genetic linkage of familial open angle glaucoma to chromosome 1q21-q31. *Nat Genet*. 1993;4(1):47-50. Epub 1993/05/01.

72. Gong G, Kosoko-Lasaki O, Haynatzki GR, Wilson MR. of myocilin glaucoma. *Hum Mol Genet.* 2004;13 Spec No 1:R91-102. Epub 2004/02/07.
73. Fingert JH, Heon E, Liebmann JM, Yamamoto T, Craig JE, Rait J, et al. Analysis of myocilin mutations in 1703 glaucoma patients from five different populations. *Human molecular genetics.* 1999;8(5):899-905. Epub 1999/04/10.
74. Allingham RR, Liu Y, Rhee DJ. The genetics of primary open-angle glaucoma: a review. *Exp Eye Res.* 2009;88(4):837-44. Epub 2008/12/09.
75. Graul TA, Kwon YH, Zimmerman MB, Kim CS, Sheffield VC, Stone EM, et al. A case-control comparison of the clinical characteristics of glaucoma and ocular hypertensive patients with and without the myocilin Gln368Stop mutation. *Am J Ophthalmol.* 2002;134(6):884-90. Epub 2002/12/10.
76. Wiggs JL, Vollrath D. Molecular and clinical evaluation of a patient hemizygous for TIGR/MYOC. *Arch Ophthalmol.* 2001;119(11):1674-8. Epub 2001/11/16.
77. Vincent AL, Billingsley G, Buys Y, Levin AV, Priston M, Trope G, et al. Digenic inheritance of early-onset glaucoma: CYP1B1, a potential modifier gene. *Am J Hum Genet.* 2002;70(2):448-60. Epub 2002/01/05.
78. Faucher M, Anctil JL, Rodrigue MA, Duchesne A, Bergeron D, Blondeau P, et al. Founder TIGR/myocilin mutations for glaucoma in the Quebec population. *Hum Mol Genet.* 2002;11(18):2077-90. Epub 2002/08/22.

79. Alward WL, Kwon YH, Khanna CL, Johnson AT, Hayreh SS, Zimmerman MB, et al. Variations in the myocilin gene in patients with open-angle glaucoma. *Arch Ophthalmol*. 2002;120(9):1189-97. Epub 2002/09/07.
80. Paglinauan C, Haines JL, Del Bono EA, Schuman J, Stawski S, Wiggs JL. Exclusion of chromosome 1q21-q31 from linkage to three pedigrees affected by the pigment-dispersion syndrome. *Am J Hum Genet*. 1995;56(5):1240-3. Epub 1995/05/01.
81. Carassa RG, Bettin P, Fiori M, Brancato R. Nd:YAG laser iridotomy in pigment dispersion syndrome: an ultrasound biomicroscopic study. *Br J Ophthalmol*. 1998;82(2):150-3. Epub 1998/06/05.
82. Balidis MO, Bunce C, Sandy CJ, Wormald RP, Miller MH. Iris configuration in accommodation in pigment dispersion syndrome. *Eye (London, England)*. 2002;16(6):694-700. Epub 2002/11/20.
83. Liebmann JM, Tello C, Chew SJ, Cohen H, Ritch R. Prevention of blinking alters iris configuration in pigment dispersion syndrome and in normal eyes. *Ophthalmology*. 1995;102(3):446-55. Epub 1995/03/01.
84. Caprioli J, Spaeth GL, Wilson RP. Anterior chamber depth in open angle glaucoma. *The British journal of ophthalmology*. 1986;70(11):831-6. Epub 1986/11/01.

85. Sokol J, Stegman Z, Liebmann JM, Ritch R. Location of the iris insertion in pigment dispersion syndrome. *Ophthalmology*. 1996;103(2):289-93. Epub 1996/02/01.
86. Mora P, Sangermani C, Ghirardini S, Carta A, Ungaro N, Gandolfi S. Ultrasound biomicroscopy and iris pigment dispersion: a case--control study. *Br J Ophthalmol*. 2009;94(4):428-32. Epub 2009/10/14.
87. Laemmer R, Bellios N, Juenemann AGM, Mardin CY. Anterior segment morphometry using optical coherence tomography in patients with primary pigment dispersion syndrome. *ARVO 2008*. E-Abstract 5072.
88. Li H, Leung CK, Cheung CY, Wong L, Pang CP, Weinreb RN, et al. Repeatability and reproducibility of anterior chamber angle measurement with anterior segment optical coherence tomography. *Br J Ophthalmol*. 2007;91(11):1490-2. Epub 2007/05/04.
89. Balidis MO, Bunce C, Boboridis K, Salzman J, Wormald RP, Miller MH. Intraobserver and interobserver reliability of the R/D score for evaluation of iris configuration by ultrasound biomicroscopy, in patients with pigment dispersion syndrome. *Eye (London, England)*. 2002;16(6):722-6. Epub 2002/11/20.
90. Bunce C. Correlation, agreement, and Bland-Altman analysis: statistical analysis of method comparison studies. *Am J Ophthalmol*. 2009;148(1):4-6. Epub 2009/06/23.

91. Nongpiur ME, He M, Amerasinghe N, Friedman DS, Tay WT, Baskaran M, et al. Lens vault, thickness, and position in Chinese subjects with angle closure. *Ophthalmology*. 2011;118(3):474-9. Epub 2010/11/03.
92. Pavlin CJ, Harasiewicz K, Foster FS. Ultrasound biomicroscopy of anterior segment structures in normal and glaucomatous eyes. *Am J Ophthalmol*. 1992;113(4):381-9. Epub 1992/04/15.
93. Radhakrishnan S, Goldsmith J, Huang D, Westphal V, Dueker DK, Rollins AM, et al. Comparison of optical coherence tomography and ultrasound biomicroscopy for detection of narrow anterior chamber angles. *Arch Ophthalmol*. 2005;123(8):1053-9. Epub 2005/08/10.
94. DeLong ER, DeLong DM, Clarke-Pearson DL. Comparing the areas under two or more correlated receiver operating characteristic curves: a nonparametric approach. *Biometrics*. 1988;44(3):837-45. Epub 1988/09/01.
95. Motulsky HJ, Brown RE. Detecting outliers when fitting data with nonlinear regression - a new method based on robust nonlinear regression and the false discovery rate. *BMC bioinformatics*. 2006;7:123. Epub 2006/03/11.
96. Laemmer R, Mardin CY, Juenemann AGM. Visualization of changes of the iris configuration after peripheral laser iridotomy in primary melanin dispersion syndrome using optical coherence tomograph. *J Glaucoma*. 2008;17(7):569-70.
97. Lagreze WD, Mathieu M, Funk J. The role of YAG-laser iridotomy in pigment dispersion syndrome. *Ger J Ophthalmol*. 1996;5(6):435-8. Epub 1996/11/01.

98. Haargaard B, Jensen PK, Kessing SV, Nissen OI. Exercise and iris concavity in healthy eyes. *Acta Ophthalmol Scand.* 2001;79(3):277-82. Epub 2001/06/13.
99. Saw SM, Chua WH, Gazzard G, Koh D, Tan DT, Stone RA. Eye growth changes in myopic children in Singapore. *Br J Ophthalmol.* 2005;89(11):1489-94. Epub 2005/10/20.
100. Zadnik K, Manny RE, Yu JA, Mitchell GL, Cotter SA, Quiralte JC, et al. Ocular component data in schoolchildren as a function of age and gender. *Optom Vis Sci.* 2003;80(3):226-36. Epub 2003/03/15.
101. Williams C, Miller LL, Gazzard G, Saw SM. A comparison of measures of reading and intelligence as risk factors for the development of myopia in a UK cohort of children. *Br J Ophthalmol.* 2008;92(8):1117-21. Epub 2008/06/24.
102. Xiang F, He M, Morgan IG. Annual changes in refractive errors and ocular components before and after the onset of myopia in chinese children. *Ophthalmology.* 2012;119(7):1478-84. Epub 2012/05/15.
103. Kimura S, Hasebe S, Miyata M, Hamasaki I, Ohtsuki H. Axial length measurement using partial coherence interferometry in myopic children: repeatability of the measurement and comparison with refractive components. *Jpn J Ophthalmol.* 2007;51(2):105-10. Epub 2007/04/03.
104. Luce DA. Determining in vivo biomechanical properties of the cornea with an ocular response analyzer. *J Cataract Refract Surg.* 2005;31(1):156-62. Epub 2005/02/22.

105. Song Y, Congdon N, Li L, Zhou Z, Choi K, Lam DS, et al. Corneal hysteresis and axial length among Chinese secondary school children: the Xichang Pediatric Refractive Error Study (X-PRES) report no. 4. *Am J Ophthalmol*. 2008;145(5):819-26. Epub 2008/03/11.
106. Lim L, Gazzard G, Chan YH, Fong A, Kotecha A, Sim EL, et al. Cornea biomechanical characteristics and their correlates with refractive error in Singaporean children. *Invest Ophthalmol Vis Sci*. 2008;49(9):3852-7. Epub 2008/05/13.
107. Rahi JS, Cumberland PM, Peckham CS. Myopia over the lifecourse: prevalence and early life influences in the 1958 British birth cohort. *Ophthalmology*.118(5):797-804. Epub 2010/12/28.
108. Saw SM, Tong L, Chia KS, Koh D, Lee YS, Katz J, et al. The relation between birth size and the results of refractive error and biometry measurements in children. *Br J Ophthalmol*. 2004;88(4):538-42. Epub 2004/03/20.
109. Krause U, Krause K, Rantakallio P. Sex differences in refraction errors up to the age of 15. *Acta Ophthalmol (Copenh)*. 1982;60(6):917-26. Epub 1982/12/01.
110. McIntyre MH. The use of digit ratios as markers for perinatal androgen action. *Reprod Biol Endocrinol*. 2006;4:10. Epub 2006/03/01.
111. Manning JT, Scutt D, Wilson J, Lewis-Jones DI. The ratio of 2nd to 4th digit length: a predictor of sperm numbers and concentrations of testosterone,

- lutinizing hormone and oestrogen. *Hum Reprod.* 1998;13(11):3000-4. Epub 1998/12/16.
112. Honekopp J, Bartholdt L, Beier L, Liebert A. Second to fourth digit length ratio (2D:4D) and adult sex hormone levels: new data and a meta-analytic review. *Psychoneuroendocrinology.* 2007;32(4):313-21. Epub 2007/04/03.
113. Cordain L, Eaton SB, Brand Miller J, Lindeberg S, Jensen C. An evolutionary analysis of the aetiology and pathogenesis of juvenile-onset myopia. *Acta Ophthalmol Scand.* 2002;80(2):125-35. Epub 2002/04/16.
114. <http://www.randomizer.org/>. Available from: <http://www.randomizer.org/>.
115. Moreno-Montanes J, Maldonado MJ, Garcia N, Mendiluce L, Garcia-Gomez PJ, Segui-Gomez M. Reproducibility and clinical relevance of the ocular response analyzer in nonoperated eyes: corneal biomechanical and tonometric implications. *Invest Ophthalmol Vis Sci.* 2008;49(3):968-74. Epub 2008/03/11.
116. D Luce. Methodology for corneal compensated IOP and corneal resistance factor for an ocular response analyzer. [cited 2013 August]; Available from: <http://doclibrary.com/MSC167/PRM/Luce-2006-13559.pdf>.
117. Helmholtz H. Ueber die Accommodation des Auges. *Albrecht von Graefes Archiv für Ophthalmologie.* 1855;2:1-74.
118. Sheppard AL, Evans CJ, Singh KD, Wolffsohn JS, Dunne MC, Davies LN. Three-dimensional magnetic resonance imaging of the phakic crystalline lens during accommodation. *Invest Ophthalmol Vis Sci.* 52(6):3689-97. Epub 2011/02/08.

119. Shah A SA, Sinapis C, Bunce C, Garway-Heath D. Inter- and intra- observer agreement of anterior segment-OCT iris profile measurements in pigment dispersion syndrome. *ARVO*. 2010;51; ARVO E-Abstract 5539.
120. Liu S, Li H, Dorairaj S, Cheung CY, Rousso J, Liebmann J, et al. Assessment of scleral spur visibility with anterior segment optical coherence tomography. *J Glaucoma*. 2009;19(2):132-5. Epub 2009/06/17.
121. Kirwan C, O'Keefe M, Lanigan B. Corneal hysteresis and intraocular pressure measurement in children using the reichert ocular response analyzer. *Am J Ophthalmol*. 2006;142(6):990-2. Epub 2006/12/13.
122. Huang Y, Huang C, Li L, Qiu K, Gong W, Wang Z, et al. Corneal biomechanics, refractive error, and axial length in Chinese primary school children. *Invest Ophthalmol Vis Sci*.52(7):4923-8. Epub 2011/01/08.
123. Chang PY, Chang SW, Wang JY. Assessment of corneal biomechanical properties and intraocular pressure with the Ocular Response Analyzer in childhood myopia. *Br J Ophthalmol*. 2010;94(7):877-81. Epub 2009/10/17.
124. Dirani M, Islam FM, Baird PN. The role of birth weight in myopia--the genes in myopia twin study. *Ophthalmic Res*. 2009;41(3):154-9. Epub 2009/03/27.
125. McFadden D, Shubel E. Relative lengths of fingers and toes in human males and females. *Horm Behav*. 2002;42(4):492-500. Epub 2002/12/19.

126. Malas MA, Dogan S, Evcil EH, Desdicioglu K. Fetal development of the hand, digits and digit ratio (2D:4D). *Early Hum Dev.* 2006;82(7):469-75. Epub 2006/02/14.
127. Honekopp J, Watson S. Meta-analysis of digit ratio 2D:4D shows greater sex difference in the right hand. *Am J Hum Biol.* 22(5):619-30. Epub 2010/08/26.
128. Barker DJ. Fetal origins of coronary heart disease. *BMJ (Clinical research ed).* 1995;311(6998):171-4. Epub 1995/07/15.
129. Schoeller DA, Kushner RF. Determination of body fluids by the impedance technique. *IEEE Eng Med Biol Mag.* 1989;8(1):19-21. Epub 1989/01/01.
130. Cordain L, Whicker RE, Johnson JE. Body composition determination in children using bioelectrical impedance. *Growth Dev Aging.* 1988;52(1):37-40. Epub 1988/01/01.
131. Houtkooper LB, Lohman TG, Going SB, Hall MC. Validity of bioelectric impedance for body composition assessment in children. *J Appl Physiol.* 1989;66(2):814-21. Epub 1989/02/01.
132. Strachan TaR, A. *Human Molecular Genetics.* 4th ed. New York: Garland Science, Taylor and Francis Group, LLC; 2011. p. 467-96.
133. Ott J. *Analysis of Human Genetic Linkage.* 2nd Edition ed. Baltimore: Johns Hopkins University Press; 1991.
134. Morton NE. Sequential tests for the detection of linkage. *Am J Hum Genet.* 1955;7(3):277-318. Epub 1955/09/01.

135. Haines JL, Pericak-Vance MA. Genetic analysis of complex disease. 2nd edition ed: John Wiley & Sons, Inc; 2006.
136. Sarfarazi M, Child A, Stoilova D, Brice G, Desai T, Trifan OC, et al. Localization of the fourth locus (GLC1E) for adult-onset primary open-angle glaucoma to the 10p15-p14 region. *Am J Hum Genet.* 1998;62(3):641-52. Epub 1998/04/29.
137. Rezaie T, Child A, Hitchings R, Brice G, Miller L, Coca-Prados M, et al. Adult-onset primary open-angle glaucoma caused by mutations in optineurin. *Science.* 2002;295(5557):1077-9. Epub 2002/02/09.
138. Porter LF, Urquhart JE, O'Donoghue E, Spencer AF, Wade EM, Manson FD, et al. Identification of a novel locus for autosomal dominant primary open angle glaucoma on 4q35.1-q35.2. *Invest Ophthalmol Vis Sci.* 2011;52(11):7859-65. Epub 2011/09/08.
139. Garway-Heath DF, Lascaratos G, Bunce C, Crabb DP, Russell RA, Shah A. The United Kingdom Glaucoma Treatment Study: a multicenter, randomized, placebo-controlled clinical trial: design and methodology. *Ophthalmology.* 2013;120(1):68-76. Epub 2012/09/19.
140. Sequencher® version 4.1.4 sequence analysis software. Gene Codes Corporation, Ann Arbor, MI USA; Available from: <http://www.genecodes.com>.
141. Ritch R. Nonprogressive low-tension glaucoma with pigmentary dispersion. *Am J Ophthalmol.* 1982;94(2):190-6. Epub 1982/08/01.

142. Bennetts JS, Fowles LF, Berkman JL, van Bueren KL, Richman JM, Simpson F, et al. Evolutionary conservation and murine embryonic expression of the gene encoding the SERTA domain-containing protein CDCA4 (HEPP). *Gene*. 2006;374:153-65. Epub 2006/03/21.
143. Ittner LM, Wurdak H, Schwerdtfeger K, Kunz T, Ille F, Leveen P, et al. Compound developmental eye disorders following inactivation of TGFbeta signaling in neural-crest stem cells. *J Biol*. 2005;4(3):11. Epub 2006/01/13.
144. Iwao K, Inatani M, Matsumoto Y, Ogata-Iwao M, Takihara Y, Irie F, et al. Heparan sulfate deficiency leads to Peters anomaly in mice by disturbing neural crest TGF-beta2 signaling. *J Clin Invest*. 2009;119(7):1997-2008. Epub 2009/06/11.
145. David D, Cardoso J, Marques B, Marques R, Silva ED, Santos H, et al. Molecular characterization of a familial translocation implicates disruption of HDAC9 and possible position effect on TGFbeta2 in the pathogenesis of Peters' anomaly. *Genomics*. 2003;81(5):489-503. Epub 2003/04/23.
146. Chung AE, Durkin ME. Entactin: structure and function. *Am J Respir Cell Mol Biol*. 1990;3(4):275-82. Epub 1990/10/01.
147. Grada A, Weinbrecht K. Next-generation sequencing: methodology and application. *J Invest Dermatol*. 2013;133(8):e11. Epub 2013/07/17.
148. Quail MA, Smith M, Coupland P, Otto TD, Harris SR, Connor TR, et al. A tale of three next generation sequencing platforms: comparison of Ion Torrent, Pacific

- Biosciences and Illumina MiSeq sequencers. *BMC genomics*. 2012;13:341. Epub 2012/07/26.
149. Sobreira NL, Cirulli ET, Avramopoulos D, Wohler E, Oswald GL, Stevens EL, et al. Whole-genome sequencing of a single proband together with linkage analysis identifies a Mendelian disease gene. *PLoS genetics*. 2010;6(6):e1000991. Epub 2010/06/26.
150. Lander ES, Schork NJ. Genetic dissection of complex traits. *Science*. 1994;265(5181):2037-48. Epub 1994/09/30.
151. Risch N, Merikangas K. The future of genetic studies of complex human diseases. *Science*. 1996;273(5281):1516-7. Epub 1996/09/13.
152. Reich DE, Lander ES. On the allelic spectrum of human disease. *Trends in genetics : TIG*. 2001;17(9):502-10. Epub 2001/08/30.
153. Burdon KP. Genome-wide association studies in the hunt for genes causing primary open-angle glaucoma: a review. *Clin Experiment Ophthalmol*. 2012;40(4):358-63. Epub 2011/12/17.
154. The International HapMap Project. *Nature*. 2003;426(6968):789-96. Epub 2003/12/20.
155. Kruglyak L. The road to genome-wide association studies. *Nature reviews Genetics*. 2008;9(4):314-8. Epub 2008/02/20.

156. Klein RJ, Zeiss C, Chew EY, Tsai JY, Sackler RS, Haynes C, et al. Complement factor H polymorphism in age-related macular degeneration. *Science*. 2005;308(5720):385-9. Epub 2005/03/12.
157. Deangelis MM, Silveira AC, Carr EA, Kim IK. Genetics of age-related macular degeneration: current concepts, future directions. *Semin Ophthalmol*. 2011;26(3):77-93. Epub 2011/05/26.
158. Baratz KH, Tosakulwong N, Ryu E, Brown WL, Branham K, Chen W, et al. E2-2 protein and Fuchs's corneal dystrophy. *N Engl J Med*. 2010;363(11):1016-24. Epub 2010/09/10.
159. Thorleifsson G, Magnusson KP, Sulem P, Walters GB, Gudbjartsson DF, Stefansson H, et al. Common sequence variants in the LOXL1 gene confer susceptibility to exfoliation glaucoma. *Science*. 2007;317(5843):1397-400. Epub 2007/08/11.
160. Schlotzer-Schrehardt U. Genetics and genomics of pseudoexfoliation syndrome/glaucoma. *Middle East Afr J Ophthalmol*. 2011;18(1):30-6. Epub 2011/05/17.
161. Williams SE, Whigham BT, Liu Y, Carmichael TR, Qin X, Schmidt S, et al. Major LOXL1 risk allele is reversed in exfoliation glaucoma in a black South African population. *Mol Vis*. 2010;16:705-12. Epub 2010/05/01.

162. Thorleifsson G, Walters GB, Hewitt AW, Masson G, Helgason A, DeWan A, et al. Common variants near CAV1 and CAV2 are associated with primary open-angle glaucoma. *Nat Genet.* 2010;42(10):906-9. Epub 2010/09/14.
163. Wiggs JL, Kang JH, Yaspan BL, Mirel DB, Laurie C, Crenshaw A, et al. Common variants near CAV1 and CAV2 are associated with primary open-angle glaucoma in Caucasians from the USA. *Hum Mol Genet.* 2011;20(23):4707-13. Epub 2011/08/30.
164. Burdon KP, Macgregor S, Hewitt AW, Sharma S, Chidlow G, Mills RA, et al. Genome-wide association study identifies susceptibility loci for open angle glaucoma at TMCO1 and CDKN2B-AS1. *Nat Genet.* 2011;43(6):574-8. Epub 2011/05/03.
165. Cichon S, Craddock N, Daly M, Faraone SV, Gejman PV, Kelsoe J, et al. Genomewide association studies: history, rationale, and prospects for psychiatric disorders. *Am J Psychiatry.* 2009;166(5):540-56. Epub 2009/04/03.
166. Chang B, Smith RS, Hawes NL, Anderson MG, Zabaleta A, Savinova O, et al. Interacting loci cause severe iris atrophy and glaucoma in DBA/2J mice. *Nat Genet.* 1999;21(4):405-9. Epub 1999/04/07.
167. Ripoll VM, Meadows NA, Raggatt LJ, Chang MK, Pettit AR, Cassady AI, et al. Microphthalmia transcription factor regulates the expression of the novel osteoclast factor GPNMB. *Gene.* 2008;413(1-2):32-41. Epub 2008/03/04.

168. Bachner D, Schroder D, Gross G. mRNA expression of the murine glycoprotein (transmembrane) nmb (Gpnmb) gene is linked to the developing retinal pigment epithelium and iris. *Brain Res Gene Expr Patterns*. 2002;1(3-4):159-65. Epub 2003/03/18.
169. Boissy RE, Zhao H, Oetting WS, Austin LM, Wildenberg SC, Boissy YL, et al. Mutation in and lack of expression of tyrosinase-related protein-1 (TRP-1) in melanocytes from an individual with brown oculocutaneous albinism: a new subtype of albinism classified as "OCA3". *Am J Hum Genet*. 1996;58(6):1145-56. Epub 1996/06/01.
170. Lynch S, Yanagi G, DelBono E, Wiggs JL. DNA sequence variants in the tyrosinase-related protein 1 (TYRP1) gene are not associated with human pigmentary glaucoma. *Mol Vis*. 2002;8:127-9. Epub 2002/05/16.
171. Hoashi T, Sato S, Yamaguchi Y, Passeron T, Tamaki K, Hearing VJ. Glycoprotein nonmetastatic melanoma protein b, a melanocytic cell marker, is a melanosome-specific and proteolytically released protein. *FASEB journal : official publication of the Federation of American Societies for Experimental Biology*. 2010;24(5):1616-29. Epub 2010/01/09.
172. Weterman MA, Ajubi N, van Dinter IM, Degen WG, van Muijen GN, Rutter DJ, et al. nmb, a novel gene, is expressed in low-metastatic human melanoma cell lines and xenografts. *Int J Cancer*. 1995;60(1):73-81. Epub 1995/01/03.
173. Seddon JM, Ajani UA, Mitchell BD. Familial aggregation of age-related maculopathy. *Am J Ophthalmol*. 1997;123(2):199-206. Epub 1997/02/01.

174. Klaver CC, Wolfs RC, Assink JJ, van Duijn CM, Hofman A, de Jong PT. Genetic risk of age-related maculopathy. Population-based familial aggregation study. *Arch Ophthalmol*. 1998;116(12):1646-51. Epub 1998/12/31.
175. Purcell S, Neale B, Todd-Brown K, Thomas L, Ferreira MA, Bender D, et al. PLINK: a tool set for whole-genome association and population-based linkage analyses. *Am J Hum Genet*. 2007;81(3):559-75. Epub 2007/08/19.
176. Purcell S. PLINK. Available from: <http://pngu.mgh.harvard.edu/purcell/plink/>.
177. R Development Core Team RfSC. R: A Language and Environment for Statistical Computing. 2011; Available from: <http://www.R-project.org>.
178. Anderson CA, Pettersson FH, Clarke GM, Cardon LR, Morris AP, Zondervan KT. Data quality control in genetic case-control association studies. *Nat Protoc*. 2010;5(9):1564-73. Epub 2010/11/19.
179. Kumar P, Henikoff S, Ng PC. Predicting the effects of coding non-synonymous variants on protein function using the SIFT algorithm. *Nat Protoc*. 2009;4(7):1073-81. Epub 2009/06/30.
180. Adzhubei IA, Schmidt S, Peshkin L, Ramensky VE, Gerasimova A, Bork P, et al. A method and server for predicting damaging missense mutations. *Nat Methods*. 2010;7(4):248-9. Epub 2010/04/01.
181. Ferrer-Costa C, Orozco M, de la Cruz X. Characterization of disease-associated single amino acid polymorphisms in terms of sequence and structure properties. *J Mol Biol*. 2002;315(4):771-86. Epub 2002/01/29.

182. Ferrer-Costa C, Orozco M, de la Cruz X. Sequence-based prediction of pathological mutations. *Proteins*. 2004;57(4):811-9. Epub 2004/09/25.
183. Wellcome Trust Sanger Institute. HapMap 3. URL: <http://www.sanger.ac.uk/resources/downloads/humans/hapmap3.html> [10 February 2012]
184. Cardon LR, Palmer LJ. Population stratification and spurious allelic association. *Lancet*. 2003;361(9357):598-604. Epub 2003/02/25.
185. Price AL, Patterson NJ, Plenge RM, Weinblatt ME, Shadick NA, Reich D. Principal components analysis corrects for stratification in genome-wide association studies. *Nat Genet*. 2006;38(8):904-9. Epub 2006/07/25.
186. Patterson N, Price AL, Reich D. Population structure and eigenanalysis. *PLoS genetics*. 2006;2(12):e190. Epub 2006/12/30.
187. Price AL, Weale ME, Patterson N, Myers SR, Need AC, Shianna KV, et al. Long-range LD can confound genome scans in admixed populations. *Am J Hum Genet*. 2008;83(1):132-5; author reply 5-9. Epub 2008/07/09.
188. Lu H, Wang X, Pullen M, Guan H, Chen H, Sahu S, et al. Genetic dissection of the Gpnmb network in the eye. *Invest Ophthalmol Vis Sci*. 2011;52(7):4132-42. Epub 2011/03/15.